Dissertations, Theses, and Masters Projects   Theses, Dissertations, & Master Projects

2011

Fine Sediment Dynamics in Dredge Plumes

Stanley Jarrell Smith II

College of William and Mary - Virginia Institute of Marine Science

FINE SEDIMENT DYNAMICS IN DREDGE PLUMES

A Dissertation

Presented to

The Faculty of the School of Marine Science

The College of William and Mary

In Partial Fulfillment

Of the Requirements for the Degree of

Doctor of Philosophy
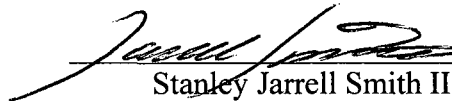
by

Stanley Jarrell Smith II
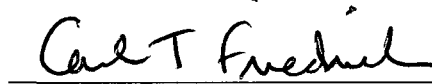
2010

APPROVAL SHEET
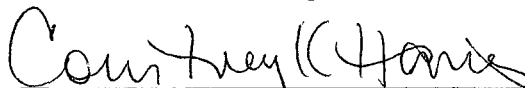
This dissertation is submitted in partial fulfillment of

the requirements for the degree of

Doctor of Philosophy

_____
Stanley Jarrell Smith II

Approved, by the Committee, October 2010

_____
Carl T. Friedrichs, Ph.D.
Committee Chairman/Advisor

_____
Robert J. Diaz, Ph.D.

_____
Courtney K. Harris, Ph.D.

_____
L. Donelson Wright, Ph.D.

_____
Lawrence P. Sanford, Ph.D.
University of Maryland
Cambridge, Maryland

TABLE OF CONTENTS

ACKNOWLEDGEMENTS

LIST OF TABLES

LIST OF FIGURES

ABSTRACT

The research presented in this study is motivated by the need to improve predictions of transport and fate of cohesive sediments suspended during dredging operations. Two techniques are presented to quantify vertical sediment flux within dredge plumes. A mass-balance approach using an Acoustic Doppler Current Profiler (ADCP) is described and de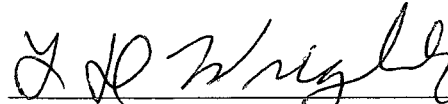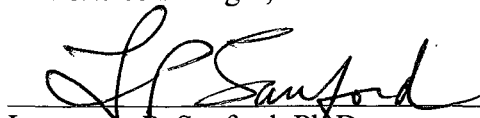monstrated to accurately estimate vertical mass flux and settling velocity for a suspension of fine sand from a dredged material placement operation.

A new digital video settling column for simultaneous measurement of particle size and settling velocity is described and evaluated. The Particle Imaging Camera System (PICS) is a single-chambered, digital video settling column, which permits rapid acquisition (within 2-3 minutes) of image sequences within dredge plumes. Image analysis methods are presented, which provide improved estimates of particle size, settling velocity, and inferred particle density. A combination of Particle Tracking Velocimetry (PTV) and Particle Image Velocimetry (PIV) techniques is described, which permits general automation of image analysis collected from video settling columns. In the fixed image plane, large particle velocities are determined by PTV and small particle velocities are tracked by PIV and treated as surrogates for fluid velocities. The large-particle settling velocity (relative to the suspending fluid) is determined by the vector difference of the large and small particle settling velocities. The combined PTV/PIV image analysis approach is demonstrated for video settling column data collected within a mechanical dredge plume in Boston Harbor. The automated PTV/PIV approach significantly reduces uncertainties in measured settling velocity and inferred floc density.

Size, settling velocities, and density of suspended sediments were measured with PICS within a trailing suction hopper dredge plume in San Francisco Bay. Results indicated that suspended sediments within the plume were predominantly in the clay and fine silt size classes, as aggregates with d>30 µm. Suspended bed aggregates (defined by densities of 1200 to 1800 kg m^{-3}) represented 0.2-0.5 of total suspended mass, and size and settling velocity of this class were time invariant. Flocs (densities < 1200 kg m^{-3}) represented 0.5 to 0.8 of total suspended mass, and size and settling velocity of flocs was seen to increase with time. The peak diameter of bed aggregates and flocs occurred near 90 µm and 200 µm, respectively, corresponding to peak settling velocities of about 1 mm s^{-1} in each case. Floc settling velocities increased with particle size $d^{1.1}$, while bed aggregate settling velocity increased like $d^{1.3}$.

Numerical modeling approaches to representing settling velocities for hopper dredge plumes are discussed in light of the experimental findings. Size-dependant settling velocities were well-described by a fractal-based relationship when the suspension was treated with discrete classes for each of the aggregate states. Time-dependent increases in floc size and settling velocity confirm that flocculation is a first-order process which should be included in numerical plume models. Correlations between settling velocity and suspended sediment concentration were weak and statistically insignificant, implying that commonly applied empirical relationships are inappropriate for dredge plumes.

FINE SEDIMENT DYNAMICS IN DREDGE PLUMES

INTRODUCTION AND SUMMARY

The objective of this research is to quantify size, settling velocity, and density of suspended fine grained sediments in dredge plumes. Fine sediments suspended during dredging operations impact surrounding ecosystems to varying degrees by altering physical and chemical characteristics of the water column and sediment bed. Ecosystem impacts include: light attenuation, nutrient loading, physiological impairment (particularly early life stages), burial, dispersal of contaminated sediments, and changes to habitat quality. Numerical sediment transport models have been developed and applied to quantify these ecosystem impacts; however evaluations of these models have indicated a general deficiency in describing the settling processes in dredge plumes. Insights gained through the present research will be transferred to numerical transport models, permitting improved impact assessment and more effective mitigation alternatives for dredging operations.

Dredges remove sediment from the bed by mechanical and/or hydraulic means. The stresses imposed by dredging operations greatly exceed stresses exerted by natural hydrodynamic processes. Consequently, dredges are capable of removing sediments previously buried 10s to 100s cm below the sediment-water interface. Due to self-weight consolidation, these dredged sediments are much denser than surficial sediments eroded by natural processes. During the dredging process, a portion of the consolidated sediment bed is fragmented and released to the water column. Additional dredging practices, such as hopper or barge overflow, also release sediment to the water column. The initial states of aggregation and consequent fate of sediments suspended by dredging operations are highly dependent upon such factors as dredging equipment and processes, sediment composition, bed density, and hydrodynamics.

Particle settling is governed by the balance of gravity, buoyancy, and drag forces. These forces are influenced by fluid density and viscosity and particle size, shape, and density. The primary influences of dredging operations on suspended sediment settling

are particle size and density. Particle density is associated with aggregation state, which includes: single mineral grains (primary particles), dense cohesive aggregates, and loose cohesive aggregates (flocs).

Flocs are formed in the water column by interparticle collisions, resulting in relatively fragile, low-density aggregations of primary particles, flocs, and denser aggregates. Floc growth is governed by competing processes of aggregation and disaggregation. Aggregation is influenced by the rate of interparticle collisions (controlled by turbulent shear and particle size and concentration) and interparticle cohesion (which influences the stickiness or likelihood that colliding particles will bond). Disaggregation occurs when turbulent stresses exceed the interparticle bonds of the floc. When aggregation outpaces disaggregation, floc size increases, floc density decreases, and with rare exception floc settling velocity increases. The opposite holds when flocs disaggregate. Floc characteristics may change rapidly (on timescales of minutes to hours), when the aggregation-disaggregation processes are imbalanced.

Dense cohesive aggregates are products of repeated aggregation/disaggregation cycles in the water column or resuspension of consolidated sediments from the bed. Dense aggregates are characterized by relatively high interparticle bonding, and therefore are more robust and less likely to disaggregate. Due to their higher density, dense cohesive aggregates settle faster than flocs of the same size.

Measuring fine-sediment size, settling velocity, and density in dredge plumes is challenging due to the small spatial scales of dredge plumes and the short time scales of fine-sediment processes within the plumes. Additionally, flocs are inherently fragile and must be sampled in situ. Consequently, measurements in dredge plumes must be taken rapidly and with particular attention to avoid floc breakup during sampling.

The first chapter of this thesis provides motivation and background regarding environmental impacts of suspended dredged material, prior research of sediment transport associated with dredging operations, theoretical background of suspended fine sediment processes, and research objectives of this dissertation.

Chapter Two describes an analysis technique to determine bulk settling rates within dredge plumes using an ADCP. This approach estimates settling velocity within a

suspended sediment plume by solving the suspended sediment mass conservation equation with longitudinal (in the flow direction) gradients in suspended sediment transport estimated from the ADCP data.

Chapter Three describes development of the Particle Imaging Camera System (PICS) and application of PICS to determine cohesive sediment aggregate states and settling velocities within a trailing suction hopper dredge plume in San Francisco Bay. Through this experiment, aggregate size, settling velocity, and density were estimated within the hopper dredge overflow plume for approximately 90 minutes following sediment release to the water column. The suspension released from the dredge was composed of silt and clay particles, nearly exclusively as dense aggregates and flocs. The dense aggregate class was composed of smaller but denser particles with time invariant size and settling velocity; the floc class demonstrated time-dependent increases in size and settling velocity.

Chapter Four presents improved image analysis methods for video settling columns. Two challenges in analysis of video settling column imagery are the automated tracking of settling particles and accounting for fluid motions within the settling column. A combination of Particle Tracking Velocimetry (PTV) and Particle Image Velocimetry (PIV) image analysis techniques is described, which permits general automation of image analysis collected from video settling columns. In the fixed image plane, large particle velocities are determined by PTV and small particle velocities are tracked by PIV and treated as surrogates for fluid velocities. The large-particle settling velocity (relative to the suspending fluid) is determined by the vector difference of the large and small particle settling velocities. The combined PTV/PIV image analysis approach is demonstrated for video settling column data collected within a dredge plume in Boston Harbor. The automated PTV/PIV approach was found to 1) significantly reduce uncertainties in measured settling velocity and inferred floc excess density, and 2) permits evaluation of much larger population statistics compared to manual methods.

Chapter Five provides a summary of the research and conclusions, followed by recommendations for continued research.

CHAPTER 1

SUSPENDED FINE GRAINED SEDIMENTS IN DREDGE PLUMES

1 INTRODUCTION

Dredging of sediments from navigation channels and ports is a vital activity for national economic security, enabling access to ports by commercial, deep-draft, ocean-going vessels (USACE, 1983). During dredging operations, sediments are removed from the channel bottom and transported by pipeline or vessel to approved dredged material placement sites. However, a portion of the sediments removed from the bed are suspended into the water column, transported from the dredging and placement sites by ambient currents, and returned to the bed through particle settling and deposition. The transport and fate of sediments suspended by dredging operations is a primary concern due to potential impacts to natural resources (USACE, 1983; Wilber and Clarke, 2001).

Elevated suspended sediment concentration (SSC) and turbidity can impose a range of environmental impacts such as gill abrasion and clogging; increased light attenuation and reduction of photic depth (impacts to micro-algae, macro-algae, and submerged aquatic vegetation); burial, smothering, and abrasion of demersal eggs; reduced growth rate of larval and juvenile organisms (leading to increased mortality and reduced recruitment); blockage of fish migration routes; degradation of spawning habitat; and dispersion of sediment-adsorbed contaminants (Newcombe and Jensen, 1996; Wilber and Clarke, 2001). Newcombe and Jensen (1996) propose that impacts to fish are a function of SSC, duration of exposure, species, and life stage. In the United States, natural resource agencies (state departments of environmental quality; state, regional, and federal fisheries agencies; and federal environmental protection) require dredging proponents (such as port authorities and the U.S. Army Corps of Engineers) to demonstrate that proposed dredging practices meet regulatory requirements established by under Section 404 of the Clean Water Act, Section 103 of the Marine Protection, Research, and Sanctuaries Act, National Environmental Policy Act of 1969, and state water quality standards.

Numerical models are among the primary tools through which dredging proponents demonstrate that a proposed dredging practice is likely to meet regulatory requirements. These models represent the processes of sediment suspension, advection, diffusion, settling, and deposition through a collection of both empirical- and physics-

based equations to predict transport and fate of sediments suspended by dredging operations (Koh and Chang, 1973; Johnson, 1990; Johnson et al., 2000; MacDonald et al., 2006). Wide variations in dredging equipment and sediment characteristics and limited knowledge of the rates of suspension and characteristics of suspended material lead to large uncertainties in model estimates of sediment transport and fate (Germano and Cary, 2005). Milligan and Hill (1998) suggest that time-variant flocculation effects must be included in sediment transport models for assessing environmental impacts in the coastal zone. Similarly, advancement of the predictive capabilities of dredged material transport, fate, and impacts are not expected until better understanding is gained of the influences of dredge and sediment types on sediment suspension and sediment dynamics.

To present, limited progress has been made in quantifying the rate of sediment suspension from various dredge types and even less progress has been made in describing suspended sediment characteristics and settling processes in dredge plumes. Limitations in present knowledge of suspension and settling in dredge plumes are largely attributable to past limitations in sampling technology. Until the early 1990s, field measurements were limited to physical pump and bottle samples analyzed for total suspended solids or sediment size distributions (McLellan et al. 1989). Limited spatial and temporal resolution available with physical sampling in dredge plumes characterized by high spatial and temporal gradients made quantifying suspension rates and settling velocities extremely challenging. Advances in the arena of optical, acoustic, and photographic instrumentation permit corresponding advances in the ability to collect information about dredge plume dynamics (Puckette, 1998; Tubman and Corson, 2000; Reine et al., 2002). Through application of these recent advances in suspended sediment sampling, the proposed research aims to increase understanding of suspended sediment characteristics and settling dynamics in dredge plumes. Better understanding of settling dynamics in dredge plumes will lead to improved predictive methods, better informed dredging operation planning, and reduced impacts to natural resources.

2 THEORETICAL BACKGROUND

A large portion of navigation dredging in coastal and estuarine environments involves the handling of cohesive sediments. Cohesive sediment properties and

processes significantly influence the settling, transport, and deposition of sediments suspended during dredging operations. A fundamental understanding of these processes and dredging operations is required to address sediment dynamics in dredge plumes.

2.1 Cohesive Sediment Flocs

Discrete clay particles are generally found in sizes ranging between 1-4 μm and are characterized by sheet-like mineral structure (Weaver, 1989; Winterwerp and van Kesteren, 2004) and varying degrees of surface charges. Kaolinite, Chlorite, and to a lesser degree other clay minerals may form stacks of tightly bound primary clay particles or flocculi (Winterwerp and Van Kesteren, 2004) with sizes on the order of 10's of μm. Coagulation and flocculation are processes by which individual silt and clay particles are bound together into structures called flocs or aggregates. Flocculi are formed by electro-chemical bonds (coagulation) between the sheet-like faces of individual clay particles. Stresses in the water column are generally insufficient to break the strong bonds of coagulated clay particles, and coagulation is therefore treated as an irreversible process from the perspective of marine sediment dynamics (Winterwerp and Van Kesteren, 2004). Flocs are bound through inter-particle forces arising from molecular attraction or polymeric binding of smaller flocs, flocculi, individual particles, and colloids (Winterwerp and Van Kesteren, 2004). Unlike coagulation, flocculation is a reversible process, governed by a balance between aggregation (bringing particles together) and disaggregation (break-up of flocs).

Krone (1963) was among the first to describe flocs as self-similar aggregates. Krone described the process as starting with primary particles (the individual clay particles or flocculi) than combine to form small, first-order flocs. The first-order flocs then combine in succession to form larger, higher-order flocs. Kranenburg (1994, 1999) and Winterwerp (1998, 2002) further suggested that this self-similarity can be mathematically described through fractal geometry and that floc properties such as size, settling velocity, and floc strength can be estimated from the fractal geometry.

2.2 Aggregation and Disaggregation

Aggregation is a process by which particles collide and are bound by various inter-particle forces. Factors influencing particle collision and aggregation include

particle number concentration, particle size, physico-chemical sediment properties, and physical and hydrodynamic processes (Van Leussen, 1994; Winterwerp and Van Kesteren, 2004; Mehta and McAnally, 2008). Processes producing particle-particle collisions include: Brownian motion (arising from random molecular motions), differential settling (from differences in settling velocity between individual grains/flocs), and turbulent shear (Mehta and McAnally, 2008). Van Leussen (1994) found that for most estuarine environments, turbulent shear influences aggregation much greater than Brownian motion for particles larger than 2-10 μm. Stolzenbach and Elimelich (1994) conclude that aggregation by differential settling of non-porous particles is reduced by deflection of the smaller particle around the path of the larger. Stolzenbach and Elimelich further conclude that aggregation by differential settling is likely to occur only between very small particles and large particles for which particle porosity may be significant. Winterwerp and Van Kesteren (2004) conclude that turbulent shear is the dominating effect bringing particles into collision in coastal and estuarine environments.

Not all particle collisions result in aggregation. Inorganic clay particles have repulsive ionic surface charges that are stronger than attractive forces unless particles come in close proximity to one another. The strength of repulsive ionic charges is related to mineralogy of the particles involved. When inorganic particles are mixed with ionic solutions (such as seawater), cations are attracted to the negative charges, weaken the repulsive forces, particle collisions and adhesion become more likely, and aggregation increases. Aside from molecular attractive forces, organic polymers secreted by bacteria and a host of aquatic microorganisms also serve to bind inorganic sediment particles and flocs. Additionally, pelagic organisms such as siphonophores, macrozooplankton, and microzooplankton ingest suspended sediments and package the ingested material into strong, dense, and rapidly settling fecal pellets. Estuaries and the coastal ocean represent some of the most biologically active regions of the marine environment, and in many instances biological influence dominates flocculation (Hill, 1992; Van Leussen, 1994, Fugate and Friedrichs, 2003).

Disaggregation is the competing process to aggregation by which shear breaks flocs apart. When shear stresses overcome the strength of bonds holding flocs together, flocs disaggregate. Shear experienced by flocs is produced by drag, turbulence, and

inter-particle collisions (Van Leussen, 1994; Mehta and McAnally, 2008). Floc fall speed and drag increase with increasing floc diameter. If shear produced by drag forces on the floc exceed the floc strength, disaggregation occurs. Turbulence induces interparticle stresses through strong velocity gradients found within turbulent eddies. Van Leussen (1994) reviews research leading to the theory that maximum floc size is limited by the size of the smallest turbulent eddies present in the water column (Kolmogorov microscale). The Kolmogorov scale is inversely related to turbulent energy in the water column. So, smaller flocs are expected in the presence of high turbulent energy and larger flocs are expected in the presence of lower turbulent energy. Wolanski and Gibbs (1994) found that mean floc size decreased with increasing turbulence of tidal currents on the Fly River delta. Additionally, inter-particle bond strength influences the break-up process. Factors such as mineralogy, organic content, floc size and density influence floc strength (Krone, 1963; Van Leussen, 1994; Wolanski and Gibbs, 1995; Winterwerp and Van Kesteren, 2004).

Aggregation and disaggregation processes are characteristically dynamic. Aggregation rates generally increase with particle concentration and shear, and disaggregation rates increase with internal shear rates exceeding aggregate strength (Winterwerp and Van Kesteren, 2004). Field measurements and laboratory experiments (reviewed by Chisholm (1999)) suggest that equilibrium floc sizes can be reached on time scales of minutes to hours, but some laboratory experiments at low shear and concentration (Lick et al. 1993) did not reach equilibrium in 30 hours. Additionally, internal shear in coastal and estuarine environments varies with tides, wave exposure, wind, and water column depth. Consequently, growth and breakup of flocs are time- and space-variant functions. Due to the characteristically loose nature of flocs formed in the water column (except fecal pellets), excess density of flocs is generally small, on the order of $50 - 300$ kg m^{-3} (Van Leussen, 1994; Winterwerp and Van Kesteren, 2004).

2.3 Particle Settling

Settling of solid particles in a fluid medium is described by the balance of forces arising from particle weight, buoyancy, and drag. For the case of sediment particles in still water, the influencing factors include density, size, and shape of the particle and water density and viscosity. Terminal velocity estimates for particles falling through a

fluid medium have been attempted for well over one hundred years, with the best known contribution attributed to G.G. Stokes (Stokes law):

$$w_s = \frac{1}{18\,\mu}\left(\rho_p - \rho\right) g\, d^2 \tag{1}$$

where w_s is settling velocity, μ is dynamic viscosity, ρ_p is particle density, ρ is fluid density, g is gravitational acceleration, and d is particle diameter. In arriving at (1) from the physical balance of gravity, buoyancy, and drag forces, Stokes made simplifying assumptions that the particle shape is spherical and the flow regime around the particle is laminar (simplifying the drag relationship). The requirement for laminar flow around the particle introduces the particle Reynolds number,

$$\mathrm{Re}_p = \frac{u\,d}{\nu} \tag{2}$$

where u is particle velocity relative to ambient fluid, d is spherical particle diameter, and ν is kinematic viscosity ($\nu = \mu/\rho$). The laminar flow requirement of (1) is met for $Re_p \ll 1$. Assuming still fluid ($u = w_s$), and mineral grain density of 2650 kg m^{-3}, Stokes Law is valid for spherical sediment particles with diameters smaller than approximately 90 μm. For larger, natural mineral grains such as sand and gravel, turbulent flow and separation resulting from irregular, non-spherical geometry complicate estimates of terminal fall velocity. Many empirical methods derived from settling column experiments have been presented to describe the settling velocity of such particles (Hallermeier, 1981; Dietrich, 1982; Van Rijn, 1984; Soulsby, 1997; and many others).

While discrete, spherical particles in the size range of fine sand, silt, and clay meet the particle Reynolds number criterion for Stokes Law, many complicating factors are introduced by cohesive sediments. First, the mineral structure of discrete clay particles is generally sheet-like (Weaver, 1989; Winterwerp and Van Kesteren, 2004) and poorly represented as spheres. Large aggregates (flocs larger than 250 μm and bed aggregates larger than 100 μm) generally exceed the laminar flow requirement of Stokes Law. Modifications to the spherical drag relationship are presented by Schlichting and Gersten (2000) and Raudkivi (1998) which extend Stokes Law to larger Re_p. The two

most common approximations to spherical drag outside the laminar region are an empirically based relationship attributed by Raudkivi (1998) to Oseen (1927):

$$C_D = \frac{24}{Re_p}\left(1+\frac{3}{16}Re_p\right)$$ (3)

and Schiller and Naumann (1933):

$$C_D = \frac{24}{Re_p}\left(1+0.150Re_p^{0.687}\right)$$ (4)

Eqn (3) is applicable for $Re_p \leq 2$ and Eqn (4) for $Re_p<800$ (Graf, 1971; Raudkivi, 1998). Winterwerp's (1998, 2002) implicit, fractal-based expression for settling velocity of flocs includes the Schiller-Naumann drag coefficient and is given by:

$$w_s = \frac{\theta g}{18\mu}(\rho_0 - \rho_w)d_0^{3-n_f}\frac{D_f^{n_f-1}}{1+0.15Re_p^{0.687}}$$ (5)

where, θ is a particle shape factor (1 for spherical particles), ρ_0 is primary particle density, d_0 is the primary particle diameter, D_f is the floc diameter, and n_f is the fractal dimension. An empirically derived, explicit settling velocity expression that closely follows the Schiller-Naumann drag approximation is given by Soulsby (1997) :

$$w_s = \frac{v}{d}\left[\left[10.36^2 + 1.049D_*^3\right]^{1/2} - 10.36\right]$$ (6)

where $D_* = \left[g\left(\rho_p/\rho -1\right)/v^2\right]^{1/3}d$.

The empirical constants in Eqn (6) were determined from settling experiments with sand. Eqn (6) neglects the effect of shape and permeability on settling velocity, is valid for particle aspect ratios less than 2, and reduces to Stokes Law for small Re_p. At higher Re_p, Soulsby's settling relationship shows close agreement with Stokes Law modified with the Schiller-Naumann drag coefficient (Eqn (4)); and therefore agrees

closely with similar expressions such as Winterwerp (1998, 2002) that use the same drag approximation.

Flocs are generally weak aggregations of organic and inorganic particles with large porosity (ratio of pore-to-solid volume). There is debate in the literature on the role of flow through flocs and the potential effects on settling velocity. Johnson et al. (1996) demonstrated for highly porous aggregates that porosity significantly increases settling velocity and leads to errors in Stokes Law by a factor of 2-10. Fox et al. (2004) found that to reconcile excess density inferred from floc camera settling velocities that Stokes Law settling velocity had to be increased by a factor of 3. Gregory (1997) determined that flocs with fractal dimensions greater than 2 (many marine, inorganic flocs) were not highly permeable. Winterwerp and Van Kesteren (2004) conclude that natural marine flocs may be treated as sufficiently impermeable to neglect the effects of flow through the floc on settling velocity. So many situations exist for which Stokes Law poorly represents the settling of cohesive sediments.

2.4 Relevance to Dredging

Navigation dredging involves mechanical disturbance and removal of consolidated sediments from harbors and navigation channels. A portion of the dredged sediments escape the dredging system and are suspended in the water column. It is hypothesized that many particles suspended during the dredging process are fragmented bed material of varying sizes and having a particle densities much greater than that of flocs. This introduces the concept of a three-phase aggregate model for suspended material in dredge plumes composed of disaggregated sediments, flocs, and bed aggregates. Although Winterwerp and Van Kesteren (2004), Fugate and Friedrichs (2002), and Mikkelsen et al. (2006) acknowledge the influence of bed aggregates eroded by natural processes on suspended sediment settling speed, no known studies quantify the fraction of suspended bed aggregates in dredge plumes.

In dredge plumes, a mix of aggregate states precludes the definition of a single, representative particle settling velocity. Instead, the suspended material is likely to have a spectrum of particle settling velocities ranging from slow-settling dispersed silts and clays to fast-settling large bed aggregates. Few direct measurements of settling velocity

in dredge plumes have been published. Mikkelsen and Pejrup (2000) measured in situ particle size spectra, inferred aggregate densities from LISST-100 and gravimetric analysis of bottle samples, and found that aggregate size increased and particle density decreased with increasing distance/time from the dredging source. This finding suggests that time-dependent flocculation may be important in estimating settling velocities in dredge plumes.

Efforts to represent dredge plumes in upper Chesapeake Bay and Narragansett Bay with numerical Lagrangian models (including a two-component cohesive sediment aggregation and settling model (Teeter, 2001) suggested that modeled settling velocities are much smaller than those in the measured plumes. A proposed hypothesis for poor representation of plume clearance rates by the model is the neglect of suspended bed aggregates. Ad-hoc inclusion of a class of 50-200 μm particles with density equal to bed density improved model agreement with measurements significantly, but no known field data exist to quantify aggregate states in dredge plumes.

3.0 Research Questions

A better understanding of settling processes must be gained before advances can be made in modeling of the far-field fate of suspended sediments during dredging operations. Primary questions addressed by this research include:

- What settling velocities are present in dredge plumes?

- Do bed aggregates significantly influence the settling and deposition of sediments in dredge plumes?

- How are aggregate states partitioned in dredge plumes? Does the partitioning vary with distance/time from the dredging operation? Does aggregate state partitioning vary with dredge type and sediment characteristics?

- If aggregation of sediments into flocs appears to be a significant factor, do present theories and models of flocculation (e.g. aggregation, disaggregation) apply to dredge plumes?

The objective of this research is to address these research questions and in doing so, provide guidance towards numerical modeling of fine sediments suspended during dredging operations.

REFERENCES FOR CHAPTER 1

Chisholm, T.A. 1999. A two-component aggregation model, PhD dissertation, School of Marine Science, College of William and Mary, Gloucester Point, Virginia. 224 pp.

Dietrich, W.E. 1982. Settling velocities of natural particles. *Water Resources Research* 18(6): 1615-1626.

Fox, J.M., Hill, P.S., Milligan, T.G., Ogston, A.S., Boldrin, A., 2004. Floc fraction in the waters of the Po River prodelta. *Continental Shelf Research* 24: 1699–1715.

Fugate, D.C. and Friedrichs, C.T. 2002. Determining concentration and fall velocity of estuarine particle populations using ADV, OBS and LISST. *Continental Shelf Research* 22: 1867-1886.

Fugate, D. and Friedrichs, C.T. 2003. Controls on suspended aggregate size in partially mixed estuaries. *Estuarine and Coastal Shelf Science* 58: 389-404.

Germano, J. D., and Cary, D. 2005. Rates and effects of sedimentation in the context of dredging and dredged material placement. DOER Technical Notes Collection (ERDC TN-DOER-E19), U.S. Army Engineer Research and Development Center, Vicksburg, MS. http://el.erdc.usace.army.mil/dots/doer/doer.html

Graf, W.H. 1971. Hydraulics of Sediment Transport. McGraw-Hill, New York. 513 pp.

Gregory, J. 1997. The density of particle aggregates. *Water Science Technology* 36(4): 1-13.

Hallermeier, R.J. 1981. Terminal settling velocity of commonly occurring sand grains. *Sedimentology* 28: 859-865.

Hill, P. 1992. Reconciling aggregation theory with observed vertical fluxes following phytoplankton blooms. *Journal of Geophysical Research* 97:2295-2307.

Johnson, B. H. 1990. User's Guide for Models of Dredged Material Disposed in Open Water, Technical Report D-90-5, U.S. Army Engineer Waterways Experiment Station, Vicksburg, MS.

Johnson, B.H.; Andersen, E.; Isaji, T.; Teeter, A.M.; Clarke, D.G. 2000. Description of the SSFATE numerical modeling system. ERDC TN-DOER-E10. U.S. Army Engineer Research and Development Center, Vicksburg, MS.

Johnson, C.P., Li, X., and Logan, B.E. 1996. Settling velocities of fractal aggregates. *Environmental Science and Technology* 30: 1911-1918.

Koh, R. C. Y., and Chang, Y. C. 1973. Mathematical Model for Barged Ocean Disposal of Waste, Environmental Protection Technology Series EPA 660/2-73-029, U.S. Environmental Protection Agency, Washington, DC.

Kranenburg, C. 1994. The fractal structure of cohesive sediment aggregates. *Estuarine, Coastal and Shelf Science* 39: 451-460.

Kranenburg, C. 1999. Effects of floc strength on viscosity and deposition of cohesive sediment suspensions. *Continental Shelf Research* 19: 1665-1680.

Krone, R.B. 1963. A study of rheological properties of estuarial sediments. Technical Bulletin No. 7, Committee on Tidal Hydraulics, U.S. Army Engineer Waterways Experiment Station, Vicksburg, Mississippi.

Lick, W., Huang, H., and Jepsen, R. 1993. Flocculation of fine-grained sediments due to differential settling. *Journal of Geophysical Research* 98(C6): 10279-10288.

MacDonald, N.J., Davies, M.H., Zundel, A.Z., Howlett, J.D., Demirbilek, Z., Gailani, J.Z., Lackey, T.C., and Smith, S.J. 2006. PTM: Particle Tracking Model; Report 1: Model Theory, Implementation, and Example Applications. Technical Report ERDC/CHL TR-06-20, U.S. Army Engineer Research and Development Center, Vicksburg, Mississippi.

McLellan, T.N, Havis, R.N., Hayes, D.F., and Raymond, G.L. 1989. Field studies of sediment resuspension characteristics of selected dredges. Technical Report HL-89-9. U.S. Army Engineer Waterways Experiment Station, Vicksburg, Mississippi.

Mehta, A.J. and McAnally, W.H. 2008. Chapter 4: Fine-grained sediment transport. In: Sedimentation Engineering: processes, management, modeling, and practice; M.H. Garcia (Ed.). ASCE manuals and reports on engineering practice; no. 110. ASCE, Reston, Virginia.

Mikkelsen, O. A. and Pejrup, M. 2000. In situ particle size spectra and density of particle aggregates in a dredging plume. *Marine Geology* 170: 443-459.

Mikkelsen, O.A., Hill, P.S., and Milligan, T.G. 2006. Single-grain, microfloc and macrofloc volume variations observed with a LISST-100 and a digital floc camera, *Journal of Sea Research* 55:87-102.

Milligan, T.G. and Hill, P.S. 1998. A laboratory assessment of the relative importance of turbulence, particle composition, and concentration in limiting maximal floc size and settling behavior. *Journal of Sea Research* 39:227-241.

Newcombe, C.P. and Jensen, J.O.T. 1996. Channel suspended sediment and fisheries: a synthesis for quantitative assessment of risk and impact. *North American Journal of Fisheries Management* 16: 693-727.

Oseen, C. 1927. Hydrodynamik, chapter 10, Akademische Verlagsgesellschaft, Leipzig.

Puckette, T.P. 1998. Evaluation of dredged material plumes: physical monitoring techniques, DOER Technical Notes Collection (ERDC-TN-DOER-E5), U.S. Army Engineer Research and Development Center, Vicksburg, Mississippi.

Raudkivi, A.J. 1998. Loose Boundary Hydraulics, fourth ed., Taylor & Francis, London.

Reine, K.J. Clarke, D.G., and Dickerson, C. 2002. Acoustic characterization of suspended sediment plumes resulting from barge overflow, *DOER Technical Notes Collection* (ERDC-TN-DOER-E15), U.S. Army Engineer Research and Development Center, Vicksburg, MS. http://el.erdc.usace.army.mil/elpubs/pdf/doere15.pdf

Schiller, L. and Naumann, A. 1933. Über die grundlegenden Berechnungen bei der Schwerkraftaufbereitung, Z. VDI, vol. 77.

Schlichting, H. and Gersten, K. 2000. Boundary-Layer Theory. Springer, Berlin.

Soulsby, R.L. 1997. *Dynamics of marine sands.* p. 134, Thomas Telford, London.

Stolzenbach, K.D. and Elimelich, M. 1994. The effect of density on collisions between sinking particles: implications for particle aggregation in the deep ocean, *Journal of Deep Sea Research I* 41(3): 469-483.

Teeter, A.M. 2001. Clay-silt sediment modeling using multiple grain classes. part 1: settling and deposition. In: Coastal and Estuarine Fine Sediment Processes, W.H. McAnally and A.J. Mehta (Eds.). Elsevier.

Tubman, M.W. and Corson, W.D. 2000. Acoustic monitoring of dredging-related suspended-sediment plumes, DOER Technical Notes Collection (ERDC-TN-DOER-E7), U.S. Army Engineer Research and Development Center, Vicksburg, Mississippi.

U.S. Army Corps of Engineers (USACE) 1983. Dredging and Dredged Material Disposal. Engineering Manual 1110-2-5025.

Van Leussen, W. 1994. *Estuarine Macroflocs and Their Role in Fine-Grained Sediment Transport*, Ministry of Transport, Pubic Works and Water Management. Den Haag.

Van Rijn, L.C. 1984. Sediment transport: part II: suspended load transport, *Journal of Hydraulic Engineering* 111: 1613-1641.

Weaver, C.E. 1989. *Clays, Muds, and Shales*. Developments in Sedimentology 44, Elsevier.

Wilber, D.H. and Clarke, D.G. 2001. Biological effects of suspended sediments: a review of suspended sediment impacts on fish and shellfish with relation to dredging activities in estuaries. *North American Journal of Fisheries Management* 21: 855-875.

Winterwerp, J.C. 1998. A simple model for turbulence induced flocculation of cohesive sediment. *Journal of Hydraulic Research* 36(3): 309-326.

Winterwerp, J.C. 2002. On the flocculation and settling velocity of estuarine mud. *Continental Shelf Research* 22: 1339-1360.

Winterwerp, J.C. and Van Kesteren, W.G.M. 2004. Introduction to the Physics of Cohesive Sediment in the Marine Environment. Developments in Sedimentology series, volume 56, Elsevier.

Wolanski, E. and Gibbs, R.J. (1995) Flocculation of suspended sediment in the Fly River Estuary, Papua New Guinea. *Journal of Coastal Research* 11(3): 754-762.

CHAPTER 2

A MASS-BALANCE, CONTROL-VOLUME APPROACH FOR ESTIMATING VERTICAL SEDIMENT FLUX AND SETTLING VELOCITY WITHIN DREDGE PLUMES

Authors: S.J. Smith and C.T. Friedrichs

ABSTRACT

A mass-balance, control-volume approach is presented for estimating vertical sediment fluxes and mass-averaged settling velocities in dredge plumes. The method requires detailed measurements of velocity and suspended sediment concentration along the control volume boundaries. An example application is presented in which horizontal fluxes at the control volume boundaries are derived from Acoustic Doppler Current Profiler data. Results of the analysis demonstrate good qualitative agreement with the general understanding of sediments at the site. The control-volume method is suitable for application to other types of dredge plumes and general sediment transport research related to vertical fluxes and settling of suspended sediments.

INTRODUCTION

Navigation dredging is a vital activity for national economic security, enabling access to ports by commercial, deep-draft, ocean-going vessels (USACE, 1983). During dredging operations, sediments are removed from the channel bottom and transported by pipeline or vessel to approved dredged material placement sites. However, a portion of the sediments removed from the bed are suspended into the water column, transported from the dredging and placement sites by ambient currents, and returned to the bed through particle settling and deposition. The transport and fate of sediments suspended by dredging operations is a primary concern due to potential impacts to natural resources (USACE, 1983; Wilber and Clarke, 2001).

Elevated suspended sediment concentration (SSC) and turbidity may impose a range of environmental impacts such as gill abrasion and clogging; increased light attenuation and reduced photic depth (impacts to micro-algae, macro-algae, and submerged aquatic vegetation); burial, smothering, and abrasion of demersal eggs; reduced growth rate of larval and juvenile organisms (leading to increased mortality and reduced recruitment); blockage of fish migration routes; degradation of spawning habitat; and dispersion of sediment-adsorbed contaminants (Newcombe and Jensen, 1996; Wilber and Clarke, 2001). Newcombe and Jensen (1996) propose that impacts to fish are a function of SSC, duration of exposure, species, and life stage. In the United States, natural resource agencies (state departments of environmental quality; state, regional, and federal fisheries agencies; and federal environmental protection) require dredging proponents (such as port authorities and the U.S. Army Corps of Engineers) to

demonstrate that proposed dredging activities meet regulatory requirements established by under Section 404 of the Clean Water Act, Section 103 of the Marine Protection, Research, and Sanctuaries Act, National Environmental Policy Act of 1969, and state water quality standards.

Numerical models are among the primary tools through which dredging proponents demonstrate that proposed dredging activities are likely to meet regulatory requirements. These models represent the processes of sediment suspension, advection, diffusion, settling, and deposition through a collection of both empirical- and physics-based equations to predict transport and fate of sediments suspended by dredging operations (Koh and Chang, 1973; Johnson, 1990; Johnson et al. 2000). Wide variations in dredging equipment and sediment characteristics and limited knowledge of the rates of suspension and characteristics of suspended material lead to large uncertainties in model estimates of sediment transport and fate (Germano and Cary, 2005). Milligan and Hill (1998) suggest that time-variant flocculation effects must be included in sediment transport models for assessing environmental impacts in the coastal zone. Similarly, advancement of the predictive capabilities of dredged material transport, fate, and impacts are not expected until better understanding is gained of the influences of dredge and sediment types on sediment suspension and sediment dynamics.

To present, limited progress has been made in quantifying the rate of sediment suspension from various dredge types and even less progress has been made in describing suspended sediment characteristics and settling processes in dredge plumes. Limitations in present knowledge of suspension and settling in dredge plumes are largely attributable to past limitations in sampling technology. Until the early 1990s, field measurements were limited to physical pump and bottle samples analyzed for total suspended solids (McLellan et al. 1989). Limited spatial and temporal resolution available with physical sampling in dredge plumes characterized by high spatial and temporal gradients made quantifying suspension rates and settling extremely challenging. Advances in the fields of optical, acoustic, and photographic instrumentation permit corresponding advances in the ability to collect information about dredge plume dynamics (Puckette, 1998; Tubman and Corson, 2000; Reine et al., 2002). These recent advances in suspended sediment sampling technologies have opened new possibilities in research directed toward

understanding of suspended sediment characteristics and settling dynamics in dredge plumes. Better understanding of settling dynamics in dredge plumes will lead to improved predictive methods, better informed dredging operation planning, reduced impacts to natural resources, and increased efficiency of dredged material management.

The purpose of this chapter is to describe a method developed for estimating vertical flux and mass-averaged settling velocities within dredge plumes. The method presented is dependent upon high-resolution velocity and suspended sediment measurements within dredge plumes. Recent advances in Acoustic Doppler Current Profiler (ADCP) technology permit both velocities and concentrations to be quantified from a moving platform.

CONTROL VOLUME APPROACH

For a dredge plume, a control volume of size $\Delta x \times \Delta y \times \Delta z$ can be defined (Figure 2-1) such that time variations of the mean suspended sediment concentration within the control volume are given by differences in spatially averaged sediment fluxes across the bounding surfaces as follows:

$$\frac{\Delta C}{\Delta t} \Delta x \Delta y \Delta z = \Delta y \Delta z \left(F_{x1} - F_{x2} \right) + \Delta x \Delta z \left(F_{y1} - F_{y2} \right) + \Delta x \Delta y \left(F_{z1} - F_{z2} \right) \qquad (1)$$

where C = suspended sediment concentration (M L^{-3}), t = time, x,y,z = Cartesian coordinates, F = suspended sediment flux (M L^{-2} T^{-1}) averaged over each boundary.

Assuming that the plume traveling through the control volume has reached steady
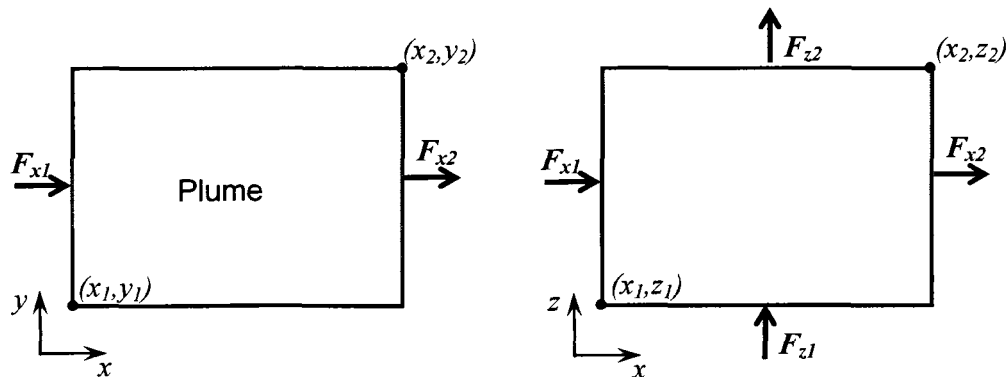
Figure 2-1. Control volume for flux balance of dredge plumes.

state (dC/dt = 0), that the lateral control-volume boundaries are outside the plume ($F_{y1} = F_{y2}$ = 0), and that there is no sediment flux through the top of the control volume at the water surface (F_{z2} = 0), the spatially averaged vertical flux across the bottom surface of the control volume reduces to:

$$F_{z1} = \frac{(F_{x2} - F_{x1})\Delta z}{\Delta x} \qquad (2)$$

To estimate vertical flux to the seabed within the defined control volume, measurements of cross-sectionally averaged horizontal fluxes at $x1$ and $x2$ are required. Neglecting horizontal turbulent diffusion, sediment flux at a point on the boundary is given by $F=uC$, where u = boundary-orthogonal velocity component. ADCPs are capable of providing both velocity and suspended sediment concentration (SSC) necessary to compute sediment flux across control volume boundaries. Acoustic backscatter has been shown to be a reliable, unobtrusive estimator of SSC (Thorne et al., 1991; Land and Bray, 2000), including measurements of dredge plumes (Battisto and Friedrichs, 2003; Reine et al. 2002; Clarke, et al. 2005). Figure 2-2 presents ADCP transects taken orthogonal to the prevailing current through a dredge plume. These
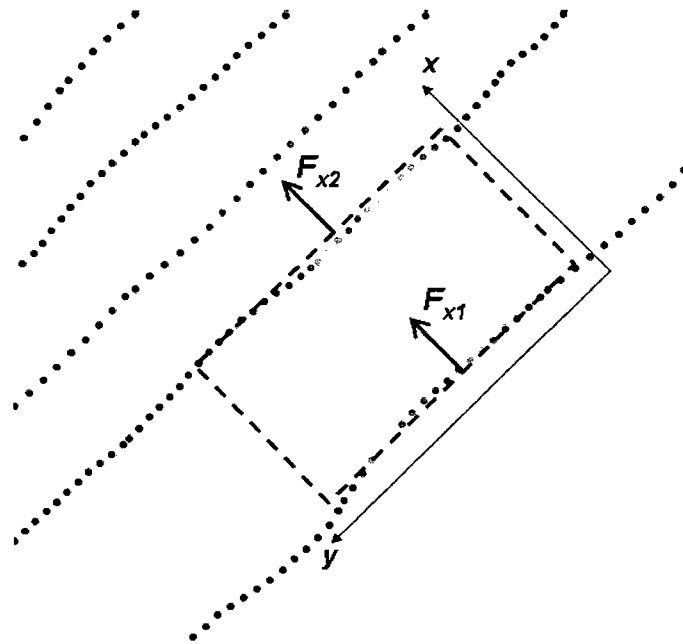
Figure 2-2. Schematic of control volume superimposed with ADCP transects serving as control-volume boundaries in the x direction.

transect lines define control-volume boundaries, with the velocity and SSC data providing basis for horizontal suspended sediment fluxes. Neglecting horizontal turbulent diffusion, the cross-sectionally averaged horizontal fluxes at $x1$ and $x2$ can each be calculated from a subsection of the ADCP transect data that includes the suspended sediment plume as follows:

$$\overline{F}_x = \frac{\sum_{i=1}^{NY}\sum_{k=1}^{NZ} u_{i,k} C_{i,k} \Delta z_k \Delta y_i}{\sum_{i=1}^{NY}\sum_{k=1}^{NZ} \Delta z_k \Delta y_i} \tag{3}$$

where the $i.k$, subscripts associated with $u_{i,k}$, $C_{i,k}$, Δy_i and Δz_k in Eq. 3 refer to ADCP bins, not the control volume.

Assuming mean vertical fluid velocities to be negligible, there are two contributions to the average vertical flux at the base of the control volume, namely gravitational settling and vertical turbulent diffusion:

$$F_{z1} = w_s C_1 - K_{z1} \frac{dC_1}{dz} \tag{4}$$

where the vertical eddy diffusivity, K_z, sediment concentration, and vertical concentration gradient are all evaluated at the height of the base of the control volume, z_1, and are all averaged across the width of the control volume, Δy. By rearranging the terms, an expression for the settling velocity at height z_1 is obtained:

$$w_s = \frac{F_{z1} + K_{z1}\frac{dC_1}{dz}}{C_1} \tag{5}$$

which requires estimation of vertical flux, vertical diffusion, and vertical concentration distribution. Note that in Eq. 5, w_s and F_{z1} are expected to be negative with the adopted positive upward convention. In the typical situation of negative vertical concentration gradient, gradient diffusion (represented by $K_z\, dC/dz$) hinders settling by exchanging lower-concentration sediment-water mixture from above with higher-concentration mixture from below. For constant vertical flux and near-bed concentration, if gradient diffusion increases, still-water settling velocity must also increase.

MEASUREMENTS

The U.S. Army Engineer Research and Development Center, Environmental Laboratory (ERDC-EL) conducted vessel-mounted ADCP surveys near a hydraulic dredging outfall to monitor dredged material plumes in the vicinity of seagrass beds in St. Andrew Bay near Panama City, Florida (Figure 2-3). A hydraulic cutterhead dredge removed sediments classified as predominantly fine sand from Port Panama City and transported the slurry through a pipeline to a spill barge (located at the "S" in "Spill Barge" in Figure 2-3) within the permitted placement area. The end of the pipeline was directed vertically downward, 3 m beneath the water surface in 12-m depth. During the study, numerous surveys were conducted during various stages of the tidal cycle, each consisting of 10 or more transects oriented perpendicular to the tidal current. The data presented in this paper are from a survey conducted during flood tide immediately down current of the placement location as shown by the transect lines in Figure 2-3. Spacing between transects ranged from 30 to 80 m, with median spacing of 40 m, and spacing between individual soundings along each transect averaged 4-5 m.. Each transect took
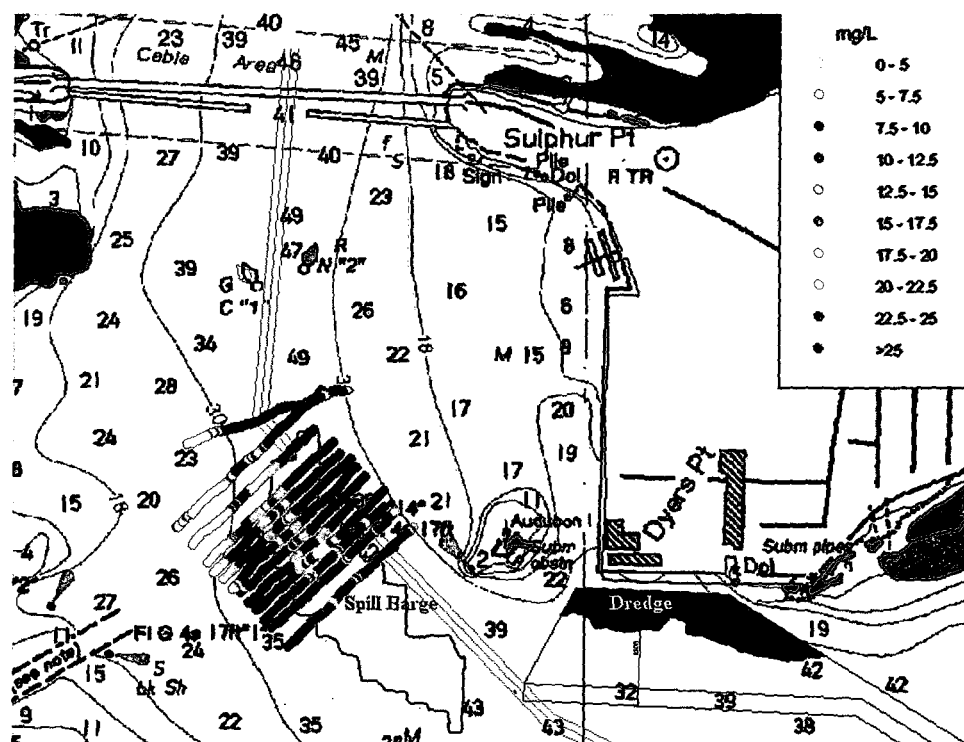
Figure 2-3. Site map of ADCP survey of dredge plume near Panama City, Florida. Colored shading along transect lines indicates depth-averaged concentration.

less than 5 minutes to complete, and the 10 transects used in this analysis were completed in less than 45 minutes, ensuring a relatively small change in the tidal hydrodynamics. Velocity and SSC data were collected with a 600 kHz ADCP. Data collection and calibration methods were performed in accordance with Land and Bray (2000) and Reine et al. (2002).

Examples of concentration and velocity data from Transect 2 (the 2nd transect north-west of the spill barge) are presented in Figure 2-4. The concentration data indicate rational trends of variation associated with the high-concentration plume down current of the discharge point. However, the velocity signal is dominated by random noise. (Mean velocity perpendicular to Transect 2 is 0.08 m s^{-1}, but the standard deviation is 0.34 m s^{-1}.) Because the investigators collecting these data were interested primarily in monitoring suspended sediment concentrations, bin spacing of the ADCP was set at 0.25 m to maximize resolution of the suspended sediment plume at the expense of velocity data quality. For a study dedicated to assessing settling dynamics of a dredge plume, bin spacing must be optimized to provide adequate vertical resolution of SSC
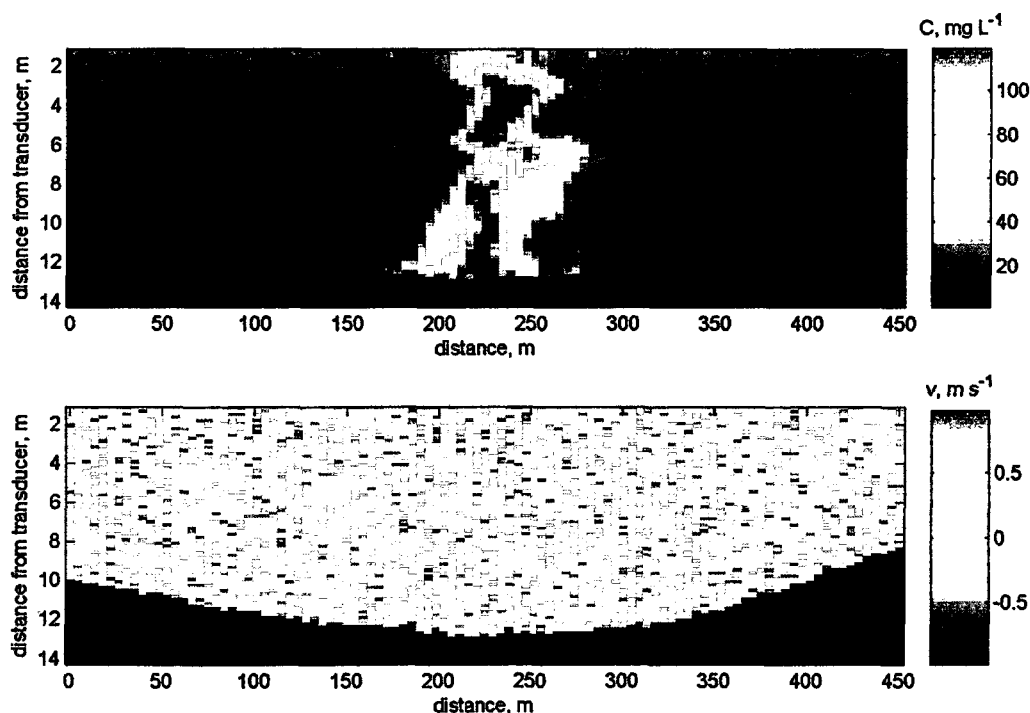
Figure 2-4. Raw concentration and velocity data from Transect 2. Velocity data represent magnitude perpendicular to the transect. (+u = NW. -u = SE).

while maintaining good quality velocity data.

A significant observation from the concentration data is the distinct signature of sediment settling from the plume with distance from the discharge point as shown in Figure 2-5. Sediment concentrations within the plume at Transect 1 are large, but progressively decrease to near-ambient levels at Transect 5. Transect 1 passes within 10 meters of the spill barge, through the high-concentration effluent of the discharge pipe. Common slurry content of hydraulic dredge effluent is approximately 15-20 percent (by volume) or 400-500 g L^{-1}. At these large concentrations, significant
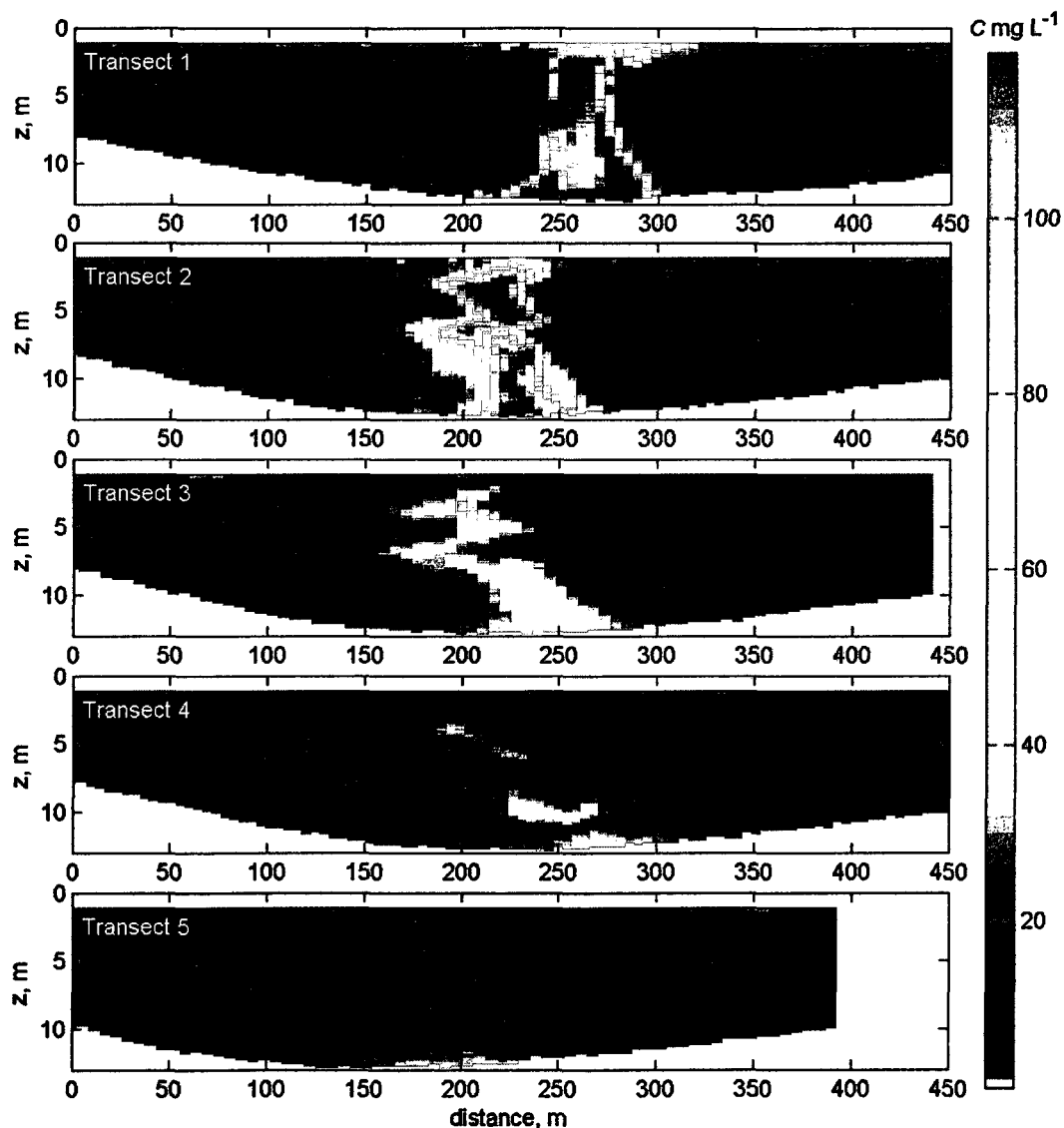
Figure 2-5. Suspended sediment concentrations for Transects 1-5. The orientation of the figures is such that flow is into the page.

acoustic energy is absorbed by suspended sediment (Thorne et al., 1991; Wren et al. 2000), resulting in lower acoustic backscatter and consequently lower inferred SSC. This effect of high sediment concentration on acoustic backscatter is shown as a zone of lower inferred concentration within the plume between 6-10 m below the transducer in Transect 1. As SSC is likely underestimated within this region, Transect 1 is omitted from later analysis.

RESULTS

Horizontal suspended sediment flux is estimated from the data collected along Transects 2 through 6. Transect 1 was omitted as previously explained due to assumed acoustic attenuation in the concentration signal resulting from large SSC. At and beyond Transect 6, the dredge plume is barely distinguished from ambient sediment concentrations. The lateral range of data used to compute horizontal fluxes was determined visually and limited to the portion of data clearly identified as a plume. As discussed previously, quality of velocity data was poor due to the small bin height selected for data collection. Due to the noisy signal, average velocities were determined for each transect and applied to the horizontal flux calculations of Eqn. 3 which are presented in Figure 2-6. Note that the cross-sectional averaged horizontal fluxes decrease from 3 to 1.3 g m^{-2} s^{-1} over a 120 m distance, with the horizontal flux gradient decreasing
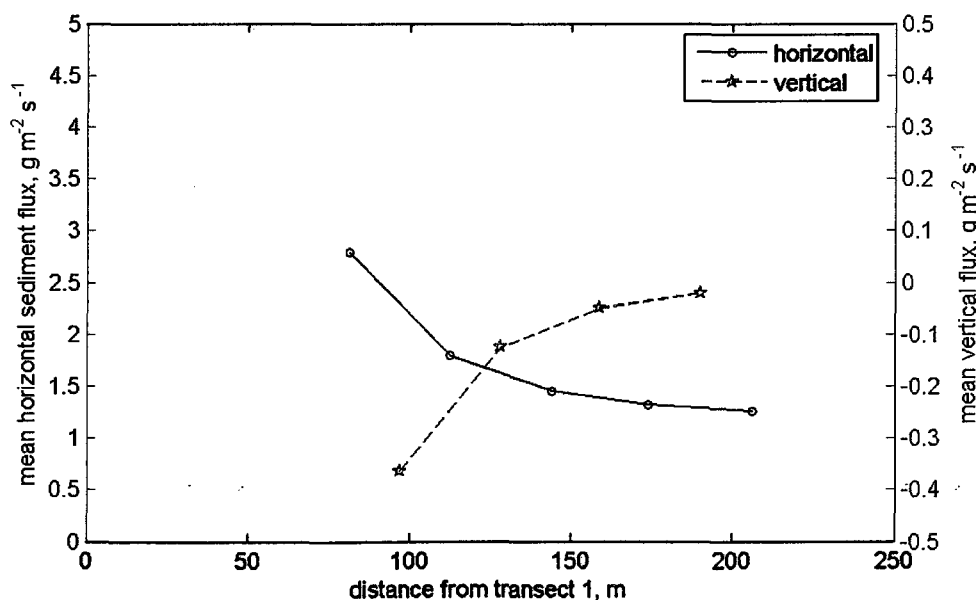
Figure 2-6. Cross-sectionally averaged horizontal and vertical fluxes for Transects 2-6.

with distance from the pipeline outfall.

Vertical flux for each control volume is estimated by Eq. 2 from the computed horizontal fluxes at each transect, distance between transects, Δx, and mean water depth (substituted for Δz), with the width of each control volume limited to the maximum width of the two bounding transects containing the dredge plume. Mean vertical sediment fluxes are plotted in Figure 2-6 at the central position of each of the four control volumes. Mean vertical flux magnitude is greatest between Transects 2 and 3 at -0.4 g m^{-2} s^{-1} and decreases by roughly an order of magnitude to -0.03 g m^{-2} s^{-1} 100 m away between Transects 5 and 6. The marked reduction in horizontal and vertical fluxes within such a short distance from the pipeline outfall suggests that much of the suspended sediment in the dredge plume deposits near the placement site.

With estimates of vertical sediment flux, near-bed sediment concentration, near-bed vertical concentration gradient, and an estimate of vertical diffusivity, Eq. 5 permits an estimate of mass-averaged sediment settling velocity. For this application, mean suspended sediment concentration and vertical concentration gradient were averaged for bins within 3 m of the bed and between the bounding transects. Velocity measurements were not of acceptable quality to directly estimate K_z from the vertical velocity profile, so an alternate, first-order approximation was estimated:

$$K_z = \frac{\kappa^2 \bar{u}}{\ln\left(\dfrac{h}{e\,z_0}\right)} z\left(1 - \frac{z}{h}\right) \tag{6}$$

assuming logarithmic vertical distribution of velocities in the benthic boundary layer, parabolic distribution of vertical eddy diffusivity, sandy bed with hydraulic roughness, z_0 $= 0.004$ m. The variables h and $\bar{u}$ represent water depth and the transect-averaged velocity, respectively. Average value of K_z for the four control volumes is 0.005 m^{2}s^{-1}. The resulting estimates of settling velocity for the four control volumes are presented in Figure 2-7. The first two control volumes, for which horizontal fluxes rapidly decrease, have an estimated settling velocity on the order of 0.02 m s^{-1}, and settling velocity decreases to 0.012 and 0.005 m s^{-1} in the final two control volumes.
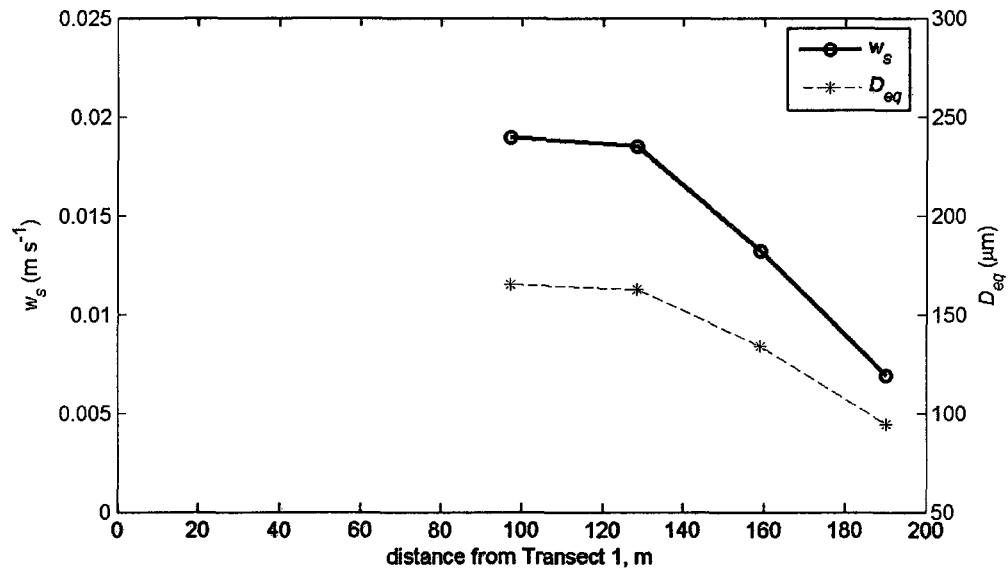
Figure 2-7. Settling velocity w_s and equivalent sand diameter, d estimated from Eq. 6.

As the dredged material in this example is predominantly fine sand and settling velocities estimated in Figure 2-7 fall in the range of expected fall velocities of fine sand, an estimate of the equivalent sand diameters can be made using an empirical estimate of sand settling velocity (Soulsby 1997):

$$w_s = \frac{v}{d}\left[\left(10.36^2 + 1.049D_*^3\right)^{1/2} - 10.36\right]$$ (7)

where v = kinematic viscosity of water, d = sediment diameter,

$D_* = \left[\dfrac{g(s-1)}{v^2}\right]^{1/3} d$, $s = \dfrac{\rho_p}{\rho}$, ρ = water density, and ρ_p = particle density. Given settling velocity and water properties, Eq. 6 is solved for d. Estimated equivalent sand diameters are presented in Figure 2-7. The trends in d follow those of w_s, decreasing with distance from the plume source, ranging from 160 µm for the first control volume down to approximately 100 µm for the last control volume. The equivalent diameters are not verifiable from the data collected for this example, but are consistent with the general classification of sediments from the dredging site. Decreasing settling velocities and inferred equivalent diameters with distance from the plume source suggest that coarser sediments deposit near the pipeline outfall and progressively finer sediments remain in suspension longer to be transported and deposited farther from the source.

Given the relatively weak currents at the site and the relatively large settling velocities of the suspended fine sand, gradient diffusion plays a minor role in opposing settling and deposition of the plume sediments. Comparing the relative strength of the settling flux (w_sC) to the gradient diffusion flux ($K_z\ dC/dz$) indicates that the magnitude of the diffusive flux is between 5 to 15 percent of the settling flux.

DISCUSSION

The control-volume approach is shown to provide reasonable results in estimating vertical fluxes to the seabed in dredging plumes, with ADCP data (velocity and concentration) providing the necessary data to estimate horizontal fluxes across longitudinal control volume surfaces. Additionally, if details of near-bed vertical diffusion and concentrations are available, a mass-averaged settling velocity estimate is possible.

Significant attention must be given to instrument configuration and experimental procedures for reliable estimates from the analysis. ADCP bin spacing must be optimized to produce good resolution of suspended sediment concentration without degrading the quality of Doppler-estimated velocities. For the example application presented in this paper (which was performed to estimate SSC only), the ADCP was configured to provide maximum resolution of SSC which caused significant errors in the velocity record. Even with the problems in the velocity data, the method was shown to provide reasonable estimates of vertical flux and settling velocity. The robustness of the method for the example application is attributed to the strong settling signature of the sandy sediments in suspension. For applications involving sediments with smaller settling velocities (such as clay and silt), the method is likely to be less forgiving regarding quality of the velocity data.

One of the founding assumptions in the method presented is steady-state nature of the plume. While plumes resulting from hydraulic pipeline placement (such as shown in the example) are characteristically steady state, other dredging operations are not. For instance, mechanical dredging with a clamshell, backhoe, or bucket dredge is characterized by discrete pulses of suspended sediment. For this case, transects should be conducted repeatedly at fixed distances from the dredging operation to obtain mean

fluxes across the control volume boundaries. Data collection becomes even more complicated for hopper dredges, in which transect lines must be run relative to a moving source. In this case, two ADCP systems transecting the dredge plume at fixed relative distances must operate in tandem.

While the control volume approach presented here has been developed with dredging applications in mind, the method is suitable for other suspended sediment research topics in a wide range of environments. Research of vertical sediment flux and deposition at river mouths, estuaries, and the inner shelf could apply the control-volume approach with sediment flux defined by ADCP transects. As with dredging applications, careful attention to spatial and temporal scales of variation in fluxes, assumptions of the analysis method, and limits in instrumentation and data collection would need to be considered.

CONCLUSION

A mass-balance control volume approach to horizontal sediment fluxes in dredge plumes is shown to provide reasonable estimates of vertical flux and mass-averaged settling velocity. The method relies on ADCP or similar instrumentation to provide suspended sediment flux at the control volume boundaries. Estimating vertical flux within the control volume requires estimates of velocity and SSC along the control volume boundaries. Further analysis of near-bed concentrations, vertical concentration gradients, and near-bed vertical diffusion allows estimation of mass-averaged settling velocity. The method presented is applicable to non-steady dredging plumes or other sources of suspended sediment with appropriate modification to data collection methods.

REFERENCES FOR CHAPTER 2

Battisto, G.M and Friedrichs, C.T. 2003. Monitoring suspended sediment plume formed during dredging using ADCP, OBS, and bottle samples. *Proceedings Coastal Sediments 2003*, CD-ROM Published by East Meets West Productions, Corpus Christi, TX ISBN-981-238-422-7, 14p.

Clarke, D.; Martin, A.; Dickerson, C.; Moore, D. 2005. Suspended sediment plumes associated with mechanical dredging at the Port of Oakland, California. Proceedings of the Western Dredging Association Twenty-fifth Technical Conference & Thirty-Seventh Texas A&M Dredging Seminar, Western Dredging Association, 187-202.

Germano, J. D., and Cary, D. 2005. Rates and effects of sedimentation in the context of dredging and dredged material placement. DOER Technical Notes Collection (ERDC TN-DOER-E19), U.S. Army Engineer Research and Development Center, Vicksburg, Mississippi. http://el.erdc.usace.army.mil/dots/doer/doer.html

Johnson, B. H. 1990. User's Guide for Models of Dredged Material Disposed in Open Water. Technical Report D-90-5, U.S. Army Engineer Waterways Experiment Station, Vicksburg, Mississippi.

Johnson, B.H.; Andersen, E.; Isaji, T.; Teeter, A.M.; Clarke, D.G. 2000. Description of the SSFATE numerical modeling system. Technical Note ERDC TN-DOER-E10. U.S. Army Engineer Research and Development Center, Vicksburg, Mississippi.

Koh, R. C. Y., and Chang, Y. C. 1973. Mathematical Model for Barged Ocean Disposal of Waste. Environmental Protection Technology Series EPA 660/2-73-029, U.S. Environmental Protection Agency, Washington, DC.

Land, J.M. and Bray, R.N. 2000. Acoustic measurement of suspended solids for monitoring of dredging and dredged material disposal. *Journal of Dredging Engineering* 2(3), 1-17.

McLellan, T.N, Havis, R.N., Hayes, D.F., and Raymond, G.L. 1989. Field studies of sediment resuspension characteristics of selected dredges. Technical Report HL-89-9. U.S. Army Engineer Waterways Experiment Station, Vicksburg, Mississippi.

Milligan, T.G. and Hill, P.S. 1998. A laboratory assessment of the relative importance of turbulence, particle composition, and concentration in limiting maximal floc size and settling behavior. *Journal of Sea Research* 39:227-241.

Newcombe, C.P. and Jensen, J.O.T. 1996. Channel suspended sediment and fisheries: a synthesis for quantitative assessment of risk and impact. *North American Journal of Fisheries Management* 16: 693-727.

Puckette, T.P. 1998. Evaluation of dredged material plumes: physical monitoring techniques. DOER Technical Notes Collection (ERDC-TN-DOER-E5), U.S. Army Engineer Research and Development Center, Vicksburg, Mississippi.

Reine, K.J. Clarke, D.G., and Dickerson, C. 2002. Acoustic characterization of suspended sediment plumes resulting from barge overflow," *DOER Technical Notes Collection* (ERDC-TN-DOER-E15), U.S. Army Engineer Research and Development Center, Vicksburg, Mississippi. http://el.erdc.usace.army.mil/elpubs/pdf/doere15.pdf

Soulsby, R.L. 1997. Dynamics of Marine Sands. Thomas Telford, London. p. 134

Thorne, P.D., Vincent, C.E., Hardcastle, P.J., Rehman, S., and Pearson, N. 1991. Measuring suspended sediment concentrations using acoustic backscatter devices. *Marine Geology* 98: 7-16.

Tubman, M.W. and Corson, W.D. 2000. Acoustic monitoring of dredging-related suspended-sediment plumes. DOER Technical Notes Collection (ERDC-TN-DOER-E7). U.S. Army Engineer Research and Development Center, Vicksburg, Mississippi.

U.S. Army Corps of Engineers (USACE) (1983). Dredging and Dredged Material Disposal. Engineering Manual 1110-2-5025.

Wilber, D.H. and Clarke, D.G. 2001. Biological effects of suspended sediments: a review of suspended sediment impacts on fish and shellfish with relation to dredging activities in estuaries. *North American Journal of Fisheries Management* 21: 855-875.

Wren, D.G., Barkdoll, B.D., Kuhnle, R.A., and Derrow, R.W. 2000. Field techniques for suspended-sediment measurement. *Journal of Hydraulic Engineering* 126(2), 97-104.

CHAPTER 3

SIZE AND SETTLING VELOCITIES OF COHESIVE FLOCS AND SUSPENDED SEDIMENT AGGREGATES IN A TRAILING SUCTION HOPPER DREDGE PLUME

ABSTRACT

A field experiment was conducted to quantify settling velocities, aggregate states, and flocculation within a hopper dredge plume. Particular interest was in determining the abundance of dense, bed aggregates suspended from the consolidated bed during dredging. A suspended sediment plume from the hopper dredge *Essayons* was sampled for a period of 90 minutes after dredging. Settling velocities and suspended particle sizes were quantified through sampling with the Particle Imaging Camera System (PICS) and automated image processing routines. The sediment plume was identified and a profiling instrumentation frame was positioned within the plume using Acoustic Doppler Current Profiler (ADCP) backscatter. Results indicated that suspended bed aggregates (defined by densities of 1200 to 1800 kg m^{-3}) represented 0.2-0.5 of total suspended mass, and flocs (densities < 1200 kg m^{-3}) represented 0.5 to 0.8 of total suspended mass. The peak diameter of bed aggregates and flocs occurred near 90 μm and 200 μm, respectively, corresponding to peak settling velocities of about 1 mm s^{-1} in each case. Floc settling velocities increased with particle size $d^{1.1}$, while bed aggregate settling velocity increased like $d^{1.3}$.

1 INTRODUCTION

Dredging of sediments from navigation channels and ports is a vital activity for economic security, enabling access to ports by deep-draft, ocean-going vessels (USACE, 1983). During dredging operations, sediments are removed from the bed and transported by pipeline or vessel to dredged material placement sites. However, a portion of the sediments removed from the bed is suspended into the water column, transported from the dredging and placement sites by ambient currents, and returned to the bed through particle settling and deposition. The transport and fate of sediments suspended by dredging operations are of primary concern due to potential impacts to natural resources (USACE, 1983; Newcombe and Jensen, 1996; Wilber and Clarke, 2001).

1.1 Environmental Impacts of Dredge Plumes

Elevated suspended sediment concentration (SSC) and turbidity may impose a range of environmental impacts such as gill abrasion and clogging; light attenuation and reduced photic depth (impacts to micro-algae, macro-algae, and submerged aquatic vegetation); burial, smothering, and abrasion of demersal eggs; reduced growth rate of larval and juvenile organisms (leading to increased mortality and reduced recruitment); blockage of fish migration routes; degradation of spawning habitat; and dispersion of sediment-adsorbed contaminants (Newcombe and Jensen, 1996; Wilber and Clarke, 2001). In the United States, natural resource agencies (state departments of

environmental quality; state, regional, and federal fisheries agencies; and federal Environmental Protection Agency) require dredging proponents (such as port authorities and the U.S. Army Corps of Engineers) to demonstrate that proposed dredging activities meet regulatory requirements established under Section 404 of the Clean Water Act, Section 103 of the Marine Protection, Research, and Sanctuaries Act, the National Environmental Policy Act of 1969, and state water quality standards.

Numerical models are commonly applied by dredging proponents to demonstrate that proposed dredging activities are likely to meet regulatory requirements. These models represent processes of sediment suspension, advection, diffusion, settling, and deposition through both empirical- and physics-based equations to predict transport and fate of sediments suspended by dredging operations (Koh and Chang, 1973; Johnson, 1990; Johnson et al. 2000; Spearman et al., 2007). Wide variations in dredging equipment, sediment characteristics, and limited knowledge of the rates of suspension and characteristics of suspended material lead to large uncertainties in model estimates of sediment transport and fate (Germano and Cary, 2005). Milligan and Hill (1998), Mikkelsen and Pejrup (2000), and Winterwerp (2002) suggest that time-variant flocculation effects must be included in sediment transport models for assessing environmental impacts in the coastal zone. Research is required to better understand the influences of dredge equipment and sediment processes on sediment suspension and sediment dynamics by dredging operations.

To date, limited progress has been made in describing suspended sediment characteristics and settling processes in dredge plumes, primarily due to available sampling technology and the challenging sampling environment. Until the early 1990s, field measurements were collected by physical pump and bottle samples and analyzed for total suspended solids (for example, McLellan et al. 1989). Fine spatial and temporal resolution is difficult to obtain with physical sampling methods. Given the relatively small spatial scales and large spatial and temporal heterogeneities of dredge plumes, quantifying dredge suspension rates and settling velocities with physical sampling is extremely challenging. Advances in the fields of optical, acoustic, and photographic instrumentation permit corresponding advances in the ability to collect information about dredge plume dynamics (Tubman et al. 1994; Land and Bray, 1998; Mikkelsen and

Pejrup, 2000). Through application of these recent advances in suspended sediment sampling, this research aims to increase understanding of suspended sediment characteristics and settling dynamics in dredge plumes. Better understanding of settling dynamics in dredge plumes will lead to improved predictive methods, better informed dredging operation planning, reduced impacts to natural resources, and increased efficiency of dredged material management.

1.2 Dredging and Aggregate States

Dredges remove sediment from the bed through mechanical and/or hydraulic stresses (Bray et al., 1997; Van Raalte, 2006). The stresses produced during dredging operations greatly exceed the typical, natural stresses exerted by hydrodynamics. Consequently, dredges are capable of removing sediments previously buried 10s to 100s cm below the sediment-water interface. Due to self-weight consolidation, these dredged sediments can be much denser than surficial sediments typically eroded by natural processes. During the dredging process, a portion of the consolidated sediments will fragment and be released to the water column. These dense bed fragments will be referred to as "bed aggregates" to distinguish them from less dense aggregates (flocs) formed in the water column through flocculation processes.

Other particulates released during dredging include primary particles (small, tightly packed flocculi of clay mineral plates or individual silt or sand particles) and flocs. Flocs released by the dredging process may originate from the low-density surficial sediment layer or may be formed during the dredging process (high-concentration and low-moderate turbulence within hopper dredges are favorable to floc formation). Flocs are also formed in the water column as the plume is transported from the dredging site. All these particulate states are important to the transport and fate of fine sediments in dredge plumes.

1.3 Flocculation

Dredging activities frequently produce SSC levels above that supported by ambient hydrodynamics. High SSC coupled with moderate turbulence leads to increased frequency of interparticle collisions and floc formation and growth (Krone, 1963; Van Leussen, 1994; Winterwerp and Van Kesteren, 2004). Flocculation rates are influenced

not only by concentration and shear, but it is increasingly recognized in the literature that biological secretions and coatings may play a significant role in influencing floc characteristics and settling velocities (Eisma, 1986; Ayukai and Wolanski, 1997; Van der Lee, 2000; Fugate and Friedrichs, 2003). Therefore, a dredge plume produced in a microbiologically active environment is likely to experience faster rates of flocculation than in less biologically active environments.

1.4 Settling Velocity

Particle settling is governed by the balance of gravity, buoyancy, and drag forces. These forces are determined by fluid properties (density, viscosity) and particle properties (density, size, shape, permeability). A common description of particle settling velocity is provided by Stokes Law, which assumes small particle Reynolds number ($Re_p = w_s d/v$ $\ll$1) and impermeable, spherical particles.

$$w_s = \frac{\left(\rho_p - \rho_w\right)gd^2}{18\mu} \tag{1}$$

where, w_s is settling velocity, d is particle diameter, g is gravitational acceleration, ρ_p is particle density, ρ_w is water density, v is kinematic viscosity, and μ is dynamic viscosity. Many investigators (Ten Brinke, 1994, Soulsby, 1997, and Winterwerp, 2002) recognize that large, fast-settling particles violate the laminar boundary assumption in Stokes' Law and have applied corrections (Schlichting and Gersten, 2000; Raudkivi, 1998) to extend Stokes Law to larger Re_p. The two most common approximations to spherical drag outside the laminar region are an empirically based relationship attributed to Schiller and Naumann (1933) by Raudkivi (1998):

$$C_D = \frac{24}{Re_p}\left(1 + 0.150 Re_p^{0.687}\right) \tag{2}$$

and Oseen (1927):

$$C_D = \frac{24}{Re_p}\left(1 + \frac{3}{16}Re_p\right) \tag{3}$$

Eqn (2) is applicable for Re_p<800 and Eqn (3) for $Re_p \leq 2$ (Graf, 1971; Raudkivi, 1998).

Winterwerp's (1998, 2002) implicit, fractal-based expression for settling velocity of flocs includes the Schiller-Naumann drag coefficient and is given by:

$$w_s = \frac{\theta g}{18\mu}\left(\rho_0 - \rho_w\right)d_0^{3-n_f}\frac{D_f^{n_f-1}}{1+0.15Re_p^{0.687}} \qquad (4)$$

where, θ is a particle shape factor (1 for spherical particles), ρ_0 is primary particle density, d_0 is the primary particle diameter, D_f is the floc diameter, n_f is the fractal dimension, and Re_p is the floc Reynolds number. An empirically derived, explicit settling velocity expression that closely follows the Schiller-Naumann drag approximation is given by Soulsby (1997) :

$$w_s = \frac{\nu}{d}\left[\left[10.36^2 + 1.049D_*^3\right]^{1/2} - 10.36\right] \qquad (5)$$

where $D_* = \left[g\left(\rho_p/\rho_w - 1\right)/\nu^2\right]^{1/3}d$

The empirical constants in Eqn (5) were determined from settling experiments with sand. Eqn (5) neglects the effect of shape and permeability on settling velocity, is valid for particle aspect ratios less than 2, and reduces to Stokes Law, Eqn (1), for small Re_p. At higher Re_p, Soulsby's settling relationship shows close agreement with Stokes Law modified with the Schiller-Naumann drag coefficient (Eqn (2)); and therefore agrees closely with similar expressions such as Winterwerp (1998, 2002) that use the same drag approximation.

There is considerable debate in the literature on the role of floc permeability on settling velocity. Johnson et al. (1996) demonstrated for highly porous aggregates that permeability significantly increases settling velocity. Gregory (1997) determined that flocs with fractal dimensions greater than 2 (characteristic of many marine, inorganic flocs) were not highly permeable. Winterwerp and Van Kesteren (2004) conclude that natural marine flocs may be treated as sufficiently impermeable to neglect the effects of flow through the floc on settling velocity.

Increases in either particle size (flocculation) or density (bed aggregates) act to increase settling velocity. These behaviors are of relevance to dredge plumes because increased settling velocity decreases both the time that a particle remains in suspension and the advected distance.

1.5 Research Objectives

To date, little research has been performed to investigate the roles of bed aggregates and flocculation on dredge plumes. The ultimate objectives of this research are to define settling processes of cohesive sediments in dredge plumes including investigation of the role of dredging equipment and bed sediment characteristics on suspended aggregate states, size spectra, vertical distributions, and settling velocity. Specific goals of this chapter are to define the relative abundance and settling characteristics of bed aggregates and flocs in a trailing suction hopper dredge plume.

This chapter describes development of a particle imaging and analysis system that is integral to the research objectives, field experiment methods and instrumentation deployed, and results from the first of three planned field experiments to quantify settling processes in dredge plumes.

2 METHODS

2.1 Instrumentation

Variability over small temporal and spatial scales of dredge plumes present challenges in sampling sediments within dredge plumes. To address these challenges, a vessel-based profiling platform was developed for collecting physical samples, measuring suspended particle size, settling velocity, currents, and turbulence. This vessel-based system permits researchers to quickly locate dredge plumes below the water surface, position profiling instrumentation within plumes, and collect pertinent data at varying water depths. Details of the instrumentation and sampling systems are provided below.

2.1.1 Acoustic Doppler Current Profiler (ADCP)

A 1200 kHz ADCP was mounted to the hull of the survey vessel. The ADCP provides real-time vertical profiles of acoustic backscatter and currents to assist with location of the dredge plume and positioning of the profiling instruments within the dredge plume. Additionally, ADCP backscatter and velocities are logged for calibration

to suspended sediment concentration and later data analysis and interpretation. The ADCP was configured with 0.25-m profiling bins and 2-sec sampling interval.

2.1.2 Profiling Frame

A profiling frame (Figure 3-1A) serves as a platform for mounting instrumentation designed for local measurements of particle size, settling velocity, and water properties within the dredge plume. The $1.1 \times 0.56 \times 0.86$ m (L×W×H) frame can be positioned to depths ranging from 0 to 15 m. All instruments attached to the profiling frame were cabled for power and communications to the surface, permitting real-time data visualization and instrument control.
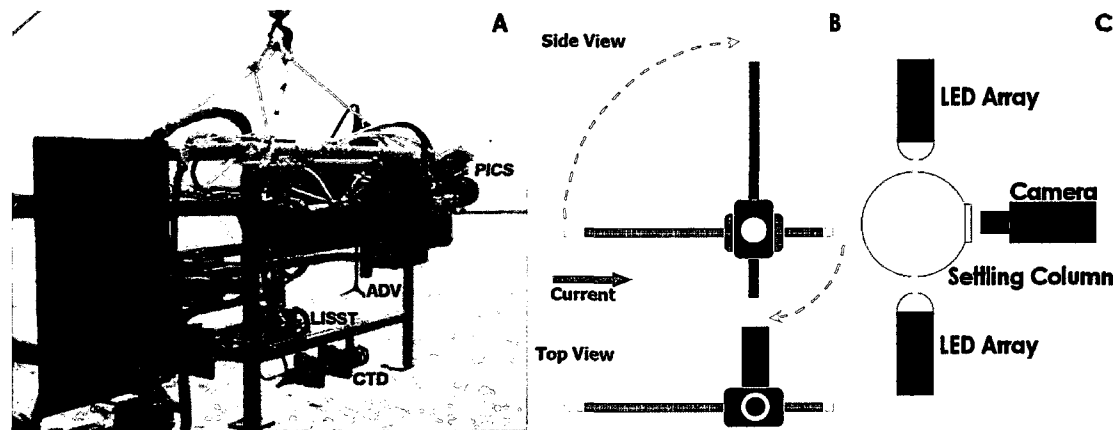
Figure 3-1. A) Instrumentation frame indicating positioning of PICS, ADV, LISST, and CTD, B) Schematic of settling column indicating sample collection and image analysis positions, C) Schematic of camera, settling column cross section, and LED lighting.

2.1.3 Particle Imaging Camera System (PICS)

To measure in-situ particle size and settling velocity, the Particle Imaging Camera System (PICS) was developed. PICS is conceptually similar to other video devices for in-situ particle settling measurements such as INSSEV (Fennessy et al. 1994), VIS (Van Leussen and Cornelisse 1993), Sternberg et al. (1996), Mikkelsen et al. (2004), and Sanford et al. (2005). The PICS sample collection, optical and lighting design, and image acquisition were designed to produce high-quality, in-situ image sequences within dredge plumes. PICS (Figure 3-1B) consists of a 1-m long, 5-cm inner diameter settling column with a mega-pixel digital video camera and strobed LED lighting. The settling column is

equipped with two pneumatically controlled ball valves at the column ends which permit sample capture and a third pneumatic actuator for rotating the column from horizontal to vertical orientation for image acquisition.

A monochrome Prosilica CV1280F digital video camera collects non-interlaced video with 1280×1024 pixel resolution at up to 20 fps with 10 bit resolution. Camera controls and image transfer are transmitted over fiber-optic Firewire cable over distances up to 500 m. The camera focuses on a 12.8×10.2 mm region in the center of the settling column (Figure 3-1B) with a 1-mm depth of focus through a 25-mm Pentax c-mount lens with extension tubes used for macro-magnification. Illumination of the field is produced by two opposing LED light arrays collimated through cylindrical lenses that produce a light sheet orthogonal to the camera lens. The LED light arrays are strobed for 30 μs with a strobe controller synchronized with camera exposure. Images are logged in raw, digital format through Matlab-based image acquisition and control software.

Data collection with PICS proceeds by positioning the profiling frame to the desired depth, capturing a sample of suspended particles by closing the ball valves at the ends of the settling column, rotating the column to vertical position, permitting turbulence within the column to dissipate (~30 to 60 sec), and collecting typically 30 sec of video. For weak currents (less than 0.15 m s^{-1}), samples are captured by raising the profiling frame with the column in its vertical position and closing the ball valves upon reaching the target depth. Upon completion of data logging, the system is positioned at the next sampling depth and the process described above is repeated. Sampling intervals with PICS range between 2-3 minutes, permitting rapid profiling of the dredge plume.

For particle tracking purposes, particles must appear in images as 3×3 or greater regions of pixels. Consequently, the PICS configuration described above is capable of imaging particles between 30 and approximately 1000 μm in diameter. (The upper size limit results from the depth of focus.) The strobe duration and length of settling column above the imaging plane permit resolution of settling velocities between 0-15 mm s^{-1}. In application within dredge plumes, PICS is limited primarily by surface waves and light scattering/attenuation. In choppy seas, oscillations are introduced into the column, which cause particles to stream in/out of the field of view on time scales that complicate or

prohibit image analysis. In the case of high particle concentrations, light scattering and attenuation result in images that are of poor quality or obscured to a degree that prohibits image analysis. The threshold at which scattering and attenuation produce problems in image analysis varies with particle size and degree of flocculation, ranging from 50-400 mg L^{-1}, depending upon the degree of flocculation in the sample.

2.1.4 Laser In-Situ Scattering and Transmissometry (LISST)

A Sequoia LISST-100c (Agrawal and Pottsmith, 2000), deployed on the profiling frame at same elevation as PICS, provided a duplicate measure of particle size. The LISST-100c uses laser diffraction principles to obtain particle size distribution (PSD) in the water column through detection of laser light scattering on 32 logarithmically spaced detectors, representing particle sizes from 2.5 to 500 μm. The LISST has a larger sampling volume which permits it to statistically sample less numerous large flocs better than PICS. On the other hand, PICS is able to detect larger flocs (on order of 1000 μm) compared to the 500 μm upper detection limit of the LISST-100c.

2.1.5 Water Density and Viscosity

Water properties (density, viscosity, and depth) were inferred from measurement of conductivity, temperature, and pressure (CTD). These measurements were logged from instrumentation mounted to the profiling frame.

2.1.6 Physical Sampling

Physical samples were withdrawn by a submersible pump for 60 seconds and sub-sampled with a churn splitter. Replicate samples were collected for approximately 10% of all samples and demonstrated consistency through later analysis. Physical samples were further analyzed in the laboratory for concentration and disaggregated PSD.

2.2 Image Analysis

Automated image processing routines were developed to enhance digital imagery, identify and track particles between successive image frames, and determine particle characteristics such as size and settling velocity. Raw grayscale images collected with PICS are first adjusted for background illumination. This procedure determines the minimum illumination level for each pixel across all frames and subtracts this value from

all frames to remove effects of non-uniform illumination and variable background intensity of the Charge-Coupled Device (CCD) elements. Grayscale images are then converted to binary with a thresholding procedure, followed by dilation and erosion. The binary images are then evaluated with a Particle Tracking Velocimetry (PTV) method, in which cross-correlation and Kalman filtering methods are applied to match particles between adjacent frames in the image sequence. Additionally, false pairing of particles was reduced by limiting changes in particle size and shape between frames. Performance of the automated particle tracking routine was verified through comparisons of the automated results to manual tracking results, and visual inspection of the automated particle track sequences.

Image analysis of the binary images permits the determination of particle characteristics such as projected area, centroid position, short and long axis lengths, and particle orientation. Prior to and following each experiment, a calibration grid is photographed with PICS for the purpose of transforming pixel space to length space in the imaged plane and verifying that optical settings remain constant during the experiment. Additional derived properties of interest such as settling velocity, particle diameter, and effective particle density are computed from observed characteristics.

A primary objective of the image analysis described above is to estimate still-water settling velocity. Although measures are taken to ensure that the fluid within the settling column is still, fluid motion within the column is influenced by vessel motions, lingering turbulence, and volume flux of settling particles. To correct measured particle displacements relative to fluid motions, small particles ranging in size from (5-20 μm) are tracked manually to determine mean vertical fluid velocity. These particles are assumed to have sufficiently small settling velocities to serve as proxy for fluid velocity, similar to the procedure described by Van Leussen (1994). The image frame is sectioned into three sectors and 12 particles (four from each sector, distributed uniformly in time) are tracked for 1-2 seconds each. Net vertical fluid velocity is determined from the mean velocity of the small particles. Image sequences with non-uniform flow fields (in space or time) are excluded from analysis. An automated method of estimating fluid velocity utilizing small particles is under development which will permit spatially and temporally variant fluid velocities estimates. The settling velocity of each particle is then determined as:

$$w_s = \frac{\Delta z}{\Delta t} - w_f \qquad (6)$$

where, Δz is vertical displacement of the particle centroid, Δt is the elapsed time over which the particle was tracked, and w_f is the estimated mean fluid velocity.

Several measures of particle dimensions are available from image analysis: min/max dimension, projected area, and diameter. Equivalent spherical diameter (*esd*) is computed as the spherical diameter producing the same projected area as the observed particle, $esd = (4A/\pi)^{1/2}$, where A is projected area of the particle. Particle density is estimated by rearranging Eqn (5):

$$\rho_p = \rho_w + \frac{\rho_w v^2}{gK_2 d^3}\left[\left(\frac{w_s d}{v} + K_1\right)^2 - K_1^2\right] \qquad (7)$$

where $K_1 = 10.36$ and $K_2 = 1.049$.

Particle classes were discriminated based on estimated density. Flocs are associated with density between 1010-1200 kg m^{-3} (excess density: 0-180 kg m^{-3}), bed aggregates: 1200-1800 kg m^{-3} (excess density: 180-780 kg m^{-3}), primary particles: 1800-3000 kg m^{-3} (excess density: 780-2000 kg m^{-3}). Density range for flocs was determined from published data (Krone, 1963; Krank et al. 1993; Van Leussen, 1994). The density range for bed aggregates extends from the upper limit of flocs to 1800 kg m^{-3} (an upper limit based on saturated bulk density of densely consolidated cohesive and mixed sediment beds and supported by published data: Torfs et al., 2001; Winterwerp and Van Kesteren, 2004). Density range for primary particles was set from the upper limit of bed aggregates to the maximum expected mineral density. The primary particle class defined here is not synonymous with primary particles defined in Eqn (4).

2.2.1 PICS Measurement Uncertainties

Measurements with video-based methods for estimating particle size, settling velocity, and particle density are subject to measurement uncertainty. Uncertainties are associated with both measurement uncertainty and systematic errors. Total measurement uncertainty is associated with both random and systematic errors. Only random error

components will be considered here; systematic errors will be addressed experimentally and presented in future work.

PICS-estimated particle size spectra were evaluated through comparison with the co-located LISST-100c particle sizer. Fifteen particle size spectra were evaluated from the field experiment presented in section 3. The SSC range for these spectra was 5 to 250 $mg \cdot L^{-1}$. PICS-estimated particle size (*esd*) was taken from the tracked particle dataset, converted to particle volume, and size spectra computed in 25 logarithmically spaced bins ranging from 20-1000 μm. The LISST-100c provides volume spectra in 32 logarithmically spaced bins between 2.5 – 500 μm.

An example of the PICS and LISST volume spectra is given in Figure 3-2A. In this example, the PICS and LISST size spectra compare favorably over the range 20-300 μm. For nearly all samples, the PICS size spectrum is less than that of the LISST in the range 20-50 μm. This observation is attributed to the imposed image processing requirement that particles be tracked for at least 1 second to be included in the dataset and the difficulty in automatically tracking small particles for long times due to low illumination and obscurance by larger particles. There is marked disagreement between the LISST and PICS in the 400-500 μm size classes, likely due to scattering from the larger particles in suspension on the inner detector rings of
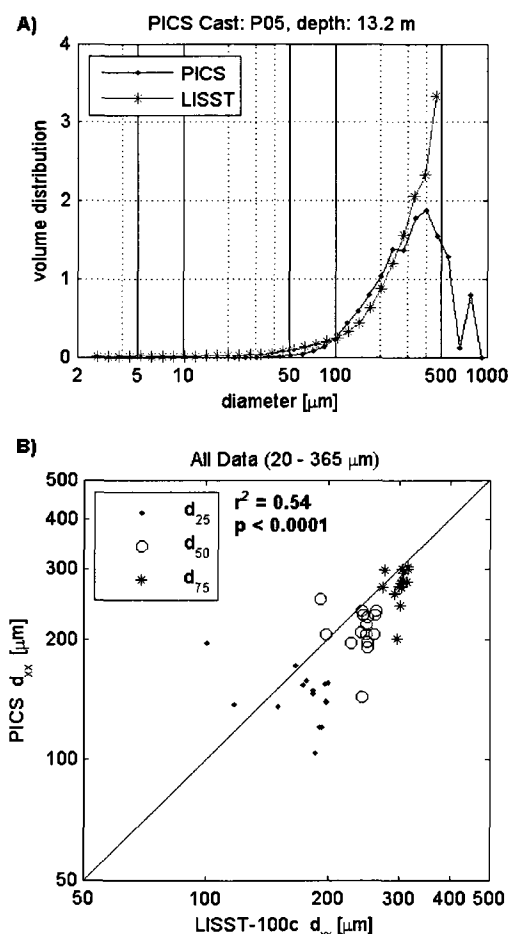
Figure 3-2. Comparison of PICS and LISST size distributions. (A) LISST volume spectrum and PICS volume spectrum from a single sample. (B) Comparison of quartile size fractions from overlapping size bins (20 – 365 μm) of PICS and LISST-100c volume spectra.

the LISST (Agrawal and Pottsmith, 2000; Mikkelsen et al. 2005).

All volume spectra were compared by computing the quartile diameters, d_{25}, d_{50}, and d_{75} for the LISST and PICS within the overlapping size bins between 20-350 μm (Figure 3-2B). The PICS diameters are on average smaller than those of the LISST by approximately 25-30 μm, but the agreement between the two devices is favorable. PICS settling experiments are not the most appropriate method to quantify particle size spectra. Size spectra will be more heavily weighted for faster settling particles due to the larger flux of these particles through the sampling volume. Also, as stated previously, smaller particles are more difficult to track in the images and may therefore be correspondingly sparse in the size spectra. An alternate sampling method for PICS for measuring suspended size spectra has been developed and will be presented in future work.

Estimated settling velocity (Eqn (6)) depends upon measured particle translation, elapsed time over which each particle was successfully tracked, and estimated mean vertical fluid velocity. Uncertainties associated with each of the measured parameters contribute to the settling velocity uncertainty as:

$$\delta w_s = \sqrt{\left(\frac{\partial w_s}{\partial (\Delta z)} \delta(\Delta z) \right)^2 + \left(\frac{\partial w_s}{\partial (\Delta t)} \delta(\Delta t) \right)^2 + \left(\frac{\partial w_s}{\partial (w_f)} \delta(w_f) \right)^2} \qquad (8)$$

assuming independent and random measurement uncertainties (Taylor, 1997). Within this expression, δ indicates the measurement uncertainty for the given parameter and partial derivatives refer to Eqn (6). Parameter uncertainties were determined experimentally from the data set presented in section 3. Particle position errors were estimated from errors in the affine transformation from pixel to length space. The mean error in the transformation was on the order of 10 μm , so $\delta(\Delta z)$ was determined to be 10^{-2} mm. Uncertainty in the differential time is related to resolution and accuracy of the computer clock. For the short duration of tracking, clock resolution is more critical than clock accuracy (drift). The resolution of the computer clock used for image acquisition was experimentally determined to be on the order of 10-20 μs, resulting in $\delta(\Delta t)=10^{-5}$ sec. Uncertainty in the estimated mean fluid velocity was determined from the small-particle tracking data and was characterized by the standard error at 90% significance. The

uncertainty, $\delta(w_f)$ was assigned a value of 0.18 mm·s^{-1}. The resulting uncertainty in settling velocity, δw_s is then 0.18 mm·s^{-1}. Uncertainties in settling velocity are dominated by uncertainty in fluid velocity; uncertainties associated with particle position and time are on the order of 10^{-3} and 10^{-5} mm·s^{-1}, respectively. Relative uncertainty in settling velocity was determined by normalizing Eqn (8) with settling velocity (Figure 3-3). Relative uncertainty in settling velocity increases sharply with decreasing settling velocity. Relative uncertainty levels of 0.1, 0.5, and 1 are associated with settling velocities of 1.8, 0.36, and 0.18 mm·s^{-1}, respectively. Other researchers have expressed measurement uncertainties in terms of the velocity-normalized standard deviations in settling velocity for tracked particles: Sternberg et al (1999), 22%; Van der Lee (2000), 10-15%; and Mikkelsen et al. (2007) 30%. These values are consistent with the error levels associated with the median settling velocities estimated from this study (section 3.3).
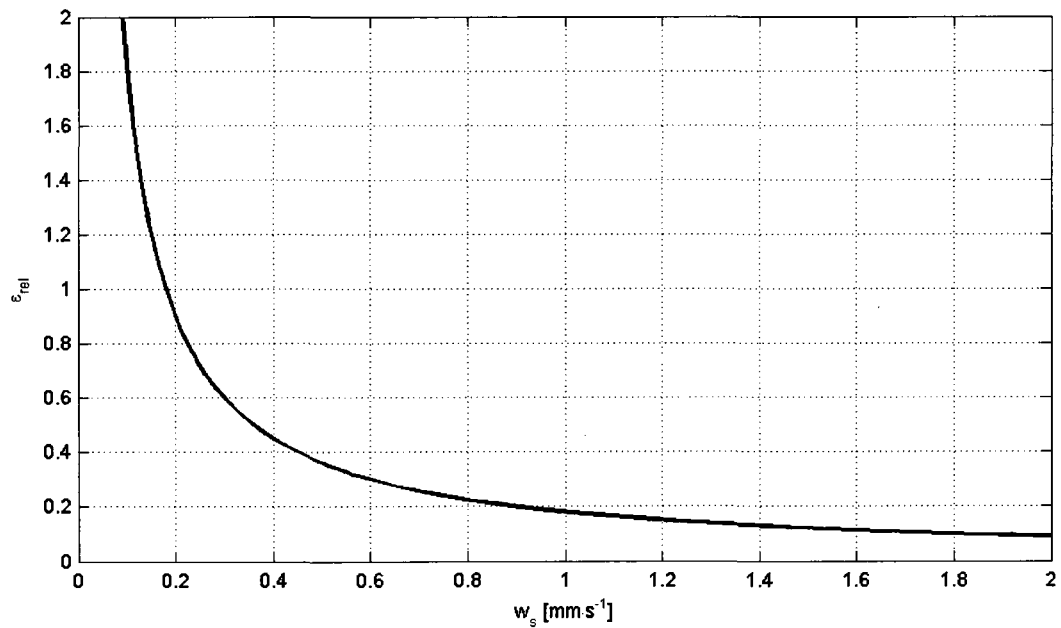
Figure 3-3. Relative uncertainty in PICS settling velocity estimates.

Uncertainty in excess density, $\rho_e = \rho_p - \rho_w$, was determined using Eqn (7) for ρ_p and employing the methods described earlier in this section. Excess density is computed from measured estimates of settling velocity, particle diameter, and fluid density and viscosity. Assuming uncertainties in fluid density and viscosity are small and

uncertainties in settling velocity and particle size are independent and random, the uncertainty in excess density is given by:

$$\delta p_e = \sqrt{\left(\frac{\partial \rho_e}{\partial w_s}\delta w_s\right)^2 + \left(\frac{\partial \rho_e}{\partial d}\delta d\right)^2} \qquad (9)$$

Applying the previously determined uncertainties, $\delta w_s = 0.18$ mm·s^{-1} and $\delta d = 0.03$ mm (converted to mks units) yields the results in Figure 3-4. The highest uncertainties are associated with small, slowly settling particles. For macroflocs (d>150 μm) settling near 1 mm·s^{-1} relative error in excess density is less than 0.4.
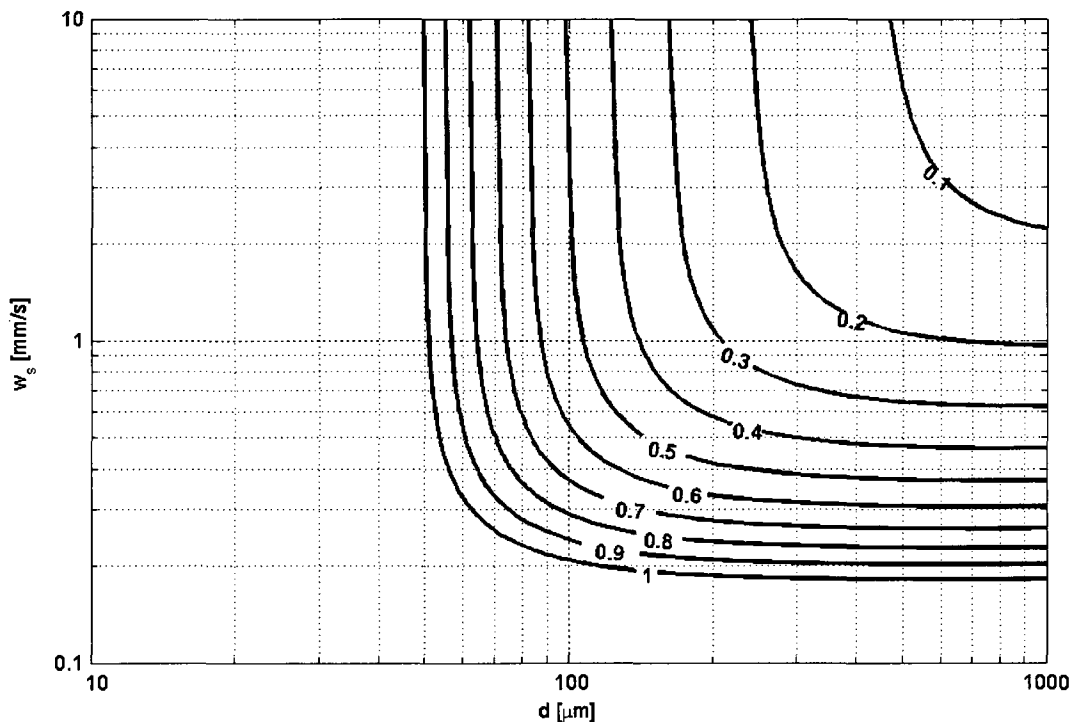
Figure 3-4. Relative uncertainty ($\delta p_e / p_e$) in excess density as function of settling velocity and particle diameter. Lines indicate relative uncertainty values.

2.3 Experiment Description

Field experiments for particle settling within dredge plumes were conducted 2-10 June 2006 at Richmond-Long Wharf in north-central San Francisco Bay, USA (Figure 3-5A). San Francisco Bay is a 4000-km^2 estuary connected to the Pacific Ocean by a

narrow strait, the Golden Gate. Tides in San Francisco are mixed diurnal/semi-diurnal with a mean tide range of 1.8 m. The primary source of freshwater and sediment input to San Francisco Bay is the Sacramento River, which enters through Carquinez Straits. Bed sediments at Richmond Harbor are predominantly fine-grained with a moderate fraction of fine sand. Recent, harbor-averaged bed sediment fractions are 38% sand, 30% silt, and 32% clay. Bed samples from the dredging location for this study were composed of 20% sand, 40% silt, and 40% clay, with total organic content (TOC) ranging from 0.7 to 1.4%. Richmond Long Wharf is a petroleum transfer facility with a dredged depth of 13.5 m MLLW. The annually averaged dredged volume is approximately 120,000 m^3.

Dredging operations in 2006 at Richmond Long Wharf were conducted with the *Essayons*, a 4600 m^3 trailing suction hopper dredge (USACE 1983). The dredge removes sediment from the bed through hydraulic suction and transports the sediment slurry through a centrifugal pump to the hopper. Shear within the dredging process is undoubtedly large, and degree of sediment disaggregation during the dredging process is

Figure 3-5. (A) Site map of San Francisco Bay and U.S. west coast (inset). Study site at Richmond Long Wharf is indicated by star. (B) Track lines of hopper dredge *Essayons* and survey vessel *Grizzly* during field experiment (10 June 2006). Diamonds on dredge path indicate start of dredging, begin of overflow, and end of dredging. Star indicates *Grizzly* position during data collection.
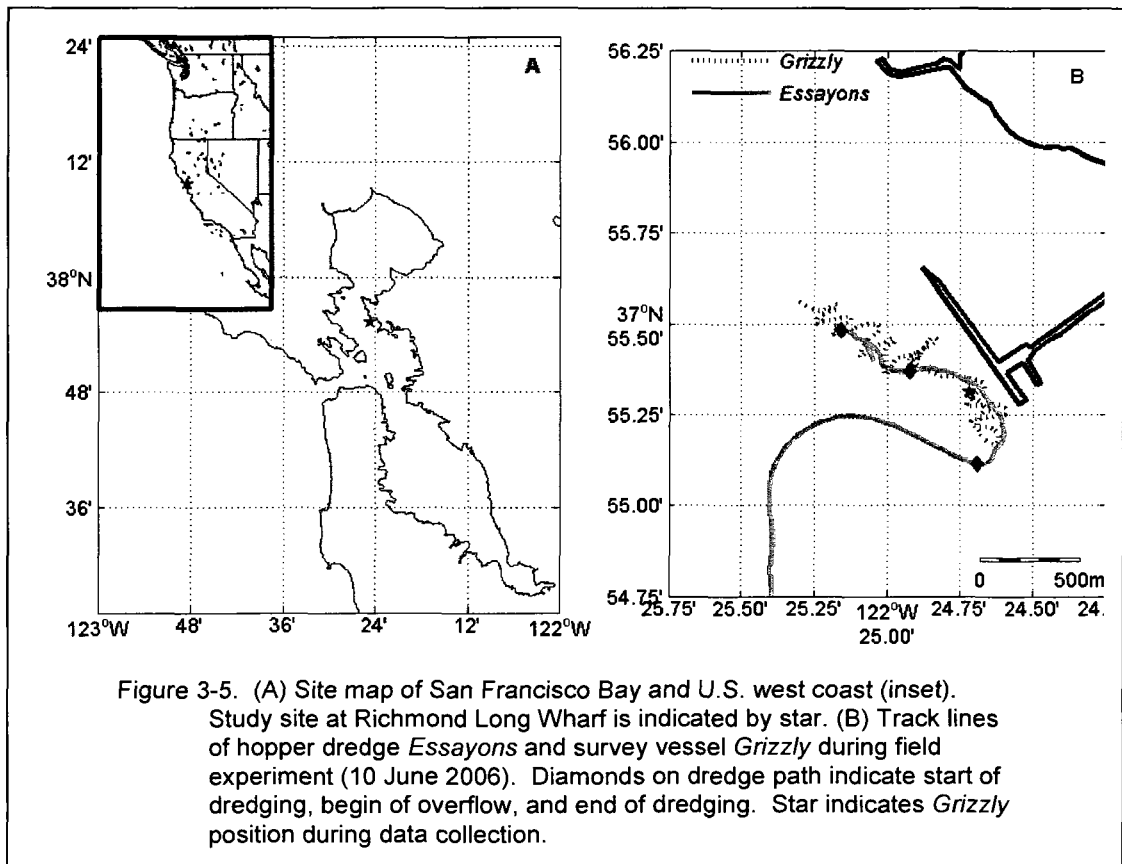
unknown. Within the hopper, turbulent conditions exist near the pump discharge, but rapidly become relatively quiescent due to the viscosity of the high sediment concentration (volume concentration is approximately 0.2, mass concentration ~ 500 kg m^{-3}). After approximately 15 minutes, the slurry level within the hopper reaches the overflow weir and the high-concentration suspension flows over the weirs and descends through the bottom of the hull to the sediment bed as a dynamic plume (Spearman et al., 2007). The dynamic plume is mixed into the water column by air entrained during overflow, mixing by the dredge propwash, and turbulent entrainment by the spreading bottom plume. Overflow was permitted for 15 minutes to increase sediment load in the hopper. *Essayons* is equipped with an anti-turbidity valve, which restricts flow through the weir structure such that entrained air is minimized, thus reducing vertical entrainment of the plume exiting the hull. The dredging cycle at Richmond Long Wharf (including transit time to the placement site) is approximately 1.5 hours.

During the experiment, a survey vessel followed the dredge, mapping plume extent with ADCP backscatter. With less than 5 minutes of dredging remaining, the survey vessel positioned to collect samples from the overflow plume. ADCP backscatter was used to determine positioning of the instrumentation frame within the dredge plume. During data collection, the instrument frame was raised and lowered through the water column to profile the suspended sediment plume. Measured positions within a profile cast were spaced nominally at 1-2 m, but this spacing was varied based on plume structure as indicated by acoustic backscatter. Each measurement position required 2-3 minutes. Vessel positioning methods varied during the experiment. During light winds, the vessel was allowed to drift with the plume during sampling. For stronger wind conditions, drifting with the plume was not possible, and the survey vessel was anchored such that the dredge plume drifted beneath the survey vessel with the prevailing currents.

3 RESULTS

Data are presented from a single dredging operation on 10 June 2006 near Richmond Long Wharf (Figure 3-5B). The hopper dredge *Essayons* commenced dredging at 18:30 UTC in the NW portion of the dredged basin and proceeded to the SE. Hopper overflow began at 18:42, and dredging was complete at 18:58. During the period

of dredging, the survey vessel *Grizzly* identified the extent of the dredge plume with ADCP backscatter. Near the end of dredging, *Grizzly* returned to a position near the mid-point of hopper overflow and set anchor within the plume for sampling. Continuous profiling and sampling within the plume was performed between 19:14 and 20:25. The sampling period occurred around the time of high tide and currents within the dredged basin were weak, generally less than 0.15 m s^{-1}.

3.1 Calibration of backscatter to SSC

ADCP echo intensity (measure of intensity of backscattered acoustic energy from particulates) was recorded continuously with bin spacing of 0.25 m. Echo intensity was converted to acoustic backscatter (dB) using TRDI (2007) coupled with the sound absorption methods of Ainslie and McColm (1998) and Richards (1998) which account for sound absorption by water and sediment. Calibration of acoustic backscatter to physical samples of SSC (Figure 3-6) was performed through an iterative procedure, resulting in the relationship: $SSC = 10^{0.0742BS-4.56}$, where BS is backscatter intensity (dB). The backscatter calibration was applied to the ADCP data during the PICS profiling period as shown in Figure 3-7. The ADCP-derived SSC data indicate that the dredge plume is heterogeneous in both space and time. Suspended sediment concentrations within the plume are largest near the bed and generally decrease with time as particulates
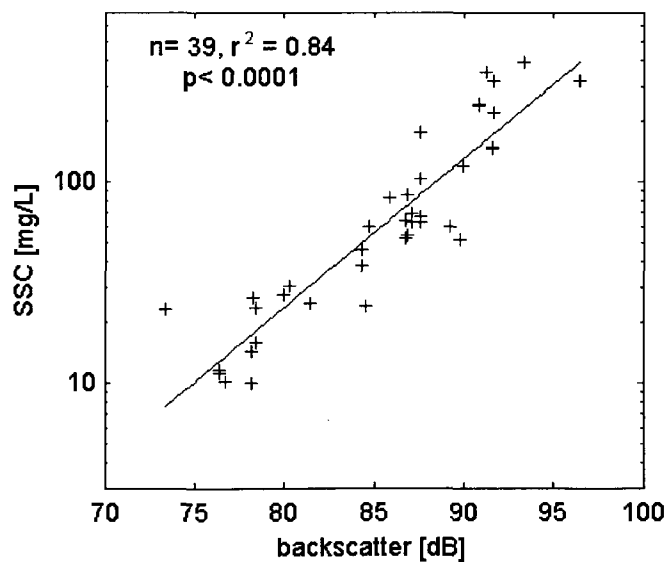
Figure 3-6. Calibration of ADCP acoustic backscatter to log(SSC) for physical samples collected 10 June 2006.
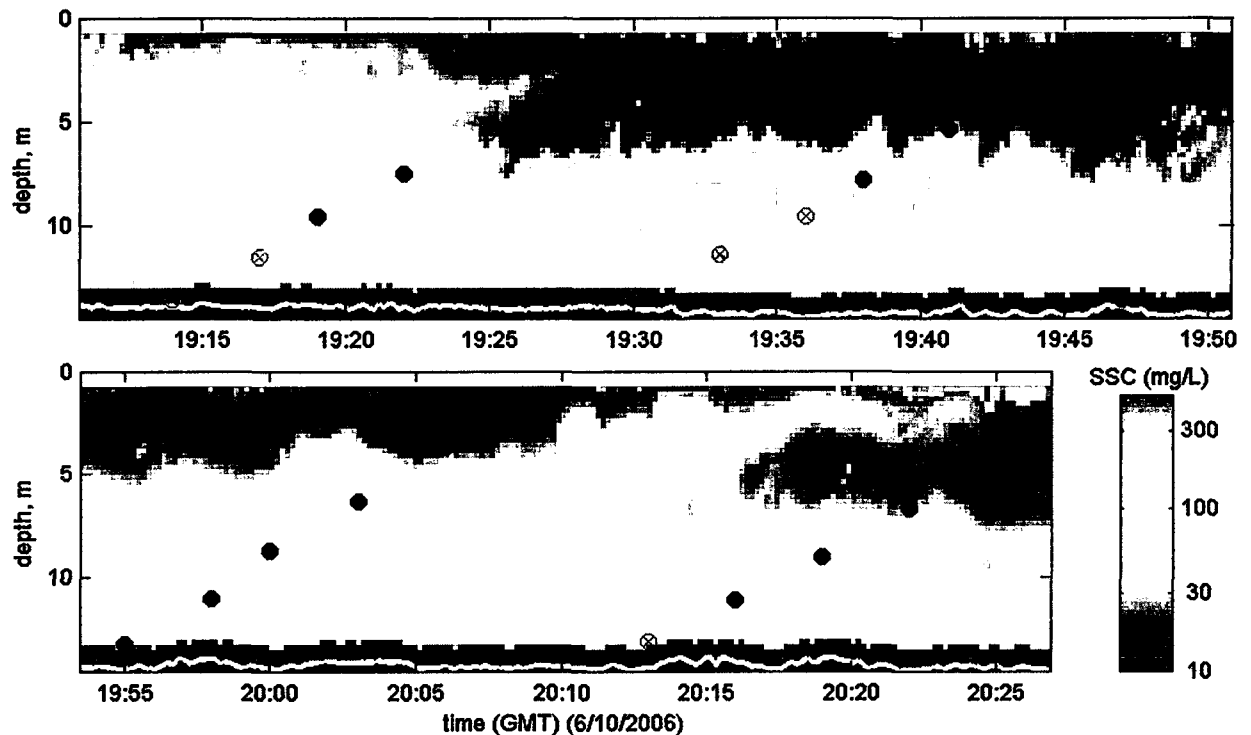
Figure 3-7. ADCP estimated SSC (mg/L) during data collection. Circles indicate time and vertical positioning of PICS during sample collection and image acquisition. Open circles with × indicate failed image (high concentration or column circulation), filled circles indicate successful image acquisition and analysis.

suspended during dredging and overflow settle from suspension. Within the plume, smaller scale features of higher sediment concentration are also evident, which complicate efforts to develop relationships from point measurements.

3.2 Physical Sample Analysis

Suspended sediment samples were collected at each of the locations indicated in Figure 3-7. Samples were collected to determine SSC and disaggregated size spectra. Size spectra from the four disaggregated samples were nearly identical and indicate that the suspended sediments in the plume were composed of 1 % sand, 46% silt, and 53% clay. This observation suggests that sand was retained in the hopper and/or settled to the bed prior to sample collection. The silt:clay ratios of the pre-dredging bed samples and suspended samples are 1.1 and 0.87, respectively. These silt:clay ratios are similar, but there are insufficient data to state with statistical significance (p=0.19) that the silt:clay ratio in suspension is the same as that from the bed.

3.3 Results of PICS Image Analysis

During the sampling period, data were collected in four casts through the water column with approximately 2-m vertical spacing to quantify suspended sediment characteristics. Measurement positions are indicated by circles in Figure 3-7. Filled circles indicate stations for which PICS image analysis was possible, open circles indicate that image analysis was not possible due either to high sediment concentration or large surface wakes from passing vessels. These casts of the instrumentation package through the water column will be referred to as Cast 03-06.

Image analysis was performed for each of the successful PICS sampling stations indicated in Figure 3-7. The 11-m station from Cast06 (time=20:16) is presented in Figure 3-8. Figure 3-8C gives settling velocity versus equivalent spherical diameter (*esd*), with 1982 particles identified in the 30-sec video sequence. For this image sequence, the mean vertical fluid velocity was estimated to be upward at 0.05 mm s^{-1}. Settling velocity was bin-averaged within 25 logarithmically spaced particle size bins between 20-1000 μm for primary particles, bed aggregates, and flocs. Each particle class is distinguished by estimated particle density. The bin-averaged values were fit by method of least squares to $w_s = Ad^m$. The m values for each particle class are indicated on each best-fit curve.

The count, sediment mass, and volume spectra for all particles are shown in Figure 3-8A. Sediment mass for each particle (excluding pore water) was estimated as

$$m_p = \frac{\pi (esd)^3}{6} \rho_s (1-\phi)$$

(10)

where ρ_s is the assumed sediment mineral density (2650 kg·m^{-3}), and $(1-\varphi) = (\rho_p - \rho_w) / (\rho_s - \rho_w)$, φ being floc porosity. The count spectrum is dominated by smaller particles, but the sediment mass and volume spectra are dominated by macroflocs ($d > 150$ μm). The mass spectra for each particle class are shown in Figure 3-8B. Primary particles range in size from 30-70 μm with a peak at 50 μm, bed aggregates range in size from 40-200 μm with a peak near 80 μm, and flocs range from 40-800 μm with peaks near 300 and 700 μm. Sediment mass fractions by particle class are 2% primary particles,
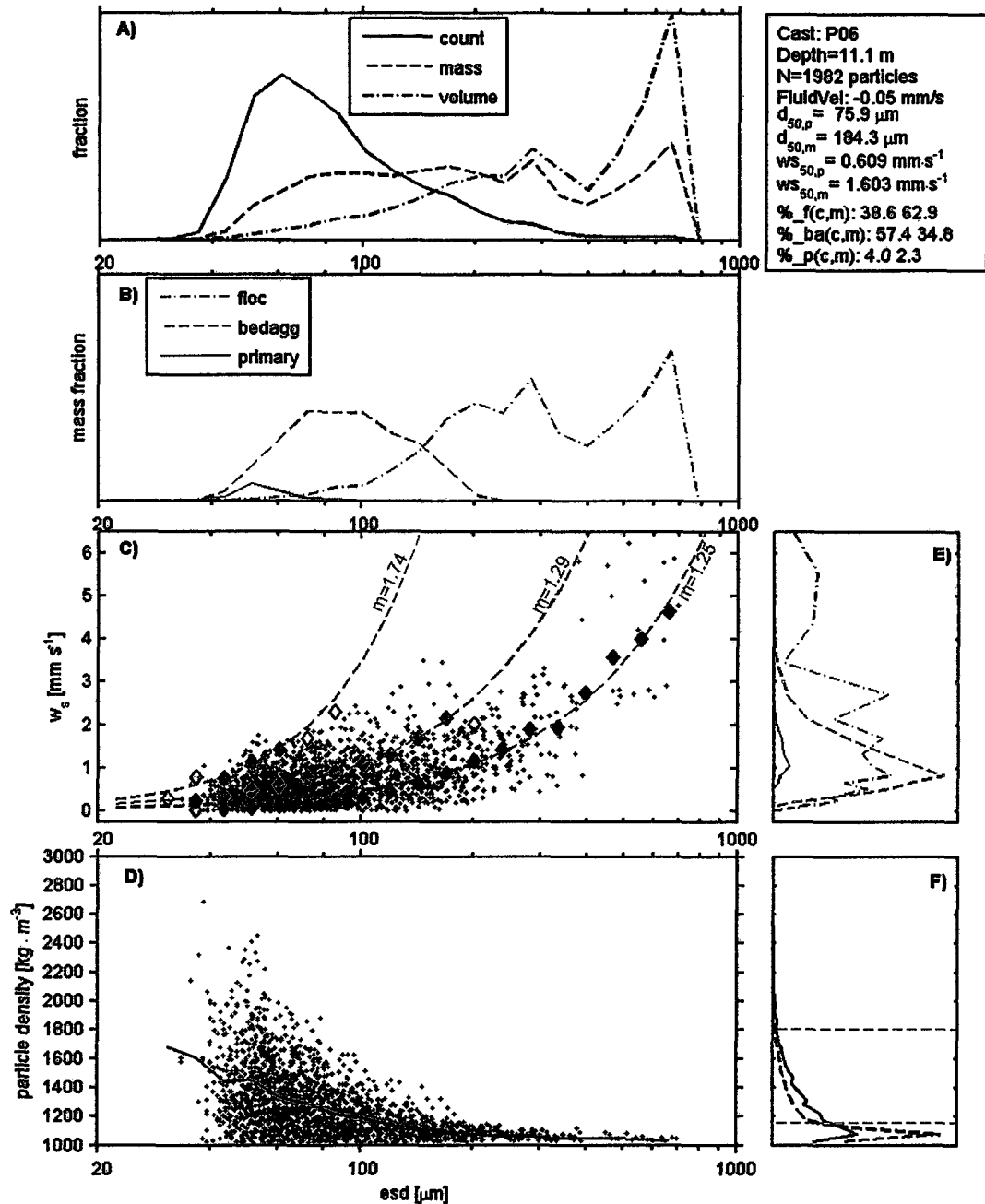
Figure 3-8. Results of image analysis for 11-m station from Cast06. A) count-, mass-, and volume-weighted particle size spectra, B) sediment mass-size spectra by particle class C) size and settling velocity for individual particles (points), bin-averaged (diamonds), and least-squares fit (to bin averages) (lines), *m* indicates the exponent of the power fit, and color indicates particle class (color scale indicated in panel B), D) Individual particle densities from Eqn (5) (points) and from bin-averaged settling velocity (line) E) mass-weighted settling velocity spectra by particle class (line styles as in B), and F) mass-weighted density distributions (line styles as in A).

35% bed aggregates, and 63% flocs. Median particle size is 76 μm by count and 180 μm by mass, indicating the relative contribution of the less abundant, but higher mass macroflocs.

In Figure 3-8E, the mass-w_s spectra for each particle class indicates peak settling velocities for primary particles and bed aggregates near 1 mm·s^{-1} and a broad distribution of settling velocity for flocs between 1 to 3 mm·s^{-1}. A secondary peak in the floc spectrum appears near 5 mm·s^{-1} for a few large, fast-settling flocs. The influence of these macroflocs is also seen in the estimated median settling velocity, which is 0.6 mm·s^{-1} by count and 1.6 mm·s^{-1} by mass.

Particle density was estimated by applying Eqn (7) to each particle's *esd* and w_s. The resulting densities are presented in Figure 3-8D, and the corresponding distribution of particle densities by count and mass are presented in Figure 3-8F. Particle densities ranged from 1020 to 2680 kg m^{-3}, with smaller particles having larger densities and range of densities.

The example provided in Figure 3-8 is intended to illustrate data available from a single PICS sample. During the field experiment, 17 such samples were collected within the dredge plume. Parameters derived from image analysis for all PICS samples are provided in Table 3-1.

Correlations between particle size, settling velocity, and mass fractions to elapsed time and SSC (from physical samples) are examined in Figure 3-9. Elapsed time is given in minutes following the end of the dredging cycle. For each correlation, the best fit line, r^2, and p-value are provided. Statistically significant increases in median floc size (d_{50}) and median settling velocity ($w_{s\,50}$) with elapsed time (Figure 3-9A-B) suggest flocculation occurred within the dredge plume. Bed aggregate diameters and settling velocities were nearly constant with time. Additionally, mass fraction of flocs and bed aggregates showed no time variance (Figure 3-9C). Floc size and settling velocity poorly correlate with SSC (Figure 3-9D-E). A statistically significant correlation exists between bed aggregates and concentration, but the slope is mild, indicating that bed aggregate size remains essentially constant with SSC. The correlations of sediment mass fraction to SSC are not statistically significant (Figure 3-9F). The small sample size (N=17) and low

Cast	Time	Elapsed Time	Depth	Fluid Velocity	N	SSC (sample)	SSC (ADCP)	d_{50p}	d_{50m}	$w_{,50p}$	$w_{,50m}$	floc	bedagg	primary
	GMT	min	m	mm/s	Count	mg/L	mg/L	µm	µm	mm/s	mm/s			
3	19:14	16	13.6	-	-	377	-	-	-	-	-	-	-	-
3	19:17	19	11.5	-	-	353	162	-	-	-	-	-	-	-
3	19:19	21	9.6	0.11	654	243	151	85	160	0.47	1.14	0.61	0.38	0.01
3	19:22	24	7.5	0.55	628	70	76	102	161	0.52	1.18	0.64	0.36	0.01
3	19:25	27	5.5	-	-	27	22	-	-	-	-	-	-	-
3	19:27	29	3.3	-0.11	432	26	26	74	173	0.56	1.27	0.60	0.38	0.02
4	19:30	32	13.5	-	-	420	-	-	-	-	-	-	-	-
4	19:33	35	11.4	-	-	397	259	-	-	-	-	-	-	-
4	19:36	38	9.6	-	-	269	179	-	-	-	-	-	-	-
4	19:38	40	7.8	-0.30	1125	174	173	142	222	1.08	1.53	0.78	0.20	0.01
4	19:41	43	5.4	0.17	2670	20	33	80	105	0.55	0.81	0.46	0.53	0.02
4	19:44	46	3.1	-0.06	239	10	15	68	160	0.46	1.19	0.61	0.36	0.03
5	19:47	49	13.6	0.39	2203	91	-	91	153	0.42	0.81	0.72	0.27	0.00
5	19:55	57	13.2	-0.35	3872	120	131	111	204	0.87	1.34	0.71	0.27	0.01
5	19:58	60	11	0.74	2110	59	75	92	205	0.39	1.21	0.80	0.20	0.00
5	20:00	62	8.7	0.68	1735	60	68	97	188	0.85	1.57	0.63	0.36	0.01
5	20:03	65	6.3	0.49	1208	42	42	83	204	0.40	1.32	0.72	0.27	0.01
5	20:06	68	3.7	0.18	776	31	14	73	128	0.62	1.14	0.48	0.49	0.03
5	20:09	71	1.6	-0.58	161	11	12	69	176	0.47	1.52	0.66	0.27	0.07
6	20:13	75	13.1	-	-	54	75	-	-	-	-	-	-	-
6	20:16	78	11.1	0.05	1982	60	116	76	184	0.61	1.60	0.63	0.35	0.02
6	20:19	81	9	0.35	1064	63	90	80	230	0.49	1.51	0.74	0.25	0.01
6	20:22	84	6.7	0.57	367	25	26	83	167	0.74	1.69	0.51	0.46	0.03
6	20:25	87	4.6	-0.49	41	12	17	74	113	0.26	1.21	0.53	0.43	0.04

Table 3-1. Summary statistics from PICS samples. | Aggregate Fractions
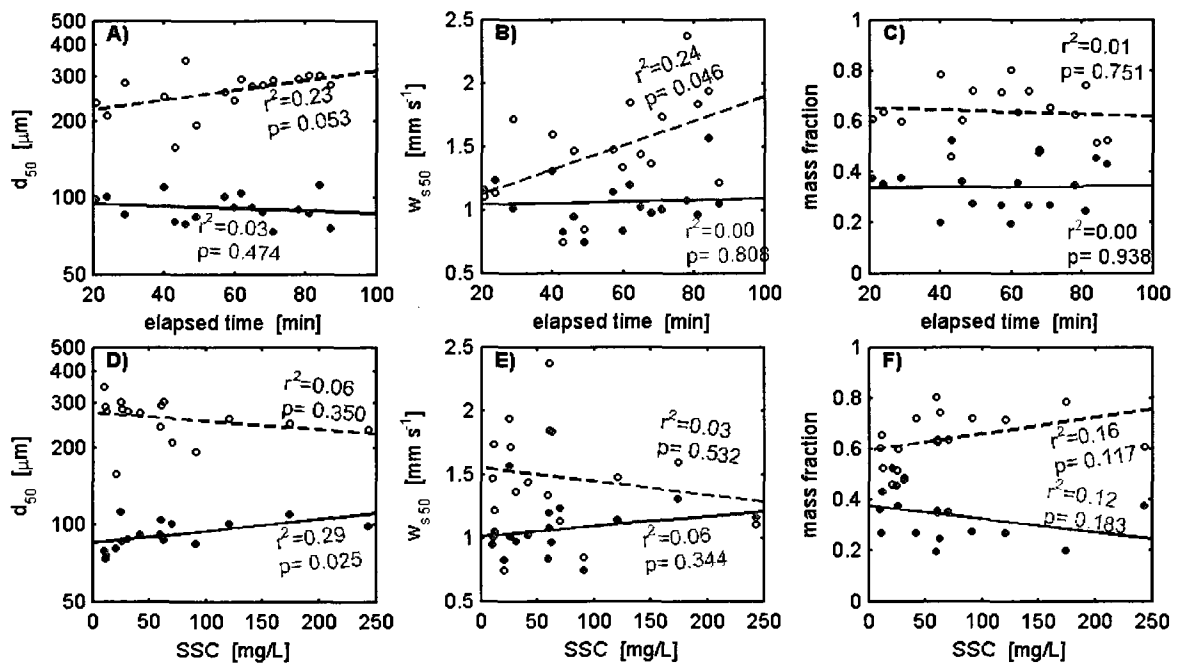
Figure 3-9. Correlations between suspended particle characteristics (d_{50}, $w_{s\,50}$, and mass fraction), elapsed time (A-C), and SSC (D-F). Sample size is 17, and r^2 and p-value for each correlation are indicated. (●) bed aggregates, (○) flocs. Lines represent best fit.

number of samples with SSC > 100 mg L^{-1} lead to poor correlation statistics, and unfortunately limit conclusions related to particle characteristics and sediment concentration.

Particle data from the 17 PICS stations were combined, resulting in a data set of 21267 tracked particles, of which 51% were flocs and 47% were bed aggregates, and 2% were primary particles. The settling velocities associated with each particle class were bin averaged in 25 logarithmically spaced bins between 20 to 1200 μm as presented in Figure 3-10B. A least-squares regression to the bin-averaged settling velocities using w_s = $A(esd)^m$ reveals that m increases from 1.12 for flocs to 1.28 for bed aggregates to 1.44 for primary particles. Data in the floc particle class for esd < 150 μm are heavily influenced by measurement uncertainty, and are excluded from the fit. Considering Winterwerp's (1998) fractal-based expression of Stokes Law, the m values suggest fractal dimensions, n_f of 2.1, 2.3, and 2.4 for flocs, bed aggregates, and primary particle classes. Variation in settling velocity was greatest for flocs with the peak variation of ±σ = 2 mm s^{-1} occurring in the 400-600 μm size range. A sediment-mass-normalized size spectrum is presented for each aggregate class (Figure 3-10A). The size spectra indicate peak bed aggregate size near 80 μm and peak floc size is approximately 200 μm, each corresponding to settling velocities of about 1 mm s^{-1} (Figure 3-10B). Flocs contribute 68% of the total sediment mass and 76% of the vertical mass transport $(m_p \times w_s)$; bed aggregates contribute 31% of sediment mass and 23% of mass transport; and primary particles contribute 1% of sediment mass and 1% of mass transport. It is likely, however, that the discrepancy between sediment mass and mass transport fractions for bed aggregates is within the error of the measurements.

4 DISCUSSION AND CONCLUSIONS

The primary objectives of this research are to determine settling velocities of suspended sediments, identify the presence and abundance of bed aggregates in suspension, and assess the role of flocculation in dredge plumes.
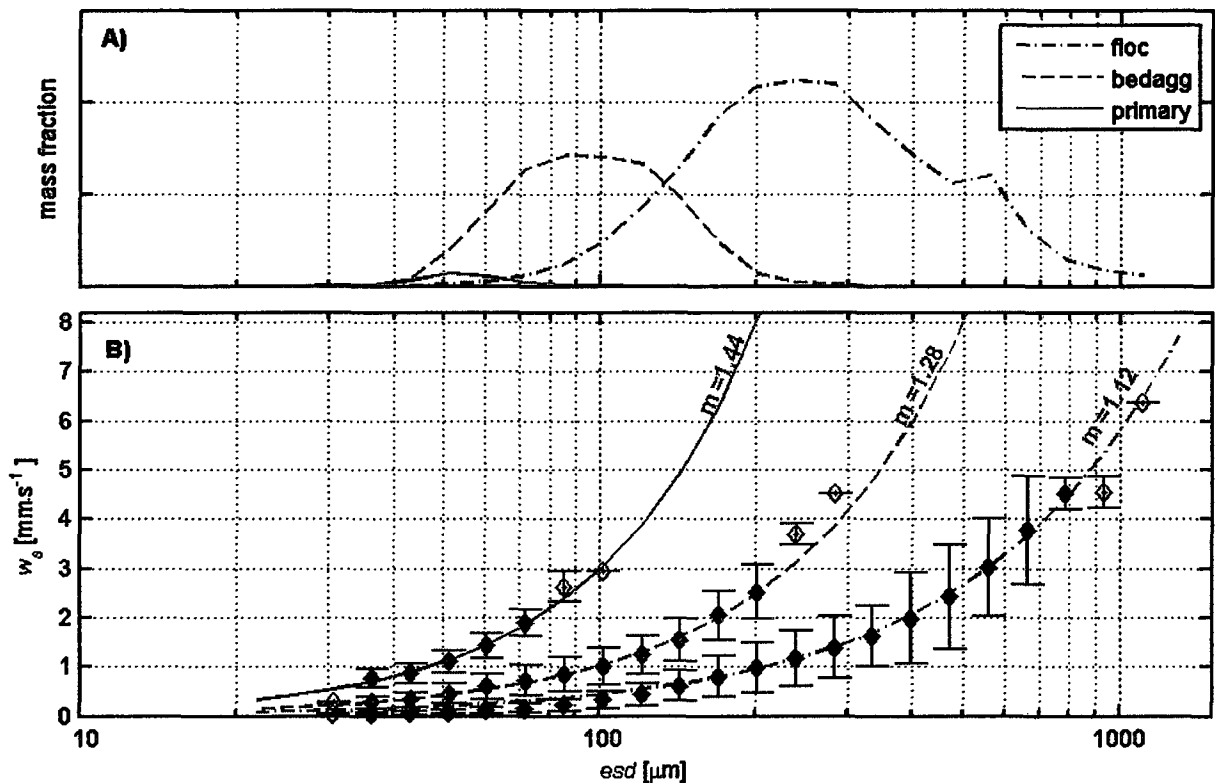
Figure 3-10. Particle characteristics for all particles sampled during 10 June 2006 experiment. A) mass-weighted particle size spectra by particle class. Size spectra are normalized to total sediment mass. B) bin averaged settling velocity of all particles (N=21267) analyzed from 17 PICS samples segregated by particle class. Hollow symbols represent bins with fewer than 10 particles and were excluded from the regression. Bars represent ±1 S.D. for each bin. Lines represent best-fit to $w_s = k \, (esd)^{\,m}$ for each particle class.

4.1 Settling Velocity

Settling velocities measured within the dredge plume ranged from 0.01 to more than 6 mm s^{-1}, with median velocities ranging between 0.8 to 1.7 mm s^{-1}. When all casts were pooled, the peak settling velocities for both bed aggregates and flocs was near 1 mm s^{-1}. The measured settling velocities are not remarkably different from those measured nearby (approximately 8 km north) in San Pablo Bay (Kineke and Sternberg, 1989; Krank and Milligan, 1992), for which mass-weighted, mean settling velocities ranged from 0.4 to 2.5 mm s^{-1}.

Krone (1963) was among the first to describe flocs as self-similar aggregates. Kranenburg (1994) and Winterwerp (1998, 2002) further suggested that this self-similarity can be mathematically described through fractal theory (Eqn (4)). Khelifa and Hill (2006) comment on the fractal based approach, suggesting that fractal dimension is
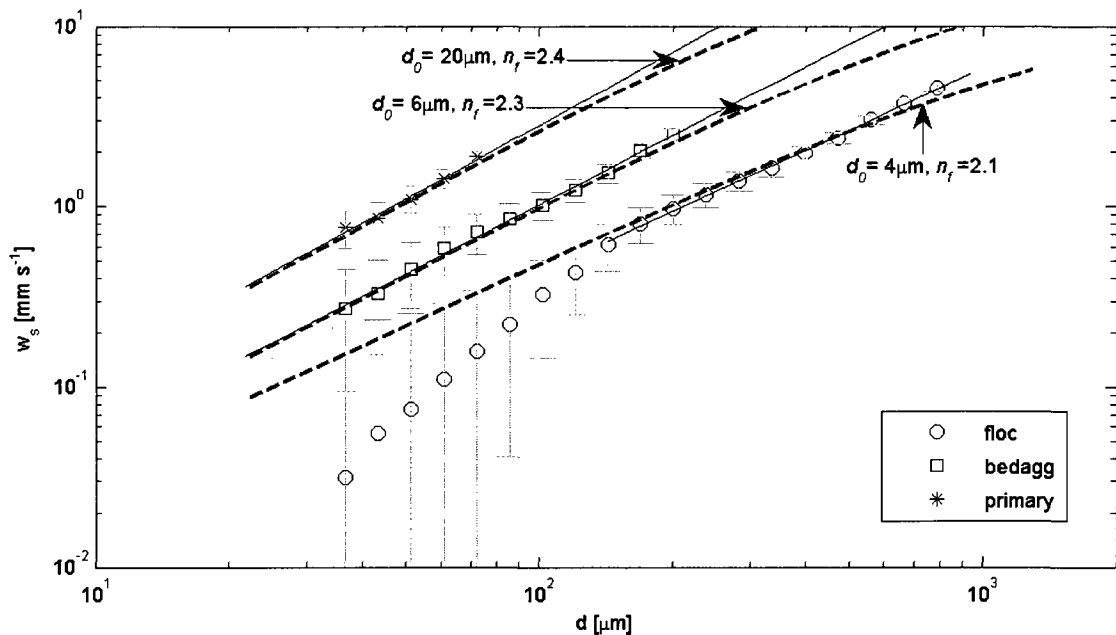
Figure 3-11. Settling velocity versus particle size. Symbols indicate bin-averaged data from Figure 3-10, bars indicate uncertainty in settling velocity, solid lines represent best-fit to data, dashed lines represent fit of Eqn (4) to data for spherical particles and ρ_0 = 2650 kg m^{-3}.

not constant, but instead decreases with increasing floc diameter. Figure 3-11 presents the bin-averaged data from Figure 3-10; error bars indicate uncertainty associated with the bin-averaged settling velocities; and solid lines indicate best fit to $w_s = A(esd)^m$. Dashed lines represent fit of Eqn (4) to the data with constant ρ_0 = 2650 kg m^{-3}; n_f as indicated from the m for each particle class; and primary particle diameter (which was determined through the least-squares fit to the data). As in Section 3.3, data in the floc particle class for esd < 150 µm are heavily influenced by measurement uncertainty, and are excluded from the fit.

Slopes of the best fit, m, suggest fractal dimensions of 2.1, 2.3, and 2.4 for the macrofloc, bed aggregate, and primary particle classes, respectively. These variable fractal dimensions are consistent with the claims of Khelifa and Hill (2006) that fractal dimension varies within populations of suspended particles. However, contrary to Khelifa and Hill, fractal dimensions within a particle class are shown to be constant with particle diameter. Khelifa and Hill's observations may be associated with the dominance of denser microflocs in the smaller size classes as shown in Figure 3-10A. If the primary

particle class were composed of individual mineral grains, a fractal dimension near 3 is expected. The lower fractal dimension of 2.4 could be attributed to biological coatings or aggregates consisting of a few silt-sized particles, which act to reduce particle density and inferred fractal dimension. Considerable natural variability (greater than measurement uncertainty) in settling velocities at a given particle size is evident in Figures 8 and 10, implying correspondingly large variation in fractal dimensions of individual particles. Figures 8 and 10 indicate that there is considerable natural variability (greater than the measurement uncertainty) in settling velocities of individual particles at a given diameter, implying correspondingly large variation in the fractal dimensions of individual particles.

Primary particle size, d_0, for the primary particle class is notably different from that of the bed aggregate and floc classes. (The reader is reminded that the primary particle size of Eqn (4) is not equivalent to the primary particle class, which is defined by inferred particle density.) The equivalent d_0 for the floc and bed aggregate particle classes suggests that they are of similar composition. However, the larger d_0 for the primary particle class suggests that this particle class is of different composition than the floc and bed aggregate classes. The larger d_0 and fractal dimension less than 3 are consistent with a class of biologically coated silt-sized particles and/or aggregates composed of a few silt-sized particles.

The fractal-based description of settling velocities (Winterwerp 1998, 2002) agrees well with measured settling velocities when applied to individual particle classes. A description of the suspended population with a single fractal dimension results in poorer agreement with the data (supporting Khelifa and Hill's argument for size-dependent fractal dimension). Considering the favorable agreement of the fractal-based settling velocity estimate by particle class, numerical modeling efforts could define suspended sediment classes with varying fractal dimensions to appropriately account for the presence of low-density flocs and robust aggregates suspended from the bed.

4.2 Bed Aggregates

Bed aggregates are defined in this paper as particles with apparent densities between 1200-1800 kg m^{-3} (excess density: 180-780 kg m^{-3}). These particles are presumed to be consolidated aggregates that were removed from the bed by the dredging

process and were not completely disaggregated during hydraulic transport through the dragarm and hopper. The fraction of bed aggregates indicated by PICS data ranged from 20 to 50% of the total sample mass and 31% of the pooled-sample sediment mass. Bed aggregates were found to have particle diameters ranging from 40-250 µm, with a median diameter of approximately 90 µm. The greater density of bed aggregates in this size range results in settling velocities of 0.5 to 3 mm s^{-1} compared to 0.1 to 1 mm s^{-1} for comparably sized flocs (Figure 3-10B); a finding that is of particular significance for estimating dredge plume clearance rates.

Bed aggregates are similar in size and density to microflocs reported in the literature. Microflocs are generally defined as flocs with diameter less than ~150 µm (Eisma, 1986; Van Leussen, 1994; Dyer et al., 1996; Mikkelsen et al., 2007) with excess densities in the range 100-1000 kg m^{-3} (Manning and Dyer, 1999). Approximately 20% of the denser bed aggregates from this study were larger than 150 µm. Krank and Milligan (1992) estimated mean density of suspended particles in San Pablo Bay, California ranging from 1030 to 1150 kg m^{-3}, but the sampling methods in their study were unable to provide particle size-density relationships. Presumably a significant portion of the particles were bed aggregates, at the upper limit of their reported mean densities. Mikkelsen and Pejrup (2000) estimated particle densities inferred from LISST-100 size spectra and gravimetric sampling in a mechanical dredging plume, resulting in mean particle densities between 1500-2300 kg m^{-3} (mean excess density 490-1300 kg m^{-3}).

The origin of microflocs in natural suspensions is attributed to progressively denser packaging of sediment through repeated aggregation/breakup processes (Van Leussen, 1994; Mikkelsen et al. 2006) and/or resuspension of partially consolidated sediments from the bed (Van Leussen, 1994; Winterwerp and Van Kesteren 2004). Considering these processes, the smaller, denser bed aggregate class could arise from incomplete disaggregation of the sediment bed and/or aggregation/breakup processes during the dredging process. Given the presence of bed aggregates soon after overflow and the time-constant characteristics of these particles, it is unlikely that they were formed in the water column during our study period.

Fast-settling bed aggregates produced during the dredging process may be preferentially retained within the hopper. Disaggregated samples collected within the plume indicate that only a small fraction of fine sand (d < 100 μm) is present in the plume, implying that either few particles with settling velocities greater than 5-7 mm s^{-1} pass the overflow weir or that few of these particles are entrained outside the dynamic plume. Bed aggregate data from the present study are consistent with the hopper retention premise, in that measured bed aggregate settling velocities did not exceed 5 mm s^{-1}.

The results of this field experiment indicate that hopper dredges suspend a substantial portion of bed aggregates, particularly during overflow. However, no PICS samples were taken at Richmond Long Wharf in the absence of dredging activities, so a direct assessment of the abundance of bed aggregates with and without dredging is not possible.

4.3 Flocs and Flocculation

Flocs contained 68% of the suspended mass and represented 76% of the vertical mass transport within the measured portion of the dredge plume. High concentrations and weak currents during this experiment were favorable for floc growth. Median floc size and settling velocity were observed to increase with time (Figures 9A,B), suggesting flocculation. Mikkelsen and Pejrup (2000) also noted an increase in particle diameter and decrease in mean particle density over a 50-minute period while conducting an experiment in a calcium carbonate dredge plume in the Øresund Sound between Denmark and Sweden.

Mehta and Lott (1987), Eisma et al. (1990), Van Leussen (1994), and Fennessy and Dyer (1996) have demonstrated the significance of macroflocs on estuarine sediment dynamics, emphasizing their relatively low abundance but large impact on vertical sediment flux. Large flocs, with diameters as large as 1200 μm were observed in the dredge plume of this study. Macroflocs (esd > 150 μm, ρ_p < 1200 kg m^{-3}) were relatively abundant within the plume, accounting for 19% of the particle count, 50% of suspended sediment mass, and 70% of the estimated vertical sediment mass transport. These observations indicate that flocculation was an active and time-dependent process within

the dredge plume; and flocs, but particularly macroflocs, dominate vertical mass flux in the passive phase of the overflow plume.

Eisma (1986), Winterwerp (1998), Van der Lee (2000), and Fugate and Friedrichs (2003) suggest that biological coatings, organic content, and browsing can significantly impact flocculation and settling. Biological influence on flocculation and settling was qualitatively observed in the PICS video sequences. Zooplankton and biologically dominated stringers were observed, and the larger flocs appeared to have stringy loops protruding or trailing behind.

The results of this field experiment suggest that the high concentrations of suspended sediment produced by hopper overflow are favorable for floc formation and growth. The chemical characteristics of sediment and water as well as biological activity in the area no doubt play a role in the degree and rates of flocculation. Spatial and temporal heterogeneities of the dredge plume precluded an assessment of time-rates of flocculation, however increases in large floc abundance with time was evident in the image sequences and data.

4.4 Modeling of Hopper Overflow Plumes

Observations from the field experiment provide several insights relevant to numerical modeling of dredge plumes. LISST and PICS data both suggest that less than 20 minutes following overflow, the passive dredge plume is in a highly aggregated state. LISST volumes in the size range 2.5 to 40 µm accounted for less than 4% of the *in-situ* suspended volume, compared to 97% for the disaggregated samples. PICS data indicate mass distributions of approximately 70% flocs and 30% bed aggregates. These data demonstrate that suspensions from hopper overflow can be initially highly aggregated. Of course, variations in sediment mineralogy, organic content, and dredge equipment (such as screens and plunging overflow) could influence the initial state of aggregation.

Milligan and Hill (1998), Mikkelsen and Pejrup (2000), and Winterwerp (2002) suggest that time-variant flocculation is important in representing cohesive sediment transport in estuarine and coastal systems. Floc size and settling velocity were observed to increase with time within the dredge plume, which supports the inclusion of time-dependent flocculation in dredge plume models. Challenges remain in this regard, as

time-dependent flocculation models, such as proposed by Van Leussen (1994) and Winterwerp (2002) include empirical constants to characterize the aggregation and breakup processes that are likely to be site and sediment specific.

Many sediment transport models allow modeling of discrete particle classes. The data presented suggest that at least two particle classes existed in the dredge plume measurements, with distinct differences in characteristics. The bed aggregate class was composed of smaller but denser particles with time invariant size and settling velocity; the floc class demonstrated time-dependent increases in size and settling velocity. These observations suggest that a multiple-class model would be advantageous in representing the behavior of dredge plumes.

Van Leussen (1994) and Van der Lee (2000) present the work of many researchers that have observed a concentration dependence of settling velocities in various estuarine settings. These observations are attributed to increased collision frequency with increase in concentration, but may also be influenced in part by resuspension/deposition exchanges with the sediment bed (Eisma, 1986). For the present study, correlations between floc size and settling velocity to SSC were weak and statistically insignificant. The SSC data for these correlations were poorly distributed and the sample size was small; consequently, the findings related to SSC and w_s should be considered inconclusive.

4.5 Dredging Operations

Trailing suction hopper dredges, through hydraulic removal and transport of sediment to the hopper, turbulent conditions within the hopper, and turbulent stresses during overflow (Land and Bray, 1998; Van Raalte, 2006) are likely to break bed aggregates into small fragments. Additionally, hopper dredges may preferentially retain larger bed aggregates within the hopper. Those bed aggregates that pass the overflow weir on the *Essayons* exit the hull in fairly close proximity to the sediment bed, making them less likely to be entrained higher into the water column. The remainder of sediment entrained into the water column appears from samples taken within 20-minutes of overflow to already exist in a highly flocculated state. This observation suggests that flocculation occurs within the high-concentration slurry within the hopper and/or very

rapidly following overflow. Within the studied hopper overflow plume, flocculation appears to have a stronger influence than bed aggregates on both suspended sediment mass and vertical sediment flux.

Mechanical dredges (clamshell, bucket) remove sediment from the bed with much less hydraulic disturbance than hydraulic or hopper dredges and are much more likely to suspend a larger fraction of bed aggregates in their plumes. Additionally, mechanical dredges introduce their losses throughout the water column, and bed aggregates are likely to be introduced near the water surface. Future research will address such questions regarding the difference in suspended particle characteristics between hopper and mechanical dredges.

REFERENCES FOR CHAPTER 3

Agrawal, Y.C. and Pottsmith, H.C. 2000. Instruments for particle size and settling velocity observations in sediment transport. *Marine Geology* 168: 89-114.

Ainslie, M.A. and McColm, J.G. 1998. A simplified formula for viscous and chemical absorption in sea water. *Journal of the Acoustical Society of America* 103(3): 1671-1672.

Ayukai, T. and Wolanski, E. 1997. Importance of biologically mediated removal of fine sediments from the Fly River plume, Papua New Guinea. *Estuarine, Coastal, and Shelf Science* 44: 629-639.

Bray, R.N., Bates, A.D., and Land, J.M., 1997. Dredging: A Handbook for Engineers. Arnold. London.

Dyer, K.R.; Cornelisse, J.; Dearnaley, M.P.; Fennessy, M.J.; Jones, S.E.; Kappenberg, J.; McCave, I.N.; Pejrup, M.; Puls, W.; Van Leussen, W.V.; and Wolfstein, K. 1996. A comparison of in situ techniques for estuarine floc settling velocity measurements. *Journal of Sea Research* 36(1/2): 15-29.

Eisma, D. 1986. Flocculation and de-flocculation of suspended matter in estuaries. *Netherlands Journal of Sea Research* 20(2/3): 183-199.

Eisma, D.; Schuhmacher, T.; Boekel, H.; Heerwaarden, J.V.; Franken, H.; Laan, M.; Vaars, A.; Eijgenraam, F.; and Kalf, J. 1990. A camera and image-analysis system for in situ observation of flocs in natural waters. *Netherlands Journal of Sea Research* 27(1): 43-56.

Fennessy, M.J. and Dyer, K.R. 1996. Floc population characteristics measured with INSSEV during the Elbe estuary intercalibration experiment. Journal of Sea Research 36(1/2): 55-62.

Fennessy, M.J., Dyer, K.R., and Huntley, D.A. 1994. INSSEV: an instrument to measure the size and settling velocity of flocs in situ. *Marine Geology* 117: 107-117.

Fugate, D. and Friedrichs, C.T., 2003. Controls on suspended aggregate size in partially mixed estuaries, *Estuarine, Coastal, and Shelf Science* 58: 389-404.

Germano, J.D., and Cary, D., 2005. Rates and effects of sedimentation in the context of dredging and dredged material placement, DOER Technical Notes Collection (ERDC TN-DOER-E19), U.S. Army Engineer Research and Development Center, Vicksburg, MS. http://el.erdc.usace.army.mil/dots/doer/doer.html

Graf, W.H. 1971. Hydraulics of Sediment Transport. McGraw-Hill, New York.

Gregory, J., 1997. The density of particle aggregates. *Water Science and Technology* 36(4): 1-13.

Johnson, B.H., 1990. User's Guide for Models of Dredged Material Disposed in Open Water, Technical Report D-90-5, U.S. Army Engineer Waterways Experiment Station, Vicksburg, MS.

Johnson, B.H., Andersen, E., Isaji, T., Teeter, A.M., and Clarke, D.G., 2000. Description of the SSFATE numerical modeling system. ERDC TN-DOER-E10. U.S. Army Engineer Research and Development Center, Vicksburg, MS.

Johnson, C.P., Li, X., and Logan, B.E., 1996. Settling velocities of fractal aggregates. *Environmental Science and Technology* 30: 1911-1918.

Khelifa, A. and Hill, P.S. 2006. Models for effective density and settling velocity of flocs. *IAHR Journal of Hydraulic Research* 44(3): 390-401.

Kineke, G.C. and Sternberg, R.W., 1989. The effect of particle settling velocity on computed suspended sediment concentration profiles, *Marine Geology* 90: 159-174.

Koh, R.C.Y. and Chang, Y.C., 1973. Mathematical Model for Barged Ocean Disposal of Waste, Environmental Protection Technology Series EPA 660/2-73-029, U.S. Environmental Protection Agency, Washington, DC.

Kranenburg, C. 1994. The fractal structure of cohesive sediment aggregates. *Estuarine, Coastal, and Shelf Science* 39: 451-460.

Krank, K. and Milligan, T.G., 1992. Characteristics of suspended particles at an 11-hour anchor station in San Francisco Bay, California, *Journal of Geophysical Research* 97(C7): 11373-11382.

Krank, K., Petticrew, E., Milligan, T.G., and Droppo, I.G. 1993. In situ particle size distributions resulting from flocculation of suspended sediment. In: Mehta, A.J. (Ed.), Nearshore and Estuarine Cohesive Sediment Transport, American Geophysical Union, pp. 60-74.

Krone, R.B. 1963. A study of rheological properties of estuarial sediments. Technical Bulletin No. 7, Committee on Tidal Hydraulics, U.S. Army Engineer Waterways Experiment Station, Vicksburg, Mississippi.

Land, J. and Bray, R.N. 1998. Acoustic measurement of suspended solids for monitoring of dredging and dredged material disposal. *Proceedings of the 15th World Dredging Congress (WODCON XV)*, Western Dredging Association, Vancouver, pp. 105-120.

Manning, A.J. and Dyer, K.R. 1999. A laboratory examination of floc characteristics with regard to turbulent shearing. *Marine Geology* 160: 147-170.

McLellan, T.N., Havis, R.N., Hayes, D.F., and Raymond, G.L. 1989. Field Studies of Sediment Resuspension Characteristics of Selected Dredges. Technical Report HL-89-9. U.S. Army Engineer Waterways Experiment Station, Vicksburg, Mississippi.

Mehta, A.J. and Lott, J.W. 1987. Sorting of fine sediment during deposition. in: Proceedings of the Conference on Advances in Understanding Coastal Sediment Processes, 1, 348-362.

Mikkelsen, O.A. and Pejrup, M. 2000. In situ particle size spectra and density of particle aggregates in a dredging plume. *Marine Geology* 170: 443-459.

Mikkelsen, O.A., Hill, P.S., and Milligan, T.G. 2006. Single-grain, microfloc and macrofloc volume variations observed with a LISST-100 and a digital floc camera. *Journal of Sea Research* 55: 87-102.

Mikkelsen, O.A., Hill, P.S., and Milligan, T.G. 2007. Seasonal and spatial variation of floc size, settling velocity, and density on the inner Adriatic Shelf (Italy). *Continental Shelf Research* 27: 417-430.

Mikkelsen, O.A., Hill, P.S., Milligan, T.G., and Chant, R.J. 2005. In situ particle size distributions and volume concentrations from a LISST-100 laser particle sizer and a digital floc camera. *Continental Shelf Research* 25: 1959-1978.

Mikkelsen, O.A., Milligan, T.G., Hill, P.S., and Moffatt, D. 2004. INSSECT—an instrumented platform for investigating floc properties close to the seabed. *Limnology and Oceanography: Methods* 2: 226-236.

Milligan, T.G. and Hill, P.S. 1998. A laboratory assessment of the relative importance of turbulence, particle composition, and concentration in limiting maximal floc size and settling behavior, *Journal of Sea Research* 39: 227-241.

Newcombe, C.P. and Jensen, J.O.T., 1996. Channel suspended sediment and fisheries: a synthesis for quantitative assessment of risk and impact. *North American Journal of Fisheries Management* 16: 693-727.

Oseen, C. 1927. Hydrodynamik, chapter 10, Akademische Verlagsgesellschaft, Leipzig.

Raudkivi, A.J. 1998. Loose Boundary Hydraulics, fourth ed., Taylor & Francis, London.

Richards, S.D. 1998. The effect of temperature, pressure, and salinity on sound attenuation in turbid seawater. *Journal of the Acoustical Society of America* 103(1): 205-211.

Sanford, L.P.; Dickhudt, P.J.; Rubiano-Gomez, L.; Yates, M.; Suttles, S.E.; Friedrichs, C.T.; Fugate, D.D.; and Romine, H. 2005. Variability of suspended particle concentrations, sizes, and settling velocities in the Chesapeake Bay turbidity maximum. In: Droppo, I.G.; Leppard, G.G.; Liss, S.N.; and Milligan, T.G. (Eds.) Flocculation in Natural and Engineered Environmental Systems, CRC Press, Boca Raton, Florida, USA.

Schiller, L. and Naumann, A. 1933. Über die grundlegenden Berechnungen bei der Schwerkraftaufbereitung, Z. VDI, vol. 77.

Schlichting, H. and Gersten, K. 2000. Boundary-Layer Theory. Springer, Berlin.

Soulsby, R.L. 1997. Dynamics of marine sands. Thomas Telford, London.

Spearman, J., Bray, R.N, Land, J., Burt, T.N, Mead, C.T., and Scott, D. 2007. Plume dispersion modeling using dynamic representation of trailer dredger source terms. In: ed: Maa, J.P.-Y.; Sanford, L.P.; and Schoellhamer, D.H. (Eds.) Estuarine and Coastal Fine Sediment Dynamics, Elsevier, Amsterdam, pp. 417-448.

Sternberg, R.W., Berhane, I., and Ogston, A.S. 1999. Measurement of size and settling velocity of suspended aggregates on the northern California continental shelf. *Marine Geology* 154: 43-53.

Sternberg, R.W., Ogston, A., and Johnson, R. 1996. A video system for in situ measurement of size and settling velocity of suspended particulates. *Journal of Sea Research* 36(1/2): 127-130.

Taylor, J.R. 1997. An Introduction to Error Analysis. second ed., University Science Books, Sausalito, California.

Teledyne RD Instruments (TRDI). 2007. WinRiver II user's guide. P/N 957-6231-00, p. 48

Ten Brinke, W.B.M. 1994. Settling velocities of mud aggregates in the Oosterschelde tidal basin (The Netherlands), determined by a submersible video system. *Estuarine, Coastal, and Shelf Science* 39: 549-564.

Torfs, H., Jiang, J. and Mehta, A.J. 2001. Assessment of the erodibility of fine/coarse sediment mixtures. In: W.H. McAnally and A.J. Mehta (Eds.), Coastal and Estuarine Fine Sediment Processes, Elsevier, pp. 109-124

Tubman, M., Brumley, B., and Puckette, P.T. 1994. Deep-water dredged-material disposal monitoring offshore of San Francisco using the PLUme Measurement System (PLUMES). Dredging '94, Proceedings of the second international conference on dredging and dredged material placement, Lake Buena Vista, Florida, USA. pp. 86-95

U.S. Army Corps of Engineers (USACE) (1983). Dredging and Dredged Material Disposal. Engineering Manual 1110-2-5025. Vicksburg, Mississippi, USA

Van der Lee, W.T.B 2000. Temporal variation of floc size and settling velocity in the Dollard estuary. *Continental Shelf Research* 20: 1495-1511

Van Leussen, W. 1994. Estuarine Macroflocs and Their Role in Fine-Grained Sediment Transport, Ministry of Transport, Pubic Works and Water Management. Den Haag.

Van Leussen, W.V. and Cornelisse, J.M. 1993. The determination of the sizes and settling velocities of estuarine flocs by underwater video system. *Netherlands Journal of Sea Research* 31(3): 231-241.

Van Raalte, G.H. 2006. Dredging techniques: adaptations to reduce environmental impact. In: Eisma, D. (Ed.), Dredging in Coastal Waters, Taylor and Francis, London, pp.1-40.

Wilber, D.H. and Clarke, D.G. 2001. Biological effects of suspended sediments: a review of suspended sediment impacts on fish and shellfish with relation to dredging activities in estuaries. *North American Journal of Fisheries Management* 21: 855-875.

Winterwerp, J.C. 1998. A simple model for turbulence induced flocculation of cohesive sediment. *IAHR Journal of Hydraulic Research* 36 (3): 309-326.

Winterwerp, J.C. 2002. On the flocculation and settling velocity of estuarine mud. *Continental Shelf Research* 22: 1339-1360.

Winterwerp, J.C. and Van Kesteren, W.G.M. 2004. Introduction to the Physics of Cohesive Sediment in the Marine Environment, Developments in Sedimentology series, volume 56, Elsevier. Amsterdam.

Chapter 4. Image Processing Methods for In Situ Estimation of Cohesive Sediment Floc Size, Settling Velocity, and Density

Authors: S.J. Smith and C.T. Friedrichs

ABSTRACT

Recent advances in development of in-situ video settling columns have significantly contributed towards fine-sediment dynamics research through concurrent measurement of suspended sediment floc size distributions and settling velocities, which together also allow inference of floc density. Two challenges in video analysis from these devices are the automated tracking of settling particles and accounting for fluid motions within the settling column. A combination of Particle Tracking Velocimetry (PTV) and Particle Image Velocimetry (PIV) image analysis techniques is described, which permits general automation of image analysis collected from video settling columns. In the fixed image plane, large particle velocities are determined by PTV and small particle velocities are tracked by PIV and treated as surrogates for fluid velocities. The large-particle settling velocity (relative to the suspending fluid) is determined by the vector difference of the large and small particle settling velocities. The combined PTV/PIV image analysis approach is demonstrated for video settling column data collected within a dredge plume in Boston Harbor. The automated PTV/PIV approach significantly reduces uncertainties in measured settling velocity and inferred floc density.

1 INTRODUCTION

Fine grained sediments in riverine, estuarine, and marine environments form flocs composed of organic and inorganic material (Eisma, 1986; Van Leussen, 1994; Ayukai and Wolanski, 1997, Williams et al., 2008). Flocs formed in suspension vary in size, shape, and density dependent upon factors such as mineralogy, organic coatings, internal shear, and sediment concentration (Eisma, 1986; Tsai et al., 1987; Ayukai and Wolanski, 1997; Manning and Dyer, 1999). The larger size of flocs results in settling velocities several orders of magnitude faster than the constituent particles (Van Leussen and Cornelisse, 1993). Additionally, the size, shape, density, and settling velocity of flocs are time-variable as influenced by time- and space-variant hydrodynamics and suspended sediment populations (Eisma, 1986; Van der Lee, 2000). Fine sediments are of key interest in estuarine and marine systems through the influence of light attenuation, delivery of sediment and nutrients to the sediment bed, and geomorphology of estuaries, river deltas, and continental shelves (Van Leussen, 1994; Ayukai and Wolanski, 1997; Hill et al., 2000; Sanford et al., 2005). Fine sediment dynamics are also important factors in engineering studies of navigation and dredging, contaminant transport, and ecosystem restoration (Tsai et al., 1987; Mehta, 1989; Santschi et al., 2005; Smith and Friedrichs, 2010).

The fragile nature of flocs requires in-situ sampling in order to accurately characterize their properties under field conditions (Gibbs and Konwar, 1983; Van Leussen and Cornelisse, 1993; Fennessy et al., 1994; Dyer et al., 1996). In-situ settling velocities have been obtained by gravimetric analysis (Owen, 1976; Cornelisse, 1996), optical methods (Kineke et al., 1989; Agrawal and Pottsmith, 2000), or imaging (Van Leussen and Cornelisse, 1993; Fennessy et al. 1994; Sternberg et al. 1996; Syvitski and Hutton, 1996; Mikkelsen et al., 2004; Sanford et al. 2005; and Smith and Friedrichs 2010). The imaging methods generally employ an underwater video camera that images flocs settling within an enclosed settling column. One advantage of the imaging methods is that settling velocity and two-dimensional size are collected concurrently for individual particles, permitting floc density estimates through application of Stokes settling or modifications of the drag relationship for higher Reynolds numbers (Oseen, 1927; Schiller and Naumann, 1933). Dyer et al. (1996) summarizes concerns with the in-situ devices, which include: floc breakup during sample capture, flocculation by differential settling within the sampler, and fluid circulation within the imaging chamber.

Fluid motions within the settling column of in-situ video devices arise from turbulence introduced during sample capture, thermally induced circulation, volume displacement of the settling particles, and motion of the settling column. Various approaches have been employed to minimize and/or account for fluid motions within the settling columns of in-situ video systems. Van Leussen and Cornelisse (1993) and Fennessy et al. (1994) employ separate sample collection and settling chambers and additionally introduce density stratification within their settling chamber to damp turbulence introduced during sample collection. This approach has resulted in general success in their systems, but Van Leussen and Cornelisse (1993) and Fennessy et al. (1994) indicate that fluid motions are still apparent in some of their experiments. To address these fluid motions, Van Leussen and Cornelisse (1993) adjust the settling velocities of large particles with fluid motions estimated by manually tracking the smallest visible particles as a surrogate for fluid motions. The two-chamber approach has an additional advantage in that particles from the capture/stilling chamber settle into clear water, which permits settling velocity estimates in high suspended sediment concentrations that would otherwise be too turbid for image acquisition.

The two-chamber devices have a significant disadvantage associated with the long measurement period required to permit particles with small settling velocities to reach the imaging zone within the settling column. For applications that require rapid measurement, such as within dredge plumes or vertical profiling experiments, the 30-40 minute measurement period limits vertical and temporal resolution of the measurements. Smith and Friedrichs (2010) developed the Particle Imaging Camera System (PICS) with a single capture and settling chamber and adopted the approach of Van Leussen and Cornelisse (1993), using the motions of the smallest visible particles as surrogates for fluid motion. Smith and Friedrichs determined the mean fluid motion from manually tracking 10 particles distributed in time and space within their image sequences. While this approach was considered better than neglecting the fluid motions, the manual tracking method is tedious, labor-intensive, and contributes a relatively large source of error in the settling velocity estimates (primarily from the time- and space-averaging of the fluid motions). An automated approach to quantifying fluid motions within the settling column, as suggested by Van Leussen and Cornelisse (1993), is sought to permit rapid sampling for a single-chamber video settling column with greatly reduced measurement error.

Particle Tracking Velocimetry (PTV) and Particle Image Velocimetry (PIV) are two image analysis methods commonly employed in fluid dynamics research. The PTV method involves tracking of individual particles, whereas PIV involves correlating motions of groups of particles. Image processing for cohesive sediment settling experiments has been predominantly confined to PTV methods, both manual (Van Leussen and Cornelisse, 1993; Fennessy and Dyer, 1996; Sanford et al. 2005; Manning and Dyer, 2002) and automated (Lintern and Sills, 2006; Smith and Friedrichs 2010). This paper describes an automated image processing method using both PTV and PIV methods to determine cohesive sediment fall velocities from in-situ video devices.

2 METHODS

The image processing methods described here were developed for the PICS (Smith and Friedrichs, 2010), but should be generally applicable to other similar systems. PICS consists of a single-chambered, 5-cm inner diameter settling column which captures

and images particle settling from a minimally disturbed suspended sediment sample. Following sample capture, turbulence within the column is allowed to dissipate (approximately 15-30 seconds) and a 30-second image sequence is collected at approximately 10 fps. The imaged region within the settling column is approximately 14 mm wide, 10 mm high, and 1 mm deep with resolution of 1360 x 1024 pixels. Image acquisition is accomplished with a monochrome Prosilica GE1380 Gigabit Ethernet camera, 25-mm Pentax c-mount lens, and 15mm extension tube. Additional description of PICS image acquisition and system characteristics is provided by Smith and Friedrichs (2010).

Challenges in analyzing the image sequences from in-situ video devices (such as PICS) include the large numbers of particles to track, the low relative abundance of large particles (which may contain most of the suspended sediment mass (Eisma, 1986; Van Leussen, 1994; Manning and Dyer, 2002; and Smith and Friedrichs, 2010), and fluid circulation within the settling column. The low abundance but large sediment mass fraction of the larger macroflocs (diameter, $d > 150$ μm) requires either large sampling volumes, or long sampling records to obtain statistically significant results. This suggests that large numbers of particles should be tracked in the video sequences. Because manual tracking methods are very labor intensive, automated image processing methods are well-suited for this task.

Two image processing methods are presented that accomplish the tasks of individually tracking larger particles (for settling velocity estimates) and tracking smaller particles for fluid velocity estimates. Large particles are defined here as particles large enough that their size may be determined with reasonable accuracy by image processing techniques. For the present analysis, the commonly applied 3x3 pixel criterion (Milligan and Hill, 1998; Mikkelsen et al., 2004; Lintern and Sills, 2006) is selected, resulting in large particles here having a minimum diameter of approximately 30 μm. Small particles are defined as particles with sufficiently small mass and settling velocity such that their motions approximate that of the fluid in which they are suspended (the small size criteria are discussed in Section 2.2.1). Specific details of the image analysis methods are provided in Sections 2.1 and 2.2; additional general background on PIV and PTV methods are provided in Adrian (1991) and Raffel et al. (2007). All image processing

routines described herein were programmed in Matlab, utilizing the Image Processing Toolbox.

2.1 Particle Tracking Velocimetry (PTV).

Large particles ($d > 30$ μm) were tracked by PTV methods. Several digital image processing operations were applied to the raw images prior to PTV, including background removal, grayscale to binary conversion, and digital erosion and dilation. First, spatial variations in illumination and CCD noise were corrected by subtracting background lighting intensity. Background illumination was determined as the modal (most frequently occurring) illumination intensity for each pixel within a video sequence. The modal pixel intensity effectively identifies the background illumination by identifying the most consistent lighting level for each pixel (including ambient lighting and pixel noise). The background illumination field is determined for an entire image sequence and is subtracted from each image frame prior to additional processing.

Next, grayscale images are converted to binary using a grayscale thresholding method. By this method, pixels with intensities equal to or exceeding the threshold intensity are assigned logical true (1) and those with pixel intensity less than the threshold are assigned logical false (0). Determination of the grayscale threshold is somewhat subjective and is either prescribed by manual inspection for a representative set of image sequences or automatically by the method described by Lintern and Sills (2006). Following the conversion from grayscale to binary, holes within the defined particles are filled by binary dilation and erosion (Gonzalez et al 2004; Lintern and Sills, 2006).

PTV is applied only to particles with equivalent spherical diameters greater than 30 μm . Here we define equivalent diameter as $d = \sqrt{4A/\pi}$, where A is two-dimensional particle area after binary conversion. The 30-μm diameter criterion is consistent with that used by Milligan and Hill (1998) and Mikkelsen et al. (2004), and represents a reasonable lower limit of particle size resolution. Each binary particle meeting the size criterion is labeled and particle metrics are stored (such as centroid position, area, equivalent spherical diameter, major/minor axis lengths, and particle orientation).

The next step in the PTV method is to match particles between adjacent video frames. This is accomplished by comparing an image subset bounding a single particle

(the kernel) in frame I to a larger subset of pixels (the target) in frame $I+1$. The initial target search area in frame $I+1$ is centered at the particle position in frame I and is set arbitrarily large to ensure a particle match (vertical and horizontal extents of the target box are 6 times the particle length and 3 times the particle width, respectively). Example particle kernel and target interrogation areas are provided in Figure 4-1.

A)

B)
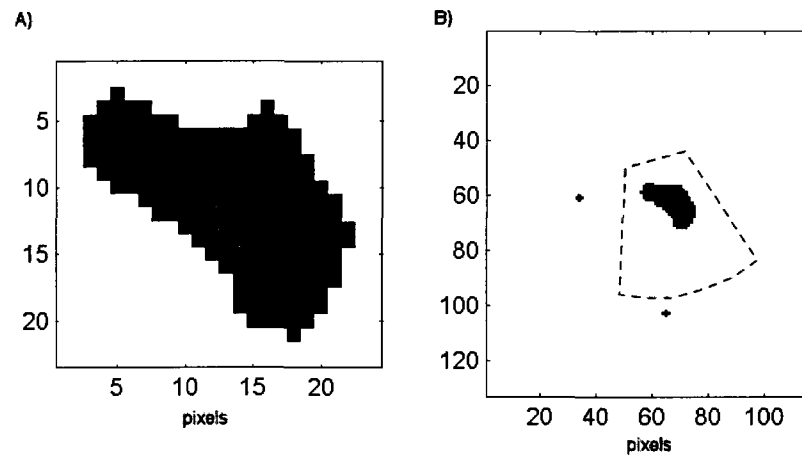
Figure 4-1. Examples of PTV kernel (A) and target (B) image zones with initial (outer rectangle) and reduced search (dashed region) areas for cross-correlation peak.

The peak normalized cross-correlation (Haralick and Shapiro, 1992; Lewis, 1995) of the kernel and target interrogation areas defines the best match between the single particle in frame I to potential matches within the target area in frame $I+1$. The cross-correlation matrix for the kernel and target from Figure 4-1 is presented in Figure 4-2. The location of maximum correlation is evaluated to determine if a valid particle exists at that location and whether its size and shape match that of the kernel particle within acceptable limits. If all of these criteria are met, then the kernel particle and target particles are labeled as matching and forward and backward references (by particle and frame indices) are associated with the matched particles. Once a successful match is determined, the velocity at frame $I+1$ is determined from the particle centroid displacement and frame interval, $V=dX/dt$, where V is the velocity vector, X is particle centroid position vector, and t is time. The velocity history of a particle is used to develop a smaller target interrogation area as shown in Figure 4-1, which reduces the computational requirements and frequency of false matches.
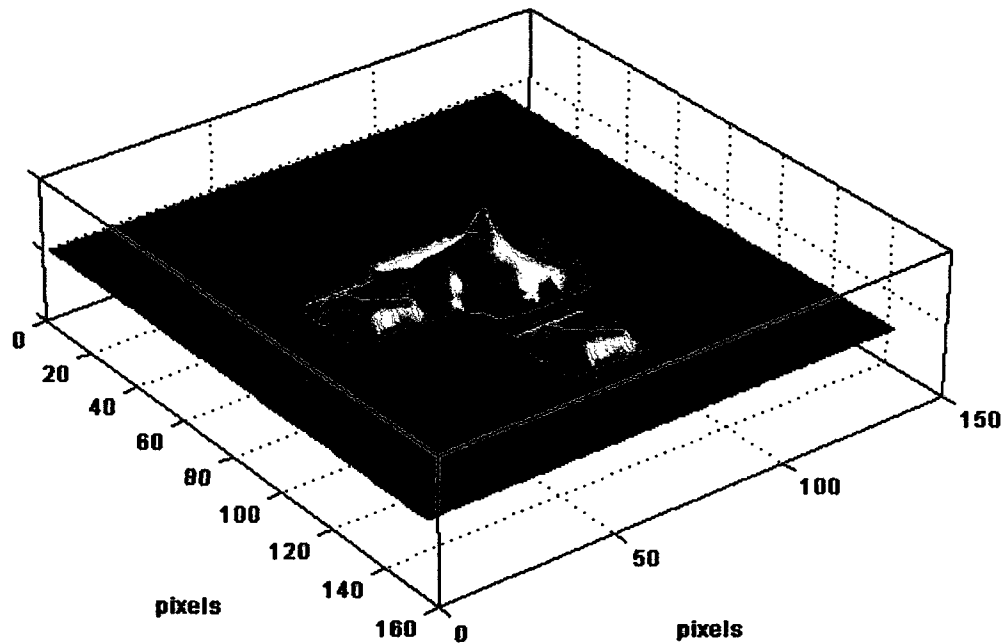
Figure 4-2. Normalized cross-correlation matrix of kernel and target from Figure 4-1.

Upon cycling through an entire video sequence, each frame includes labeled binary particles with information regarding the matched particles in adjacent frames. From this mapping of particle matches, sequences of matched particles following through all frames may be constructed. The ensemble of matches for a single particle across all possible frames is referred to here as a thread. A thread includes descriptive data (such as size, shape, location, velocity) about the single particle as it progresses from frame to frame in the image sequence. The collection of threads provides the basis for determining relationships between particle size, shape, and settling velocity.

2.2 Particle Image Velocimetry (PIV)

Particle velocities determined by the PTV method are relative to the fixed reference frame of the image (or camera). For settling velocity, the particle velocity relative to the fluid is sought, which requires an estimate of the fluid velocity relative to the image frame. A common application of PIV methods is to estimate fluid velocities from the motions of suspended particles sufficiently small to approximate fluid motions. In the present application, PIV will be applied to digitally filtered image sequences

including only small particles to estimate space- and time-variant fluid velocity fields through which the larger particles settle.

2.2.1 Small Particle Selection

PIV tracer particles must be sufficiently small in size, mass, and settling velocity to closely approximate fluid motions. Ideal PIV tracer particles are smaller than the scale of fluid motion to be measured, capable of scattering sufficient light to be detected by the imaging device, and neutrally buoyant (Westerweel, 1993; Raffel et al., 2007). Within video setting columns, we rely on natural tracer particles and the tracer characteristics cannot be tailored to meet experimental requirements. Instead, the natural tracers will be evaluated to estimate the particle size range that meets the application requirements related to frequency response and settling bias.

Frequency response of small particles in accelerating flows is influenced by the excess particle density and drag. The Stokes response time, $\tau_s = d^2 \rho_p /(18\mu)$, is commonly used to evaluate the frequency response of potential PIV tracer particles (Bec et al., 2006, Raffel et al., 2007), where d is particle diameter, ρ_p is particle density, and μ is fluid dynamic viscosity (0.0018 to 0.0008 kg·m^{-2}·s^{-1} for water between 0 and 30°C). For τ_s much less than the time scales of interest, the tracer particles are considered to appropriately follow fluid velocities, with near-equal amplitude and phase (Hjelmfelt and Mockros, 1966). For video settling columns, the small particles to be tracked by PIV methods are individual silt-sized mineral grains ($\rho_p \approx 2700$ kg·m^{-3}) or microflocs composed of clay, silt, and organic matter (1020 $< \rho_p <$ 1500 kg·m^{-3}). Evaluating the limiting case for 30 μm mineral particles, the estimated Stokes response time is 10^{-4} s, much smaller than the 0.5- to 2-s time scales of interest within the settling column.

Because the natural tracers are generally not neutrally buoyant, settling of the tracer particles introduces some degree of bias in the vertical component of the estimated fluid velocities. Stokes settling, $w_s = (\rho_p - \rho_w) g d^2 /(18\mu)$ describes the settling velocity of spherical particles at small particle Reynolds number ($Re_p = w_s d / v \ll 1$), where ρ_w is fluid density, g is gravitational acceleration, and v is fluid kinematic viscosity. Stokes settling velocity was estimated for particles ranging in diameter and

density from 10-30 μm and 1100-2700 kg· m^{-3} (Figure 4-3). For the case in which much of the suspended material is aggregated (and has lower density), the 10-20 μm size range has an estimated settling bias between 4 x 10^{-3} and 2 x 10^{-1} mm·s^{-1}. Numerous studies suggest that in natural muddy environments few suspended particles in the 10-20 μm size range are completely disaggregated (Krank and Milligan, 1992; Mikkelsen and Pejrup, 2000; Droppo, 2004; Smith and Friedrichs, 2010) with particle densities equal to mineral density (2700 kg· m^{-3}). Therefore, in most cases, the settling bias is likely to be within the lower portion of the stated range. Choosing particles smaller than 15 μm will reduce the settling bias, but the gains in doing so are largely offset by the lower light scattering potential and practical limits of resolving such particles with the present optics.
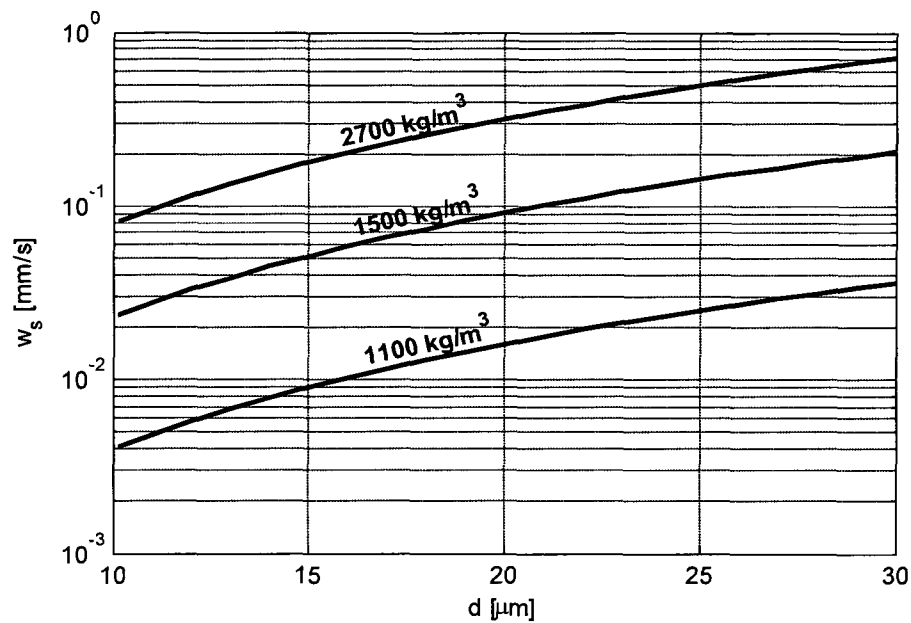
Figure 4-3. Stokes settling velocity estimate for candidate small particle diameters and densities.

2.2.2 Image Processing

The initial step of the PIV analysis includes image pre-processing to remove background illumination, conversion of grayscale images to binary, and region property estimates of the binary image as described in Section 2.1. The resulting binary image is filtered to remove particles with sizes exceeding the small particle criterion. To provide equal weighting of the small particles during cross-correlation, each small binary particle

is replaced with a 3x3 binary representation. The 3x3 representation was implemented to allow some spatial jitter in the frame-to-frame cross-correlation, which was found through experimentation to provide more stable peaks in the cross-correlation than alternate methods.

The PIV method involves binning the image into subregions, or interrogation areas. For the present application, the 1380 x 1024 image frame was subdivided into 10 x 8 interrogation areas with corresponding pixel dimensions of 136 x 128 and spatial dimensions of approximately 1.4 x 1.3 mm. An example image with defined interrogation areas is presented in Figure 4-4A. The inset in Figure 4-4B shows small particles within a single interrogation area. The darker-shaded small particles are from frame I and the lighter-shaded particles are from frame $I+1$.

The interrogation area from frame I is cross-correlated to a larger interrogation area from frame I +1 with 50% overlap. The resulting cross-correlation for the inset interrogation area from Figure 4-4 is presented in Figure 4-5. The peak correlation in Figure 4-5 represents the mean displacement of the small particles between frames I and I +1. Defining the correlation peak in this discrete fashion (based on the pixel location of the peak correlation) limits velocity resolution to 1 pixel/frame interval or approximately 10 μm / 0.1 sec = 0.1 mm/s. While this can be considered sufficient for the present application, sub-pixel resolution of particle displacements is possible through peak-fit estimators to a resolution of better than 0.1 pixel displacement (Westerweel, 1993; Raffel et al., 2007). Implementing a peak-fit estimator to the PIV would then increase the velocity resolution for the PICS to the order of 0.01 mm/s.

The final step in PIV analysis involves detection and replacement of spurious vectors. Spurious vectors result from peak correlations between the kernel and target interrogation areas away from the true displacement vector and generally result from small numbers of tracer particles within the interrogation area. Spurious vectors are readily apparent to the eye as shown in the upper right interrogation area of Figure 4-6A. Research in digital PIV methods has lead to efficient algorithms for detection and replacement of spurious vectors. The normalized median test (Westerweel, 1994; Westerweel and Scarano, 2005) is a robust and computationally efficient method
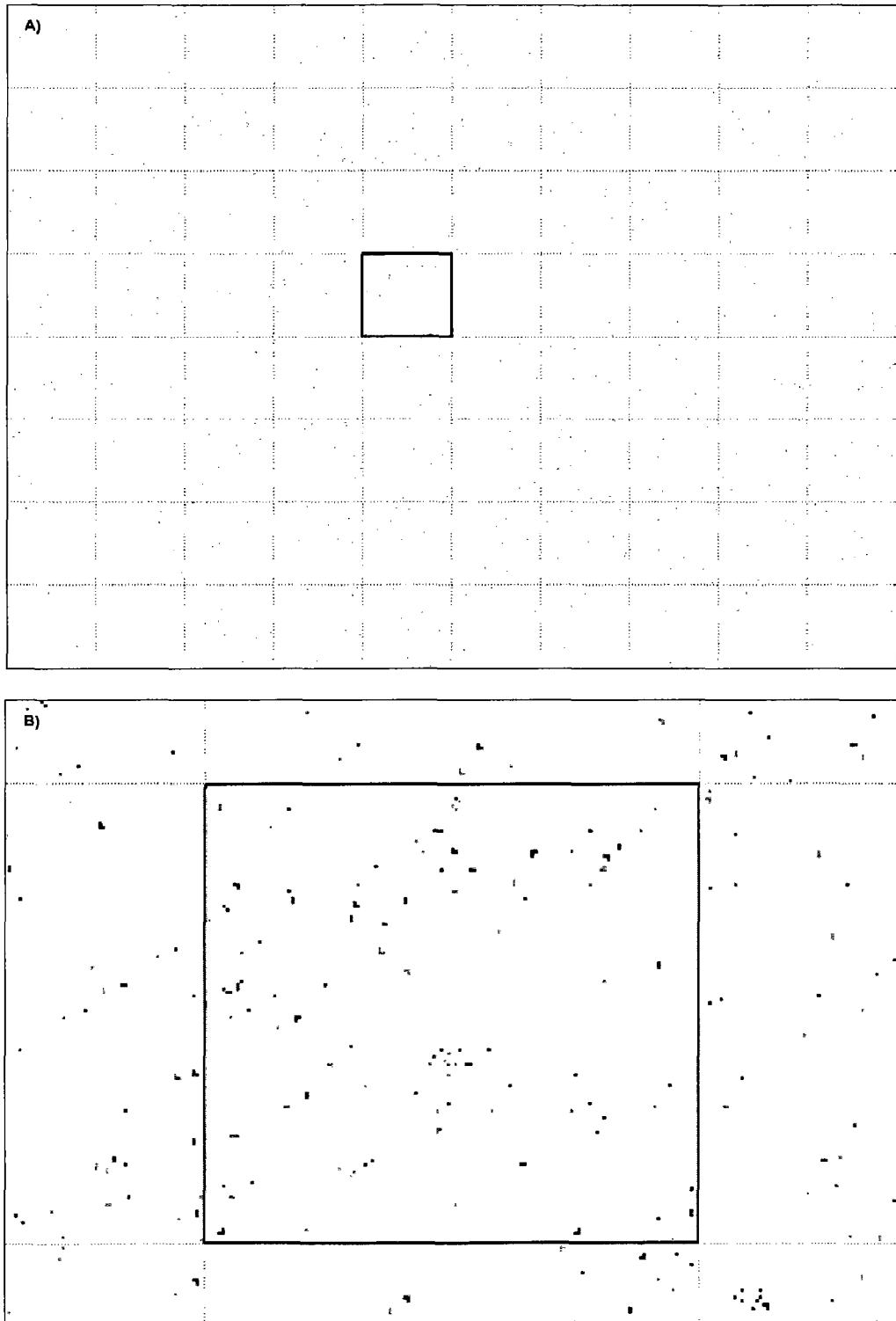
Figure 4-4. A) Image with interrogation areas (1.4 mm x 1.3 mm) for PIV analysis. B) A single interrogation area (from the bold box in A) indicating small particles from two temporally adjacent frames. The lighter-shaded particles are from frame *I* and the darker-shaded particles are from frame *I*+1.
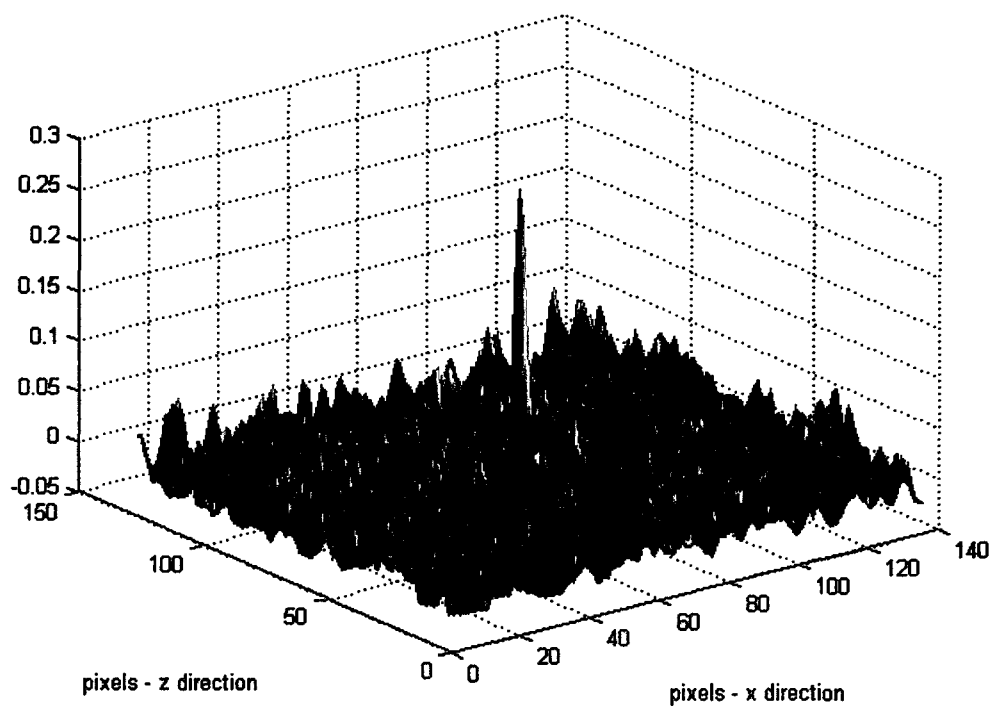
Figure 4-5. Cross-correlation matrix for interrogation area from Figure 4-4. The peak
determines the displacement vector of small particles between frames.
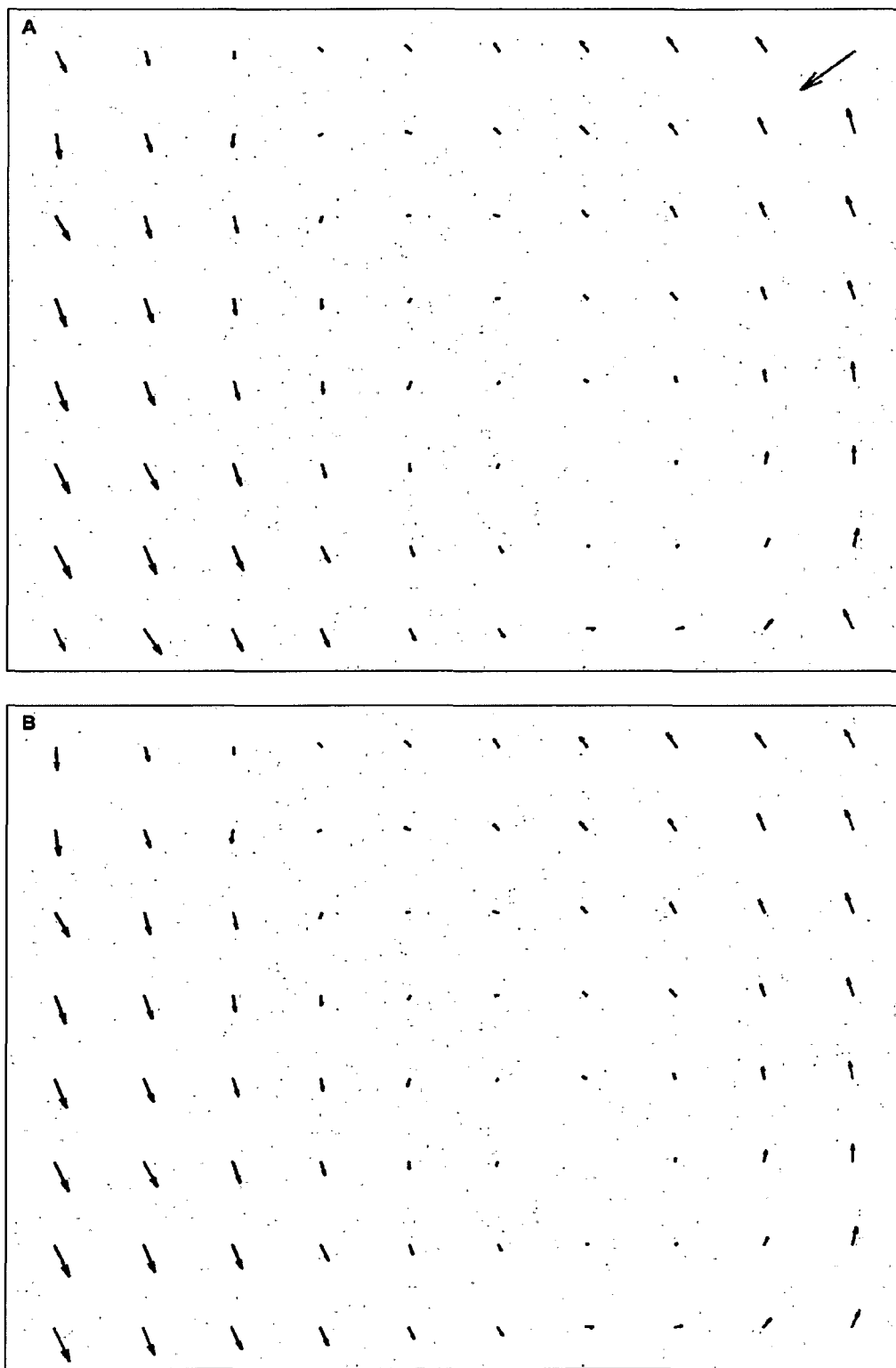
Figure 4-6. PIV determined velocity vectors. Boxes indicate interrogation areas (1.4 mm x 1.3 mm)
A) vectors resulting from the PIV cross-correlation, including spurious vectors (red). B)
vectors following spurious vector detection and replacement (replaced vectors indicated in
red). Maximum velocity in (B) is 1.5 mm/s.

for detecting spurious vectors. The normalized median test detects spurious vectors by identifying large local deviations in velocity field compared to neighboring interrogation areas. A particular strength of the normalized median test is that a single detection threshold may be developed and applied to a wide range of flow conditions for a particular application. For the present application, the user is required to experimentally determine the detection threshold until satisfactory results are obtained. The experimentally determined threshold can then be applied generally for a set of settling experiments.

Replacement of spurious vectors is accomplished through a two-step process in the spatial and temporal domains. In the spatial domain, spurious vectors detected with the normalized median test are replaced with an inpainting method. Digital inpainting is a method developed for image restoration for which corrupted portions of an image are smoothly filled based on the neighboring valid portions of the image. The numerical basis for the inpainting method applied here is numerical solution of the Laplacian, $\nabla^2 U = 0$, for detected spurious vectors. This approach is particularly well suited for fluid dynamics applications as it follows potential flow theory – albeit in only two dimensions. The code implemented in the PICS image analysis software is INPAINT_NANS, authored by John D'Errico. The spatially replaced spurious vectors are then analyzed for outliers in the time domain, which are replaced by linear interpolation. In Figure 4-6B, the seven spurious vectors of Figure 4-6A have been detected and replaced.

2.2.3 PIV Limitations

A potential limitation of the PIV method for fluid velocity estimates inside video settling columns is tracer concentration. Adrian (1991) and Raffel et al. (2007) suggest that PIV analysis requires a minimum seeding level of five particles per interrogation area. In the natural environment, the operator has little control on the abundance of small tracers. Most settings with suspended fine grained sediments have sufficient fine particulates for PIV analysis, but imaging these particles may prove challenging due to image resolution, lighting, or sensor limitations. First, the optical magnification should be sufficiently large to resolve the largest of the tracer particles with 2-4 pixels. To

maximize small particle detection, a high-quality, low-light sensitive, low-noise camera and sufficient lighting are essential. Additionally, adjustments of the camera sensor gain and/or lighting intensity may be required to utilize the full range of digital image intensity (bit depth) recorded by the camera. Further discussion of imaging requirements is provided in Section 3.6.

Additional limitations of the PIV method include: velocity resolution, spurious vector detection and replacement, and tracer settling bias. The PIV methods described above are relatively simple and could be implemented with commercial or open-source PIV software. Potential improvements to the methods presented in Section 2.2.2 include saving alternate cross-correlation peaks and application of sub-pixel displacement resolution. Saving of alternate peaks from the cross-correlation matrix would permit evaluation of these peaks during spurious vector replacement, reducing the number of inpainting replacements. Application of Kalman filtering for alternate peak detection based on velocity history (as with the PTV methods) could assist in identifying the most likely peaks in the correlation matrix. Application of sub-pixel displacement resolution through peak-fitting functions would permit greater velocity resolution by approximately one order of magnitude. These suggested improvements will increase robustness and precision of the PIV velocity estimates, but do not address settling bias. In the proposed application, settling bias is difficult to estimate precisely, given the unknown settling velocity of the small tracer particles.

2.3 Fluid-Referenced Settling Velocities

The PTV velocities of large particles (Section 2.1) and the PIV velocities of small particles (Section 2.2), which approximate fluid motions within the image plane, are used to estimate relative motions of the large particles to the surrounding fluid. The relative motion of the large particles to the surrounding fluid is given by:

$$\mathbf{V}_r(t) = \mathbf{V}(\bar{x}, t) - \mathbf{u}(\bar{x}, t) \tag{1}$$

where, V_r is the time-dependent, velocity of the particle relative to the fluid, V is the space- and time-dependent velocity of the particle (in the fixed reference frame relative to the camera), u is the space- and time-dependent fluid velocity (also in the fixed reference

frame), and $\bar{x} = x\hat{i} + z\hat{k}$ is 2-D spatial position. The fluid velocity components, u_x and u_z, are estimated by bi-linear interpolation at each particle centroid from the PTV results throughout the image sequence. (The velocity field is extended to the image boundaries with the inpainting method described in Section 2.2.) The settling velocity (vertical component of the particle velocity relative to the fluid) is then defined as:

$$w_s = \frac{\Delta z}{\Delta t} - w_f \tag{2}$$

where Δz is vertical displacement of the particle centroid, Δt is the elapsed time over which the particle was tracked, and w_f is the vertical fluid velocity component.

2.4 Measurement Uncertainty.

Measurements with video-based methods for estimating particle size, settling velocity, and particle density are subject to measurement uncertainties. Smith and Friedrichs (2010) evaluated uncertainties for the PICS associated with random and independent experimental errors using a small set of manually tracked particles to determine the mean fluid velocity. This section assesses measurement uncertainty of the automated PIV-based fluid velocity estimates, following the methods presented in Smith and Friedrichs (2010).

2.4.1 Settling velocity.

Estimated settling velocity (Eqn (2)) depends upon measured particle translation, elapsed time over which each particle was successfully tracked, and estimated vertical fluid velocity. Uncertainties associated with each of the measured parameters contribute to the settling velocity uncertainty as:

$$\delta w_s = \sqrt{\left(\frac{\partial w_s}{\partial(\Delta z)}\delta(\Delta z)\right)^2 + \left(\frac{\partial w_s}{\partial(\Delta t)}\delta(\Delta t)\right)^2 + \left(\frac{\partial w_s}{\partial(w_f)}\delta(w_f)\right)^2} \tag{3}$$

assuming independent and random measurement uncertainties (Taylor, 1997). Within this expression, δ indicates the measurement uncertainty for the given parameter and partial derivatives were derived by differencing Eqn (2). Parameter uncertainties, $\delta(\Delta z)$ and $\delta(\Delta t)$, were determined experimentally (Smith and Friedrichs, 2010) to be about 10^{-2}

mm, and 10^{-5} sec, respectively. Uncertainty in the PIV-estimated fluid velocity was determined from numerical experiments with a sinusoidal vertical velocity field with 2 mm s^{-1} amplitude and 4.3 s period. Randomly placed small particles (with zero settling velocity) were transported within this velocity field, converted to digital video, and tracked by the PIV software. The PIV-estimated velocities were then compared to the prescribed velocities, resulting in an RMS error, $\delta(w_f)$, of 0.025 mm s^{-1}.

Applying the determined parameter uncertainties to Eqn (3) gives an uncertainty in w_s equal to 0.026 mm s^{-1}. The PIV-estimated fluid velocity is the largest contributor of random uncertainty at 96 percent, followed by the particle positioning uncertainty (4 percent), and the negligibly small timing uncertainty. Relative settling velocity uncertainties ($\delta w_s/w_s$) for the automated and manual PIV methods were determined by normalizing Eqn (3) with settling velocity (Figure 4-7). The automated PIV method significantly reduces (by factor of 7) the settling velocity measurement uncertainty over the manual fluid velocity method. Relative uncertainty levels of 0.1, 0.5, and 1 are associated with settling velocities of 0.26, 0.05, and 0.026 mm·s^{-1}, respectively.
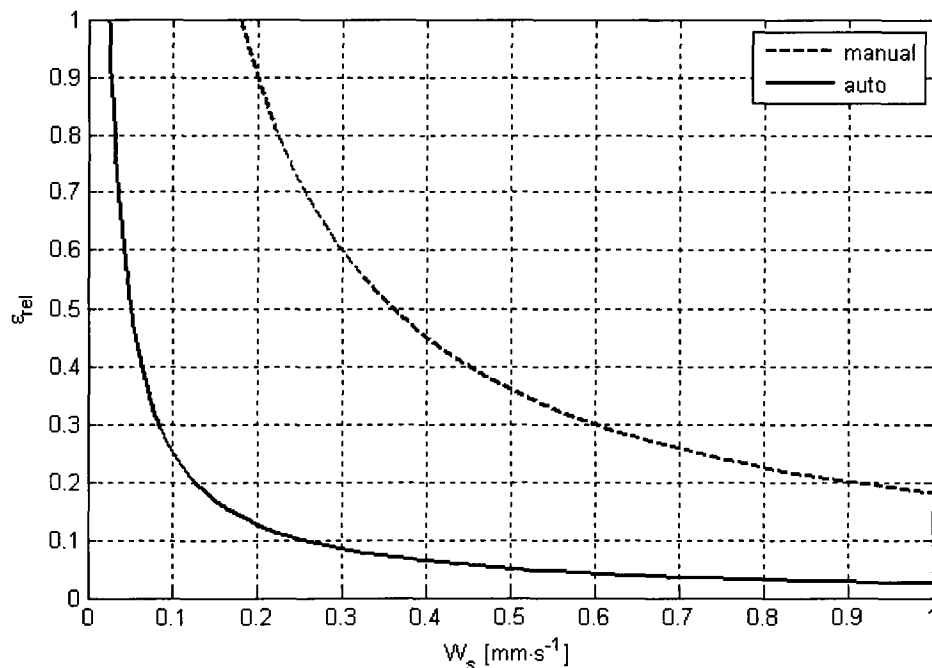

Figure 4-7. Relative error ($\varepsilon_r = |\delta w_s / w_s|$) in settling velocity estimate for manual method (Smith and Friedrichs, 2010) and automated PIV method.

2.4.2 Excess density

Smith and Friedrichs (2010) rearranged Soulsby's (1997) empirical settling velocity expression to estimate excess particle density

$$\rho_e = \rho_p - \rho_w = \frac{\rho_w v^2}{gK_2 d^3}\left[\left(\frac{w_s d}{v} + K_1\right)^2 - K_1^2\right]$$

(4)

where ρ_p is particle density, ρ_w is water density, v is kinematic viscosity, g is gravitational acceleration, d is particle diameter, $K_1 = 10.36$ and $K_2 = 1.049$. By Eqn (4), excess particle density is estimated from measurements of settling velocity, particle diameter, fluid density, and fluid viscosity. Assuming uncertainties in fluid density and viscosity are small and uncertainties in settling velocity and particle size are independent and random, the uncertainty in excess density is given by:

$$\delta\rho_e = \sqrt{\left(\frac{\partial\rho_e}{\partial w_s}\delta w_s\right)^2 + \left(\frac{\partial\rho_e}{\partial d}\delta d\right)^2}$$

(5)

where the partial derivatives refer to terms in Eqn (4). The relative error in excess density was determined by applying the previously determined uncertainties, $\delta w_s = 0.026$ mm·s^{-1} and $\delta d = 0.02$ mm (Smith and Friedrichs, 2010) and normalizing the result ($\delta\rho_e / \rho_e$) (Figure 4-8). The largest uncertainties are associated with small, slowly settling particles. For macroflocs ($d > 150$ μm) settling faster than 0.1 mm·s^{-1} relative error in excess density is less than 0.35.

3 RESULTS AND DISCUSSION

To demonstrate the PTV and PIV methods described in Section 2, they are applied here to a single settling velocity video (of 33 total) conducted within a clamshell dredging plume in Boston Harbor on September 11, 2008. The dredged bed material at the site was characterized as 54 percent sand, 37 percent silt, and 9 percent clay. The PICS water sample was collected and image acquisition performed approximately 60 m down current from the dredging source at a depth of 10 m below the water surface. Image acquisition began approximately 20-40 sec following collection of the PICS water sample, and images were recorded at 8 frames per second for 30 sec (240 frames). In the
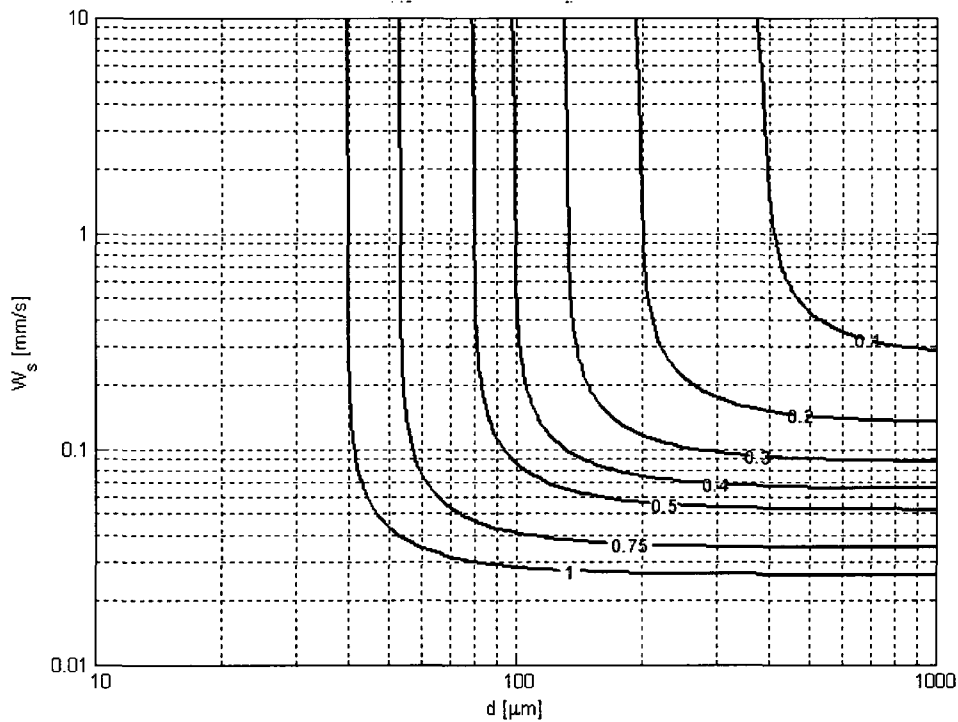
Figure 4-8. Contours of excess density relative error ($\varepsilon_r = |\delta\rho_e / \rho_e|$) for automated PIV method.

following sections, the results and performance of the PTV and PIV are examined and compared to alternate image processing methods.

3.1 PTV Particle Tracking

PTV processing was performed on the image sequence. Background illumination was defined as the modal illumination level for each pixel sampled randomly from 50 frames. Grayscale thresholding was determined by the automatic thresholding method of Lintern and Sills (2006), resulting in a grayscale threshold of 13/255, and the minimum particle size for PTV tracking was set to 30 µm. For the 240 image frames, 2785 particles were tracked with thread lengths greater than 4 frames (0.5 seconds). Particles ranged in size from 32 to 550 µm, with vertical velocities (positive upward) ranging from -9.9 to 4.6 mm/s, and thread lengths from 4 to 145 frames.

An example of particle image pairs and PTV-estimated particle velocities is presented in Figure 4-9. To more clearly indicate particle displacements, particles are shown from frames I and $I+3$, resulting in a frame interval of 0.375 sec. All imaged
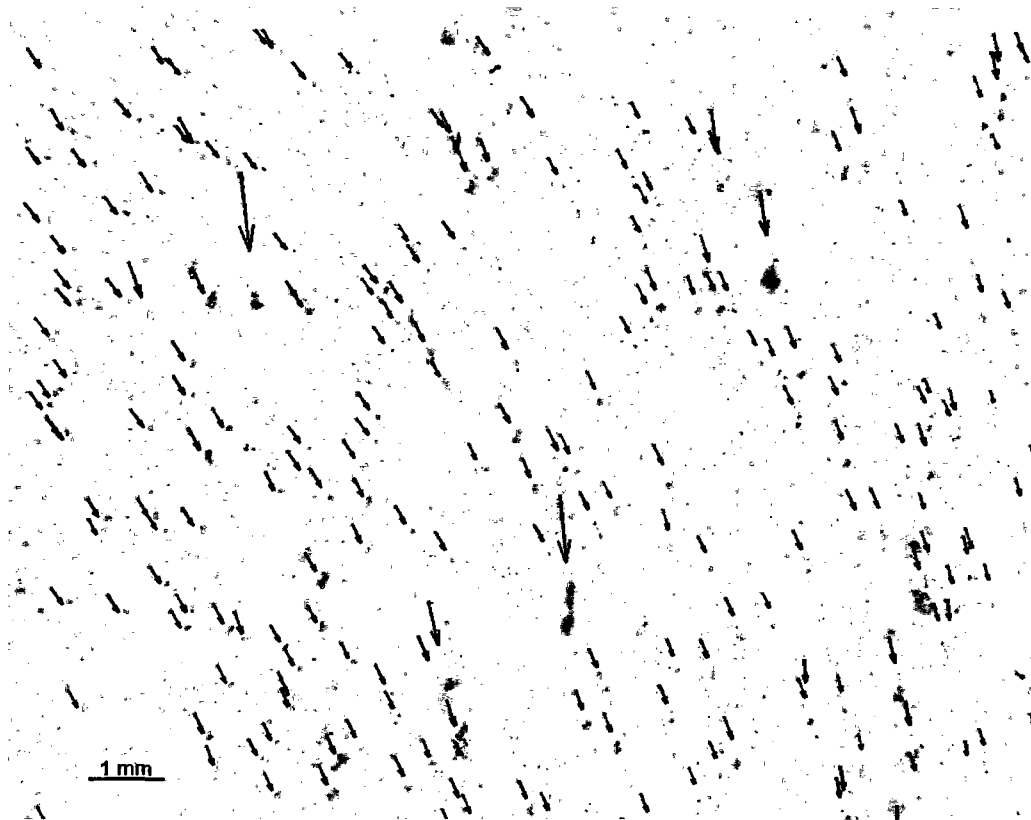
Figure 4-9. Particle images and displacement vectors from PTV analysis. Particle displacements are indicated from two superimposed image frames (separated by 0.375 sec). Particle images are negative representations of the raw images with logarithmic intensity scaling. Particle intensity from the first image is decreased by 25 percent to better indicate direction of motion. Vector lengths are scaled for display purposes and do not correspond to the length scale provided.

particles (including those not resulting in a particle thread) are shown, and image intensities are displayed with a logarithmic scale to effectively visualize the large, bright particles and smaller, dimly illuminated particles. The velocity vectors for displacements between frames I and $I+1$ are positioned on the tracked particles from frame I. In Figure 4-9, the influence of fluid motions on the settling particles is evident by comparing the directions of the more slowly settling particles to the faster settling particles, which reinforces the requirement to adjust particle settling velocities with estimates of fluid motion.

3.2 PIV Fluid Velocity Estimates

PIV analysis was performed on the small particles in the image sequence to estimate fluid velocities within the image plane. The background illumination determined during the PTV analysis was subtracted from all image frames, followed by grayscale to binary conversion with a threshold of 4/255 (to better define the fainter small particles). Only binary particles smaller than 21 μm were retained for the PIV analysis.

The PIV interrogation areas were established as a 10x8 grid (136 x 128 pixels or 1.46 x 1.37 mm) with 50% overlap for the second of the image pairs. Spurious vectors were detected with the normalized median test (Westerweel and Scarano, 2005) on a 3x3 interrogation area neighborhood without boundary buffering. Spurious vector replacement in the space- and time-domains was performed as described in Section 2.2. The PIV analysis results in 19200 velocity vectors of which 1392 (7 percent) were detected and replaced as spurious. The mean vertical fluid velocity estimated from the PIV analysis was -0.30 mm/s (downward) with a probability distribution as defined in Figure 4-10. The negative (downward) mean fluid velocity in this example represents the average fluid motion within the central portion of the settling column cross-section. Mean fluid velocities at the imaging plane were both positive and negative during this field experiment (see Figure 4-11).
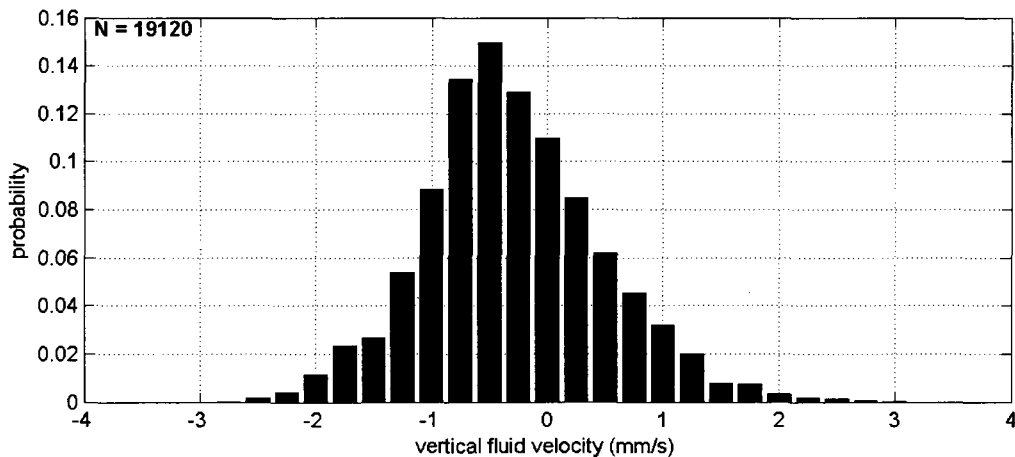
Figure 4-10. Histogram of vertical fluid velocities from a single image sequence (240 frames). Mean vertical velocity is -0.3045 mm/s (downward).
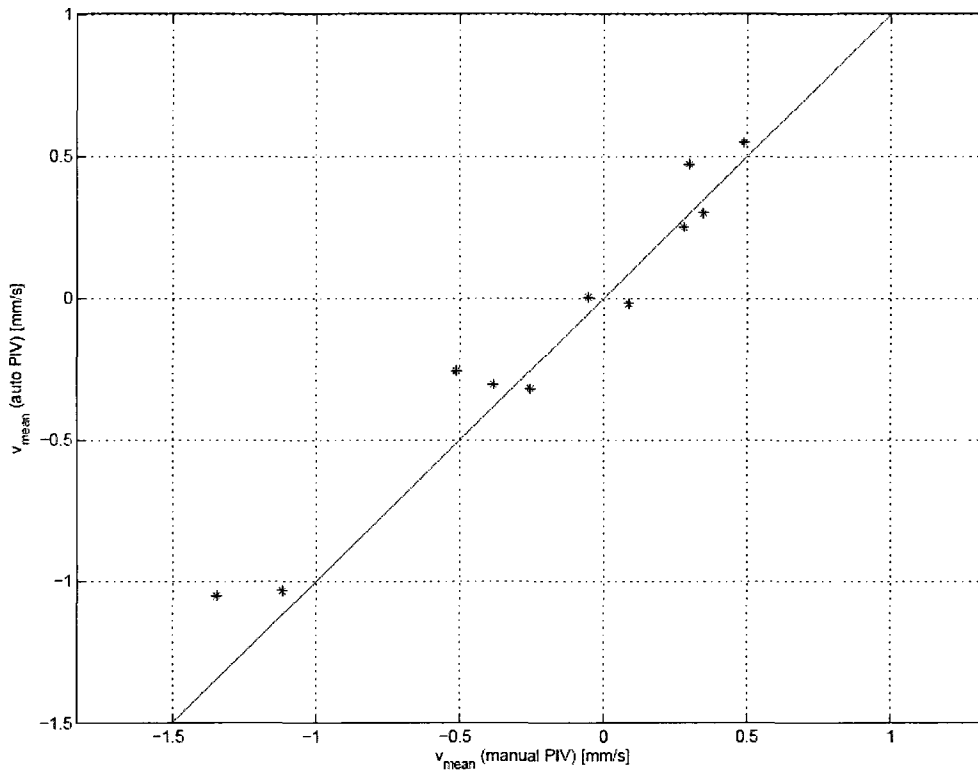
Figure 4-11. Comparison of mean vertical fluid velocities determined from automatic PIV and manual PIV methods for 11 image sequences.

Manual tracking of small particles using the method described by Smith and Friedrichs (2010) was performed on the example image sequence. By this method, ten small particles (uniformly distributed in space and time) are selected and tracked manually to determine the mean vertical fluid motions. The manual tracking method results in a mean vertical velocity of -0.38 mm/s (compared to -0.30 mm/s by the automated PIV method). Additionally, mean vertical fluid velocities were estimated by the manual tracking method for eleven of the image sequences collected from the Boston Harbor field experiment and compared to the automated PIV method (Figure 4-11). The comparison reveals that the manual method results in a reasonably accurate mean fluid velocity from a small sample of particle velocities. Most results of the manual method are within 0.1 mm/s of the automated method, but a few experiments are in error by as much as 0.2 to 0.3 mm/s. The larger of these differences are relatively large compared to the settling velocities of interest (on the order of 0.1 to 0.5 mm/s).

3.3 Settling Velocity

Settling velocities of flocs and bed aggregates (the larger particles) are corrected with the spatially and temporally variant fluid velocities estimated from the PIV analysis as described in Section 2.3. Three individual particle threads from the PTV analysis are selected to illustrate the PIV corrections to PTV velocities to result in fluid-relative settling velocities. Figure 4-12 provides PTV particle velocity, PIV fluid velocity, and net settling velocity for particles of 51, 100, and 200 um. Each of these particles was settling through a time- and space-variant velocity field. Vertical fluid oscillations were induced by vessel motions associated with wind waves and passing vessel wakes, resulting in peak vertical fluid velocities on the order of 1-2 mm·s^{-1}. Particle velocities largely follow the fluid velocities with a negative (downward) bias reflecting the particle settling velocity. Subtracting the fluid velocity from the particle velocity results in a near-constant settling velocity of the particles relative to the fluid.

Improvements gained through automated PIV determination of time- and space-variant fluid velocities are quite apparent in comparing the settling velocity estimates for all tracked particles (Figure 4-13). In Figure 4-13A, PTV particle velocities were corrected with the mean vertical fluid velocity estimated by the manual method (manually tracking 10 small particles); Figure 4-13B provides the settling velocities corrected with PIV-estimated fluid velocities for the same image sequence. The automated PIV method effectively reduces the spread in settling velocity by accounting for the variance in vertical fluid velocity. The bin-averaged (by particle size) settling velocities between the two methods are generally consistent, especially for the larger, faster-settling particles. Figure 4-14 presents a direct comparison of the bin-averaged settling velocities between the two methods. The negative bias of the manual method relative to the automated method is attributed to the larger estimate of mean fluid velocity (-0.38 mm/s versus -0.30 mm/s) by the manual method. Otherwise, the bin-averaged settling velocities determined with the manual method are comparable to the automated PIV method.

Thread Number: 4810 (38); d= 51 μm; X=13.2 mm; $w_{s\,mean}$ = 0.34 mm/s

Thread Number: 644 (55); d=100 μm; X=10.2 mm; $w_{s\,mean}$ = 0.62 mm/s

Thread Number: 3533 (82); d=200 μm; X= 9.2 mm; $w_{s\,mean}$ = 0.57 mm/s
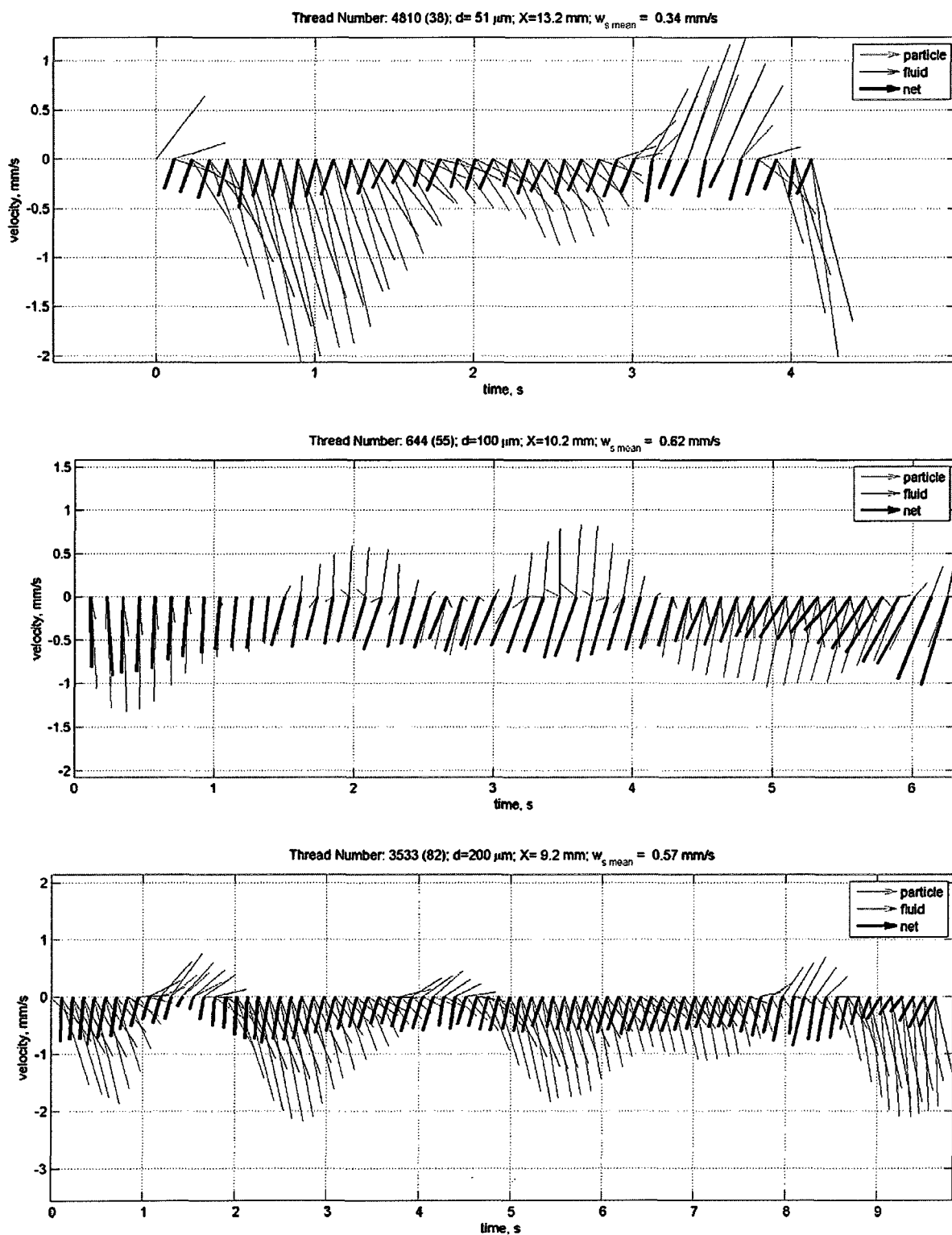
Figure 4-12. Time-series velocities for three tracked particles of size 51, 100, and 200 μm. Vectors indicate particle velocity (red), local fluid velocity (blue), and net velocity (black).

Figure 4-13. Settling velocity versus particle diameter. A) corrected with mean vertical velocity estimated from 10 manually tracked small particles, B) corrected with fluid velocities estimated by PIV method. N=2785 tracked particles, filled diamonds indicate bin-averaged velocities for bins with 3 or more particles, dashed lines indicate +/- 1 S.D.
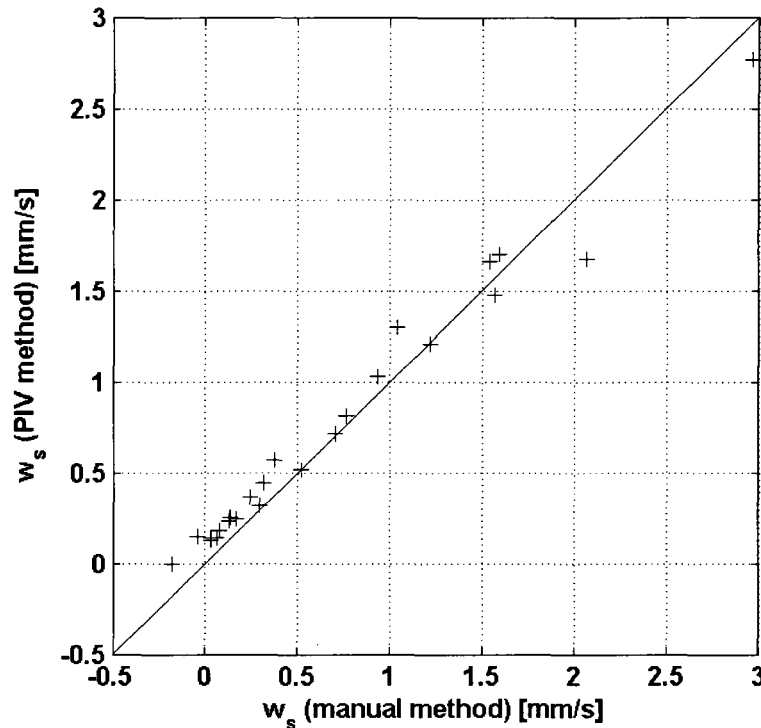
Figure 4-14. Comparison of bin-averaged settling velocities with manual and automatic PIV methods for particle tracking data from Figure 4-13.

3.4 Particle Density

A further benefit of the automated PIV method is more accurate estimation of individual particle densities from the combined particle size and settling velocity information (Figure 4-15). Particle densities were estimated using settling velocities corrected with the manual method (Figure 4-15A) and the automated PIV method (Figure 4-15B). As seen with settling velocity, the automated PIV method analogously reduces the spread in particle density by accounting for spatial and temporal variation in the vertical fluid velocity. Variations in manual and PIV estimates of particle density are similar for particle sizes larger than 200 μm, but the manual method results in significantly greater variance (by a factor of 2-5) for particle sizes smaller than 100 μm. Differences between the automatic-PIV and manual-method estimates of particle density (bin-averages) are presented in Figure 4-16. The differences are small for particles larger than 100 μm. For particle diameters between 50-100 μm, density differences between 10-60 kg·m^{-3} are attributed to differences in estimated mean fluid velocity (Figure 4-14).
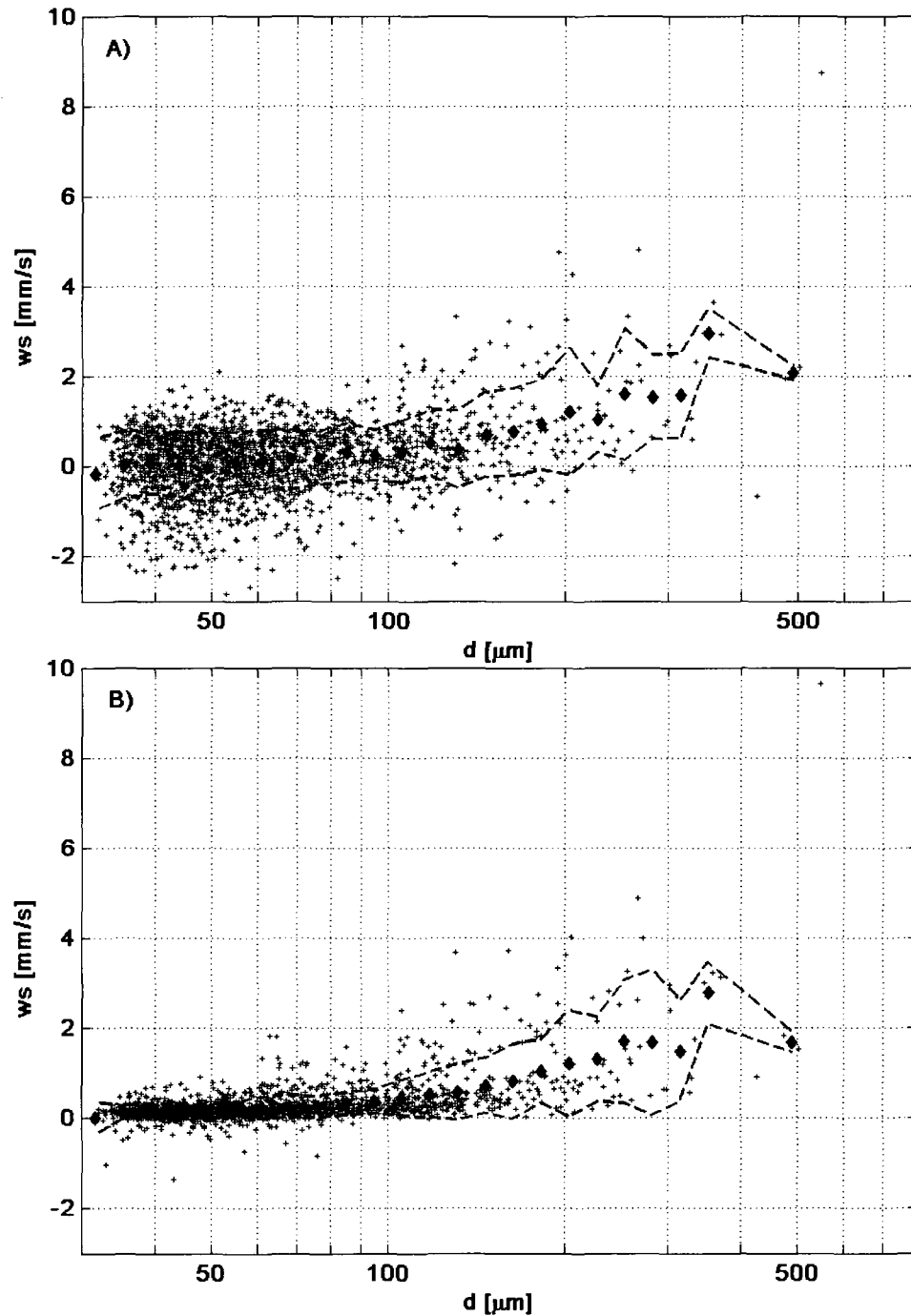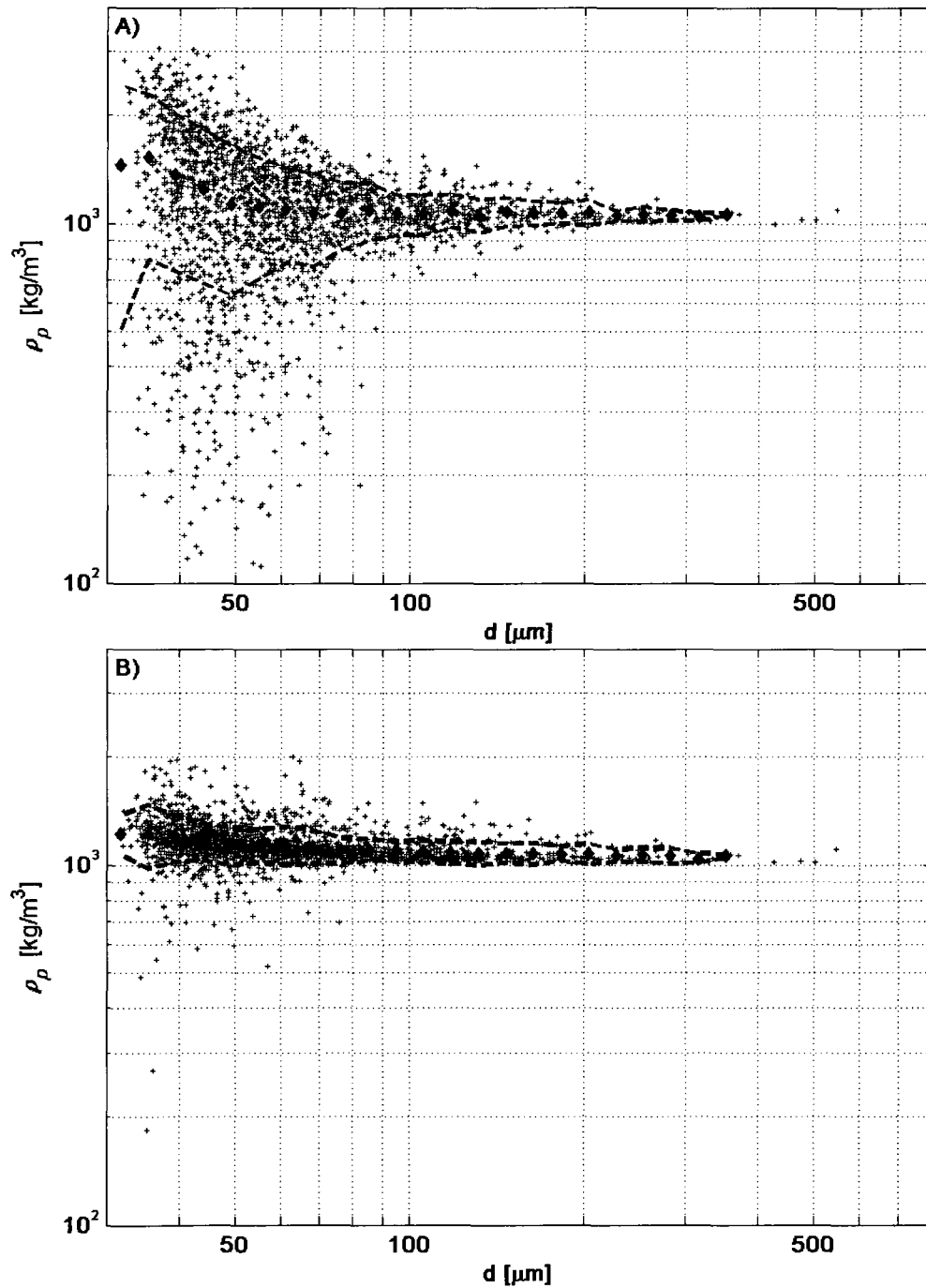
Figure 4-15. Particle density versus particle diameter. A) corrected with mean vertical velocity estimated from 10 manually tracked small particles, B) corrected with fluid velocities estimated by PIV method. N=2785 tracked particles, filled diamonds indicate bin-averaged densities for bins with 3 or more particles, dashed lines indicate +/- 1 S.D.
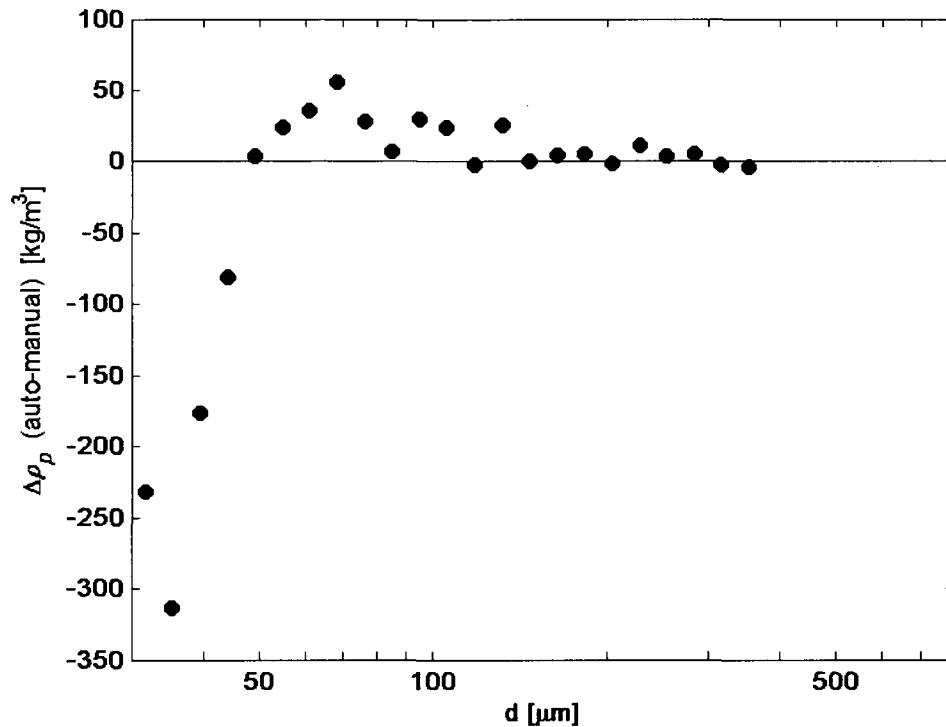
Figure 4-16. Difference between bin-averaged (by size) particle densities between manual and automatic PIV methods for particle tracking data from Figure 4-15.

The manual correction method estimates larger densities for particle diameters less than 50 μm, which is a data processing artifact associated with exclusion of negative densities from the analysis.

3.5 Computational Requirements

Fully automated PTV and PIV image analysis greatly reduces the time required to analyze video settling column images compared to manual or semi-automated analysis. The following discussion defines the computational effort required for the automated methods with presently available computing hardware. The automated analysis presented herein was performed on a system with dual 2.66 GHz Intel® Xeon® E5430 quad-core processors and 3GB of RAM. The PIV and PTV analyses were written and executed in Matlab®, utilizing the Image Processing Toolbox™ for most image processing functions.

Computational requirements for PTV analysis depend upon the number, size, and settling velocity of tracked particles and number of frames in the video. Most of the computational load is associated with the normalized image cross-correlations performed

during the particle matching process. The computational load for this process is dependent upon the number of matches required and the size of the kernel and target images. Wall clock times to complete PTV analysis on a 1380 x 1024 video with 240 frames range between 2-20 minutes. Time required to track 1000 particles over 240 frames is generally 5-8 minutes.

Computational requirements for PIV analysis are dependent upon image size, number of frames, and subdivision level. Similar to PTV analysis, most of the computational load is associated with the kernel-template matching with normalized image cross-correlation. PIV analysis on 1380 x 1024 video with 240 frames and 10 x 8 image subdivision took approximately 50 minutes to complete.

Manual processing is labor intensive, requiring the user to match particles between adjacent frames, determine particle size, and estimate settling velocity. Semi-automated processing routines (for which the user determines particle matching and image processing routines determine particle size and settling velocity) reduce processing time but still demand substantial human resources compared to fully automated methods. Semi-automated PTV analysis takes approximately 1-2 minutes per particle, and fluid velocity estimates require another 2-3 minutes per particle. By these estimates, tracking 1000 particles in a 240-frame image sequence would require approximately 50-80 hours of human interaction, compared to less than 1-minute of human interaction and 1 hour of computer time for the fully automated PTV/PIV method presented here.

3.6 Application Requirements and Limitations

PTV and PIV processing require high-quality images. To apply the automated PTV and PIV image processing routines described in this chapter, the imaging system design should address several key requirements including: magnification, resolution, light intensity, and frame rate. First, the acquired images should have sufficient magnification to resolve the largest of the small PIV tracer particles with 2-4 pixels. At high magnification (near 1:1), lens quality is important and balancing depth-of-field and diffraction limits becomes challenging. Increasing magnification also reduces the field of view (sample size). Sample size reduction is undesirable for imaging of macroflocs, which generally occur in low abundance but contain large sediment mass. Image size

and magnification should be balanced such that the small PIV tracers are sufficiently resolved while maximizing the sample volume to capture the largest numbers of particles for PTV particle tracking and analysis. Magnification and frame rate also influences the maximum resolvable particle velocities by PTV. Frame rate should be sufficiently fast to capture approximately 5 particle images for the fastest settling particles.

Light intensity and contrast are key elements for PIV and PTV analysis. The imaging sensor must receive sufficient reflected light from a wide range of particle sizes in suspension with sufficient contrast to discern these particles from reflected and scattered light within the settling column. The small PIV tracer particles represent a particular challenge, given their low-intensity reflections. Factors influencing light intensity registered by the image sensor include: lighting intensity, lens size, light reflection by viewing ports and lens elements, extension tubes, image sensor fill factor and quantum efficiency. Use of high-intensity and focused lighting, high-quality lenses with anti-reflective coatings, and high-sensitivity, low-noise image sensors addresses many of these issues. Contrast between the imaged particles and surrounding fluid can be improved by reducing internal reflections and light scattering surfaces within the settling column. Additionally, the dynamic range (bit depth) of recorded images should be fully utilized through adjustment of the lighting source or camera gain, keeping in mind that camera gain also amplifies sensor noise.

Light scattering and particle obscuration increase with increasing suspended sediment concentration. The smaller and less bright PIV tracer particles are impacted at lower concentrations than larger PTV-tracked particles. Concentrations at which PIV and PTV analysis are impacted are dependent upon particulate size and degree of aggregation. Experience with the PICS suggests that suspended sediment concentrations between 50 mg/L (for disaggregated fine silt) and 300 mg/L for well-aggregated suspensions can impact image analysis.

4 SUMMARY AND CONCLUSIONS

Fluid motions within video settling columns have been a persistent challenge that in many cases limits the experimental potential of such devices. Researchers (Van Leussen and Cornelisse, 1993; Fennessy et al. 1994) have employed physical measures

such as separate capture and settling chambers, reductions in thermal input, and introduction of density gradients to damp turbulence and reduce fluid motions. Additionally, efforts have been made to quantify fluid motions by manually tracking small particles (Van Leussen and Cornelisse, 1994; Smith and Friedrichs, 2010). An automated method to define spatial and temporal variations in fluid motions is presented and evaluated, by which the population of particles smaller than 20 µm is tracked by PIV to approximate fluid motions. Application of the PIV method to correct velocities of larger particles (tracked with PTV methods) permits accounting for time- and space-variant fluid velocities within the settling column and results in more accurate settling velocities and densities for the tracked larger particles (> 30 microns in diameter). The bin-averaged (by size) settling velocities and densities determined by the manual and automated PIV methods were generally similar; however estimates of settling velocity and density for individual particles were greatly improved by use of the automated method, and mean biases associated with manual evaluation of individual video samples were also reduced.

Automated particle tracking and fluid velocity estimates offer several advantages, both experimentally and during post-experimental analysis. Fluid velocity corrections during image analysis permits faster sampling during field experiments, through use of a single sampling and settling chamber. The single-chamber design of video settling devices allows rapid profiling of the water column with image sequences recorded on the order of 2-minute intervals instead of 10-40 minute intervals with two chambered devices. Automated PTV tracking of large particles and PIV estimates of fluid velocities enables tracking of large numbers of particles, which provides better statistical characterization of size, settling velocity, and density of suspended particle populations. The automated PIV fluid velocity correction method significantly reduces measurement uncertainty in both settling velocity and inferred particle density.

REFERENCES FOR CHAPTER 4

Adrian, R.J. 1991. Particle-imaging techniques for experimental fluid mechanics, *Annual Review of Fluid Mechanics* 23: 261-304.

Agrawal, Y.C. and Pottsmith, H.C. 2000. Instruments for particle size and settling velocity observations in sediment transport. *Marine Geology* 168: 89-114.

Ayukai, T. and Wolanski, E. 1997. Importance of biologically mediated removal of fine sediments from the Fly River plume, Papua New Guinea. *Estuarine and Coastal Shelf Science* 44: 629-639.

Bec, J., Biferale, L., Boffetta, G., Celani, A., Cencini, M., Lanotte, A., Musacchio, S., and Toschi, F. 2006. Acceleration statistics of heavy particles in turbulence. *Journal of Fluid Mechanics* 500: 349-358.

Cornelisse, J.M. 1996. The field pipette withdrawal tube (FIPIWITU), *Journal of Sea Research* 36(1/2): 37-39.

Droppo, I.G. 2004. Structural controls on floc strength and transport. *Canadian Journal of Civil Engineering* 31: 569-578.

Dyer, K.R.; Cornelisse, J.; Dearnaley, M.P.; Fennessy, M.J.; Jones, S.E.; Kappenberg, J.; McCave, I.N.; Pejrup, M.; Puls, W.; Van Leussen, W.V.; and Wolfstein, K. 1996. A comparison of in situ techniques for estuarine floc settling velocity measurements. *Journal of Sea Research* 36(1/2): 15-29.

Eisma, D. 1986. Flocculation and de-flocculation of suspended matter in estuaries. *Netherlands Journal of Sea Research* 20(2/3): 183-199.

Fennessy, M.J., Dyer, K.R., and Huntley, D.A. 1994. INSSEV: an instrument to measure the size and settling velocity of flocs in situ. *Marine Geology* 117: 107-117.

Gibbs, R.J. and Konwar, L.N. 1983. Sampling of mineral flocs using niskin bottles. *Environmental Science and Technology*: 17(6): 374-375

Gonzalez, R.C., Woods, R.E., and Eddins, S.L. 2004. Digital Image Processing Using Matlab. Pearson Prentice Hall, Upper Saddle River, New Jersey, USA.

Haralick, R.M. and Shapiro, L.G. 1992. Computer and Robot Vision, Vol II, pp. 316-317, Addison-Wesley, Reading, Massachusetts.

Hill, P.S., Milligan, T.G., and Geyer, W.R. 2000. Controls on effective settling velocity of suspended sediment in the Eel River flood plume. *Continental Shelf Research* 20: 2095-2111.

Hjelmfelt, A.T. and Mockros, L.F. 1966. Motion of discrete particles in a turbulent fluid. *Journal of Applied Sciences Research* 16: 149-161.

Kineke, G.C., Sternberg, R.W., and Johnson, R. 1989. A new instrument for measuring settling velocities in situ. *Marine Geology* 90: 149-158.

Krank, K. and Milligan, T.G. 1992. Characteristics of suspended particles at an 11-hour anchor station in San Francisco Bay, California. *Journal of Geophysical Research* 97(C7): 11,373-11,382.

Lewis, J.P. 1995. Fast template matching. *Vision Interface 95*, pp. 120-123. Canadian Image Processing and Pattern Recognition Society, Quebec City, Canada, May 15-19, 1995.

Lintern, G. and Sills, G. 2006. Techniques for automated measurement of floc properties, *Journal of Sedimentary Research* 76: 1183-1195.

Manning, A.J. and Dyer, K.R. 1999. A laboratory examination of floc characteristics with regard to turbulent shearing. *Marine Geology* 160: 147-170.

Manning, A.J. and Dyer, K.R. 2002. The use of optics for the in situ determination of flocculated mud characteristics. *Journal of Optics A: Pure and Applied Optics* 4: S71-S81.

Mehta, A.J. 1989. On estuarine cohesive sediment suspension behavior. *Journal of Geophysical Research* 94(C10): 14303-14314.

Mikkelsen, O.A. and Pejrup, M. 2000. In situ particle size spectra and density of particle aggregates in a dredging plume. *Marine Geology* 170: 443-459.

Mikkelsen, O.A., Milligan, T.G., Hill, P.S., and Moffatt, D. 2004. INSSECT—an instrumented platform for investigating floc properties close to the seabed. *Limnology and Oceanography: Methods* 2: 226-236.

Milligan, T.G. and Hill, P.S. 1998. A laboratory assessment of the relative importance of turbulence, particle composition, and concentration in limiting maximal floc size and settling behaviour. *Journal of Sea Research* 39: 227-241.

Oseen, C. 1927. Hydrodynamik, chapter 10, Akademische Verlagsgesellschaft, Leipzig.

Owen, M.J. 1976. Determination of the settling velocities of cohesive sands. Hydraulics Research Report No. IT161.

Raffel, M., Willert, C.E., Wereley, S.T., and Kompenhans, J. 2007. Particle Image Velocimetry, 2nd edition, Springer, Heidelberg.

Sanford, L.P.; Dickhudt, P.J.; Rubiano-Gomez, L.; Yates, M.; Suttles, S.E.; Friedrichs, C.T.; Fugate, D.D.; and Romine, H. 2005. Variability of suspended particle concentrations, sizes, and settling velocities in the Chesapeake Bay turbidity maximum. In: Droppo, I.G.; Leppard, G.G.; Liss, S.N.; and Milligan, T.G. (Eds.) Flocculation in Natural and Engineered Environmental Systems, CRC Press, Boca Raton, Florida, USA.

Santschi, P.H., Burd, A.B., Gaillard, J.-F., and Lazarides, A.A. 2005. Transport of materials and chemicals by nanoscale colloids and micro- to macro-scale flocs in marine, freshwater, and engineered systems. In: Droppo, I.G.; Leppard, G.G.; Liss, S.N.; and Milligan, T.G. (Eds.) Flocculation in Natural and Engineered Environmental Systems, CRC Press, Boca Raton, Florida, USA.

Schiller, L. and Naumann, A. 1933. Über die grundlegenden Berechnungen bei der Schwerkraftaufbereitung, Z. VDI, vol. 77.

Smith, S.J. and Friedrichs, C.T. 2010. Size and settling velocities of cohesive flocs and suspended sediment aggregates in a trailing suction hopper dredge plume. *Continental Shelf Research* (in press) doi:10.1016/j.csr.2010.04.002.

Soulsby, R.L. 1997. Dynamics of Marine Sands. Thomas Telford, London.

Sternberg, R.W., Ogston, A., and Johnson, R. 1996. A video system for in situ measurement of size and settling velocity of suspended particulates. *Journal of Sea Research* 36(1/2): 127-130.

Syvitski, J.P.M. and Hutton, E.W.H. 1996. In situ characteristics of suspended particles as determined by the floc camera assembly FCA. *Journal of Sea Research* 36(1/2): 131-142.

Taylor, J.R. 1997. An Introduction to Error Analysis. second ed., University Science Books, Sausalito, California.

Tsai, C.-H., Iacobellis, S., and Lick, W. 1987. Flocculation of fine-grained lake sediments due to a uniform shear stress. *Journal of Great Lakes Research* 13(2): 135-146.

Van der Lee, W.T.B 2000. Temporal variation of floc size and settling velocity in the Dollard estuary. *Continental Shelf Research* 20: 1495-1511.

Van Leussen, W. 1994. Estuarine Macroflocs and Their Role in Fine-Grained Sediment Transport, Ministry of Transport, Pubic Works and Water Management. Den Haag.

Van Leussen, W.V. and Cornelisse, J.M. 1993. The determination of the sizes and settling velocities of estuarine flocs by underwater video system. *Netherlands Journal of Sea Research* 31(3): 231-241.

Westerweel J. and Scarano, F. 2005. Universal outlier detection for PIV data, *Experiments in Fluids* 39: 1096-1100

Westerweel, J. 1994. Efficient detection of spurious vectors in particle image velocimetry data. *Experiments in Fluids* 16: 236-247

Westerweel, J. 1993. Digital Particle Image Velocimetry: Theory and Application. Delft University Press, Delft, The Netherlands, 199 pp.

Williams, N.D., Walling, D.E., and Leeks, G.J.L. 2008. An analysis of the factors contributing to the settling potential of fine fluvial sediment. *Hydrological Processes* 22: 4153-4162.

CHAPTER 5. SUMMARY, CONCLUSIONS, AND RECOMMENDATIONS

OVERVIEW

Dredging of sediments from navigation channels and ports is a vital activity for economic security, enabling access to ports by deep-draft, ocean-going vessels (USACE, 1983). During dredging operations, sediments are removed from the bed and transported by pipeline or vessel to dredged material placement sites. However, a portion of the sediments removed from the bed is suspended into the water column, transported from the dredging and placement sites by ambient currents, and returned to the bed through particle settling and deposition. The transport and fate of sediments suspended by dredging operations are of primary concern due to potential impacts to environmental quality. Furthermore, these potential impacts are directly related to the settling velocities and cohesive sediment dynamics of the dredge-suspended sediments.

The research presented in this dissertation examines influences of dredge equipment and suspended sediment processes on cohesive aggregates and settling velocities of sediments suspended during dredging operations. The first chapter provides background material regarding environmental impacts of suspended dredged material, prior research, and research objectives. Chapter two describes an analysis technique to determine bulk settling rates within dredge plumes using an Acoustic Doppler Current Profiler (ADCP). Chapter three describes development of the Particle Imaging Camera System (PICS) and application of PICS to determine cohesive sediment aggregate states and settling velocities within a trailing suction hopper dredge plume in San Francisco Bay. Chapter four describes automated image processing techniques employed to achieve higher accuracy settling velocity and particle density estimates from a single-chambered video settling column such as PICS.

SUMMARY AND CONCLUSIONS

Chapter One describes the motivation for research of settling processes in dredge plumes. Environmental concerns related to suspended dredged material include physiological stresses (particularly to larval and juvenile stages), light attenuation, habitat degradation, and interruption of reproductive cycles, among others. Numerical models are frequently applied to estimate fate of dredged material, and ecosystem impacts are inferred from these model predictions. Recent assessments of numerical model

predictions indicate that the modeled suspensions settle from the water column at slower rates than the observations suggest. The comparisons between modeled and measured behavior imply that: 1) dredged sediments are not initially completely disaggregated (as assumed by the numerical settling algorithms) and/or 2) flocculation rates (and settling velocities) within the dredge plume are faster than predicted from empirical relationships developed from naturally suspended cohesive sediments.

To better understand suspended sediment settling within dredge plumes, two experimental methods were proposed to quantify settling rates and initial aggregate states within dredge plumes. The first method is a bulk settling velocity estimate, which relies on ADCP-derived measurements of sediment flux. The second method involves measuring individual particle size and settling velocity within dredge plumes with a digital video settling column and inferring particle density from the observations. Field experiments were proposed within hopper dredge and mechanical dredge plumes to examine differences in initial states of aggregation near the dredge and flocculation rates as the suspended sediment plume is transported from the dredging site.

Chapter Two describes a mass-balance approach to estimate bulk settling velocities within dredge plumes. This method alone will not address all research questions posed, but has advantages over the individual particle approach in lower data collection and analysis costs. The mass-balance approach estimates settling velocity within a suspended sediment plume by solving the suspended sediment mass conservation equation with longitudinal (in the flow direction) gradients in suspended sediment transport estimated from the ADCP data. The mass-balance approach was demonstrated to work well for a dredge plume composed of relatively fast settling fine sand introduced from a near-constant and stationary source. In practice, the mass-balance method was difficult to implement in field experiments, particularly with moving sources (such as trailing suction hopper dredges). The mass-balance method may be able to achieve settling velocity estimates for stationary or near-stationary sources (mechanical dredges), but is unable to resolve aggregate states (a primary objective of this research).

Chapter Three describes application of the PICS within a trailing suction hopper dredge plume in San Francisco Bay. Through this experiment, size, settling velocity, and

particle density were estimated within a hopper dredge overflow plume for approximately 90 minutes following sediment release to the water column. The data suggest that at least two particle classes existed in the dredge plume measurements, with distinct differences in characteristics. The bed aggregate class was composed of smaller but denser particles with time invariant size and settling velocity; the floc class demonstrated time-dependent increases in size and settling velocity. In-situ particle size distributions indicate less than 4% of suspended volume in the 4-10 μm range compared to 97% when physical samples were disaggregated. These data indicate that although the suspension released from the dredge is composed of silt and clay particles, these particles are present in an aggregated state. Flocs represented approximately 70% of the suspended sediment mass, with the remaining 30% represented by denser bed aggregates. Flocs were found to increase in size and settling velocity with elapsed time following release; however bed aggregate size and settling velocity remained constant with time.

Settling of flocs and bed aggregates was well-described by Winterwerp's (1998, 2002) fractal-based settling velocity relationship. Khelifa and Hill (2006) suggest that fractal dimension increases with floc size. The PICS data from the dredge plume suggest that flocs and bed aggregates have similar primary particle size, but differing fractal dimensions. Fractal dimensions were found to be size-invariant within density-defined particle classes, but the increased population of bed aggregates (or microflocs) at smaller sizes are consistent with Khelifa and Hill's assertion of a size-dependent fractal dimension for the full population of suspended particles.

The data collected within the plume provide valuable insights into numerical modeling approaches for dredge plumes. Considering the favorable agreement of the fractal-based settling velocity estimate by particle class, numerical modeling applications could define discrete suspended sediment classes with varying fractal dimensions to appropriately account for the presence of low-density flocs and dense, robust aggregates suspended from the bed. Increased size and settling velocity of the floc class with time suggests that flocs interact, but interactions between bed aggregates and flocs are unknown.

Van Leussen (1994) and Van der Lee (2000) present the work of many researchers that have observed a concentration dependence of settling velocities in various estuarine settings. These observations are attributed to increased collision frequency with increase in concentration, but may also be influenced in part by resuspension/deposition exchanges with the sediment bed (Eisma, 1986). For the present study, correlations between floc size and settling velocity to suspended sediment concentration (SSC) were weak and statistically insignificant. Considering the weak correlations between settling velocity and SSC, an empirical relationship between settling velocity and plume concentration is not justified for dredge plumes.

Chapter Four presents improved image analysis methods for video settling columns. Two challenges in analysis of video settling column imagery are the automated tracking of settling particles and accounting for fluid motions within the settling column. A combination of Particle Tracking Velocimetry (PTV) and Particle Image Velocimetry (PIV) image analysis techniques is described, which permits general automation of image analysis collected from video settling columns. In the fixed image plane, large particle velocities are determined by PTV and small particle velocities are tracked by PIV and treated as surrogates for fluid velocities. The large-particle settling velocity (relative to the suspending fluid) is determined by the vector difference of the large and small particle settling velocities. The combined PTV/PIV image analysis approach is demonstrated for video settling column data collected within a dredge plume in Boston Harbor. The automated PTV/PIV approach was found to 1) significantly reduce uncertainties in measured settling velocity and inferred floc excess density, and 2) permits evaluation of much larger population statistics compared to manual methods.

FUTURE RESEARCH AND DEVELOPMENT

Deployment of the PICS within dredge plumes has yielded the first quantitative data to determine initial aggregation states and settling velocities of sediment suspended by dredging operations. The development of PICS and associated image and data analysis methods will enable further research in suspended cohesive sediment transport processes for dredge plumes and natural suspensions in coastal and estuarine systems. Over the short- and long-term, future research, development, and publication of PICS

should include: 1) published results of PICS validation experiments, 2) publication of observations from a mechanical dredging dataset (Boston Harbor), 3) additional investigations of estuarine sediment dynamics including flocculation and the role of dense bed aggregates in natural systems, and 4) application to biological processes.

PICS Validation Experiments

Limited PICS uncertainty analysis and validation has been conducted (Chapter three) based upon field measurements. Laboratory experiments are proposed to assess the accuracy to which PICS estimates settling velocity, particle size, and excess particle density. Initial efforts to conduct these laboratory experiments were attempted with manufactured particles (polystyrene divinyl-benzene, PSDVB) with mono-sized particles of known density (1.05 g cm^{-3}). The surface luster of PSDVB microspheres produced locally high reflectivity that did not permit particle size to be determined with the current lighting configuration of PICS. Natural particles with narrow-banded size distributions, spherical shape, and known hydrated density have been evaluated, and corn (~90 μm diameter) and pecan (~50 μm diameter) pollen have been identified as promising candidates for the laboratory experiments. In these experiments, size, settling velocity, and excess density estimated by PICS will be compared to the independently determined values.

Dredge Plumes

A PICS field experiment was conducted in September 2008 within a mechanical dredge plume in Boston Harbor. These data have been processed, analyzed, and presented at the 2009 International Cohesive Sediments Conference (INTERCOH). The data indicate that the mechanical dredge plume was composed of 37% flocs, 56% bed aggregates and 7% primary particles. This dataset will be prepared for publication in an engineering journal, such as ASCE *Journal of Waterways, Ports, Coastal, and Ocean Engineering*.

To date, PICS field experiments have been focused on the properties and processes of sediments released during dredging. Additional ecosystem concerns are associated with placement of dredged material by hopper dredges, scows, and hydraulic

pipelines. Future research will focus on settling processes in plumes produced during dredged material placement.

Coastal and Estuarine Fine Sediment Processes

The value of PICS in quantifying size and settling velocities of suspended cohesive sediments has already been recognized at the US Army Engineer Research and Development Center (ERDC). Several field experiments involving PICS have been planned and/or executed. Completed field experiments include South San Francisco Bay, CA; New Bedford Harbor, MA; Cochiti Lake, NM; and Mississippi Sound, MS. Planned field experiments include light attenuation studies in Currituck Sound, NC; propwash studies near San Diego, CA; and channel sedimentation studies in Galveston Bay, TX.

During field experiments in South San Francisco Bay, the strong tidal currents were observed to suspend a relatively large fraction of dense flocs that would be classified as bed aggregates. The relatively large settling velocity of these dense, robust flocs plays an important role in the tidally modulated suspended sediment response in systems with pronounced, regular exchange of sediment between the sediment bed and water column. Prior research such as that of Fugate and Friedrichs (2003) have suggested that dense, robust fine-sediment aggregates originating either from the consolidated bed or from fecal pellets are important in the Chesapeake Bay region and likely elsewhere. Application of a video settling column, such as PICS, in these systems will improve the understanding and role of both loosely bound flocs and denser muddy aggregates in estuarine and coastal fine-sediment processes.

Observations from high-shear cohesive sediment erosion experiments suggest that sediments eroded from recently deposited and weakly consolidated flocs are eroded from the sediment surface as low-density flocs (Amos and Mosher, 1985; Thomsen and Gust, 2000). As erosion progresses deeper into the consolidated sediment bed, sediments are increasingly eroded as a combination of individual particles and dense, robust, muddy aggregates and bed fragments. During erosive events (such as storms or seasonally high shear), the initial state of mobilized fine sediments is of interest, and largely unknown. Recently, PICS has been coupled with a high-shear cohesive sediment erosion flume (Sedflume) to quantify the initial aggregate states and settling velocities immediately

following erosion from the sediment bed. Presently, we are in the early stages of interpreting and understanding these data. Coupling of PICS with a cohesive sediment erosion device may offer important insights into suspended sediment processes during high energy events. To extend this research beyond the current laboratory applications, a robust, system suitable for long-term and high-energy deployment should be developed and deployed to examine the suspended population characteristics during high-energy events.

Biological Research

Flocs observed in dredge plumes, particularly macroflocs, have been noted to be bound in part by biological "stringers", filament-like material presumably composed of extracellular polymeric substances (EPS). It is increasingly recognized that EPS may play important, if not dominant, roles in the flocculation process for suspended cohesive sediments through increasing the stickiness and therefore the aggregation efficiency of interparticle collisions. Laboratory and field experiments to examine the role of EPS or other organic material in mediating flocculation are recommended. Such experiments would combine an imaging system such as PICS and organic analyses to characterize organic content and molecular weight of polymeric substances contained in the suspension.

Imaging systems such as PICS may also be applied in direct observations of abundance and/or mobility of micro-scale, planktonic organisms. Frequently, copepods, amphipods, phytoplankton, and other microorganisms are observed in video collected with PICS. For mobility studies of such organisms, the lighting modules of PICS could be exchanged for wavelengths (such as red or UV) that are not visible by the biota of interest. A recent application of PICS was to quantify the size and settling velocity of various developmental stages of winter flounder (*Pseudopleuronectes americanus*) eggs. These 800-μm eggs were resolved with sufficient detail by PICS to characterize the eggs as fertilized and embryo development stage within the eggs. The data resulting from these experiments was later used for Lagrangian numerical modeling of egg dispersal from spawning grounds over the 6-10 day interval between spawning and larvae emergence (Lackey, et al., 2010).

REFERENCES FOR CHAPTER 5

Amos, C.L. and Mosher, D.C. 1985. Erosion and deposition of fine-grained sediments from the Bay of Fundy. *Sedimentology* 32: 815-832.

Eisma, D. 1986. Flocculation and de-flocculation of suspended matter in estuaries. *Netherlands Journal of Sea Research* 20(2/3): 183-199.

Fugate, D. and Friedrichs, C.T., 2003. Controls on suspended aggregate size in partially mixed estuaries, *Estuarine, Coastal, and Shelf Science* 58: 389-404.

Khelifa, A. and Hill, P.S. 2006. Models for effective density and settling velocity of flocs. *IAHR Journal of Hydraulic Research* 44(3): 390-401.

Lackey, T.C., Kim, S-.C., Clarke, D., and Smith, J. 2010. Transport and fate of winter flounder eggs near dredging operations. Proceedings of Western Dredging Association Conference, San Juan, Puerto Rico, 6-9 June 2010.

Thomsen, L. and Gust, G. 2000. Sediment erosion thresholds and characteristics of resuspended aggregates on the western European continental margin. *Deep-Sea Research I* 47: 1881-1897.

U.S. Army Corps of Engineers (USACE) (1983). Dredging and Dredged Material Disposal. Engineering Manual 1110-2-5025. Vicksburg, Mississippi, USA

Van der Lee, W.T.B 2000. Temporal variation of floc size and settling velocity in the Dollard estuary. *Continental Shelf Research* 20: 1495-1511

Van Leussen, W. 1994. Estuarine Macroflocs and Their Role in Fine-Grained Sediment Transport, Ministry of Transport, Pubic Works and Water Management. Den Haag.

Winterwerp, J.C. 2002. On the flocculation and settling velocity of estuarine mud. *Continental Shelf Research* 22: 1339-1360.

Winterwerp, J.C. 1998. A simple model for turbulence induced flocculation of cohesive sediment. *IAHR Journal of Hydraulic Research* 36 (3): 309-326.

VITA

STANLEY JARRELL SMITH II

Born January 9, 1969 in Columbia, South Carolina. Graduated in 1992 and 1994 from Clemson University with Bachelor and Master of Science in Civil Engineering. Employed by the U.S. Army Engineer Research and Development Center, Coastal and Hydraulics Laboratory (Vicksburg, Mississippi) in 1994. Enrolled in the College of William and Mary, School of Marine Science in August 2004, and received a Doctor of Philosophy degree in Physical Sciences in January 2011.